Mid-infrared soliton self-frequency shift and supercontinuum sources based on As_2Se_3 chalcogenide microwires

Alaa Al-kadry

Department of Electrical & Computer Engineering
McGill University
Montréal, Canada

April 10, 2014

A thesis report submitted to McGill University in partial fullfillment of the requirements for the degree of Doctor of Philosophy.

Abstract

In this thesis, I propose tunable mid-Infrared (IR) sources based on the soliton self-frequency shift (SSFS) and supercontinuum (SC) generation in As_2Se_3 microwires. First, I present two methods to maximize the SSFS in microwires with diameter profiles varying non-uniformly along the soliton propagation path. There are two steps in each method. The first step consists in selecting the input microwire diameter that leads to the highest rate of soliton frequency shift per unit length. The second step consists of gradually increasing the microwire diameter along the soliton path such that a wavelength-shifting soliton experiences only weak perturbations from the third-order dispersion and avoids shedding its energy into non-solitonic radiation. The optimized profile supports solitons with different input energies that allow the tuning of a self-frequency shifted soliton over a spectral range of 860 nm in the mid-IR wavelength regime using only a 10 cm microwire length. The results are compared with the SSFS generated in microwires with uniform diameter profile to illustrate the enhancement of wavelength shift in the designed non-uniform microwire. This is the first study of the SSFS in As_2Se_3 microwires.

Second, I present the limitations of the two-photon absorption (TPA) effect on generating a mid-IR SC using femtosecond pump soliton sources operating at 1550 nm wavelength. A solution to avoid this effect is given based on the SSFS process. Also, I provide an analytical expression to obtain the full spectrum of the TPA of As_2Se_3 glass. This calculated spectrum is inserted in a numerical simulator to compare the calculated SC to experiments with better precision. A wide SC spectrum spanning from 1260 to 2200 nm

by using a 10 cm long As_2Se_3 microwire was successfully generated. This was achieved by self-frequency shifting the pump soliton toward longer wavelengths in standard silica fiber before being launched into the microwire.

Finally, I present a numerical model to maximize the SC generation in tapered fibers. Using this model, the optimal pulse parameters and the optimum structure of a tapered fiber for a maximum bandwidth of SC are determined. Based on this model, a mid-IR SC source based on a As_2Se_3 microwire and a thulium-doped fiber laser is presented. The SC source generated a continuous spectrum extending from 1400 nm to 2810 nm in a 10 cm long As_2Se_3 microwire from low-energy pulses of 124 pJ. This is the largest SC spectrum obtained in As_2Se_3 microwires. I discuss the limitations of the absorption band of OH impurity on extending the generated SC further to the mid-IR regime, and the effects of water absorption in reducing the energy contained in the spectrum.

Résumé

Dans cette thèse, j'introduis des sources accordables pour l'infrarouge moyen (MIR), basées sur l'auto-décalage fréquentiel de solitons (SSFS) ainsi que la génération de super-continuum (SC) dans des micro-fils de chalcogénure As_2Se_3. Premièrement, je présente deux méthodes permettant de maximiser le SSFS dans des micro-fils dont le diamètre varie de manière non-uniforme durant la propagation du soliton. Chaque méthode est composée de deux étapes. La première étape consiste à sélectionner le diamètre d'entrée du micro-fil qui induit un taux maximal d'auto-décalage fréquentiel par unité de longueur. La seconde étape consiste à augmenter graduellement le diamètre du micro-fil dans la direction de propagation de façon à ce que le soliton se déplaçant en longueur d'onde ne subisse que de faibles perturbations induites par la dispersion d'ordre trois et ne se déleste pas de son énergie par la création d'ondes dispersives. Le profil optimisé permet la propagation de solitons de différentes énergies, permettant un déplacement spectral par auto-décalage fréquentiel sur une plage de 860 nm dans le MIR en utilisant des micro-fils d'une longueur de 10 cm seulement. Les résultats obtenus sont comparés avec le SSFS générés dans des micro-fils dont le diamètre est constant dans la direction de propagation, afin d'illustrer les améliorations en termes de décalage fréquentiel issues du design de micro-fils non-uniformes. Il s'agit de la première études de SSFS dans des micro-fils de chalcogénure As_2Se_3.

Deuxièmement, je présente les limitations dues aux effets de l'absorption à deux photons (TPA) lors de la génération d'un SC dans le MIR en utilisant des impulsions

solitoniques femtosecondes à une longueur d'onde centrale de 1550 nm. Une façon de s'affranchir de ces effets, basée sur le procédé de SSFS, est proposée. De plus, je présente une expression analytique permettant d'obtenir le spectre intégral de la TPA intrinsèques aux verres de chalcogénure As_2Se_3. Ce spectre calculé est inséré dans un simulateur numérique afin de comparer le SC calculé aux expériences réalisées avec une meilleure précision. Un large spectre de SC s'étendant entre 1260 et 2200 nm a pu être généré en utilisant un micro-fil de chalcogénure As_2Se_3 d'une longueur de 10 cm. Ceci a été rendu possible par l'auto-décalage fréquentiel d'un soliton de pompe vers des longueurs d'ondes plus élevées dans de la fibre de silice standard avant une entrée dans le micro-fil.

Finalement, je présente un modèle numérique qui permet de maximiser la génération de SC dans des fibres effilées. De par ce modèle, les paramètres optimaux de l'impulsion d'entrée, ainsi que la structure optimale d'une fibre effilée sont déterminés en vue de maximiser la bande passante du SC induit. En se basant sur ce modèle, une source SC pour le MIR basée sur un micro-fil de As_2Se_3 et un laser à fibre dopée thulium est présentée. La source SC, pompée par des impulsions à basse énergie de 124 pJ, génère un spectre continu s'étendant entre des longueurs d'onde de 1400 nm et 2810 nm dans un micro-fil de chalcogénure As_2Se_3 d'une longueur de 10 cm. Je décris les limitations induites par la bande d'absorption des impuretés OH. Ces dernières empêchent aux SC induit de s'étendre plus loin dans le MIR. Les effets de l'absorption de l'eau, réduisant l'énergie contenue dans le spectre, sont aussi discutées.

Acknowledgements

Firstly, my great gratitude goes to Prof. Martin Rochette, my supervisor, for his unlimited support. I am deeply indebted to him, he taught me how to seek results, and useful skills such as scientific writing and presentation skills. Under his guidance, I had the opportunity to participate in conferences that have advanced my professional skills and experience. His confidence in me and his endless encouragement has motivated me to work hard during the study. I would like to express my sincere thoughts to all of those who helped me to carry out this graduation project. I wish to thank Chams Baker for showing the procedures of fabrication for tapered fibers, Thibault North for his collaboration, and Mohammed El Amraoui and Younès Messaddeq for their collaboration in providing the chalcogenide (ChG) As_2Se_3 fibers.

I would like to thank Prof. Andrew Kirk, Prof. Thomas Szkopek, and Prof. Martin Rochette for being on my advisory committee.

I would like to thank my father and mother for their support and encouragements. Also, I sincerely thank my wife and uncle for their help and the support they gave during my study. Thanks should be also addressed to my brother and sisters.

Contents

Acronyms

ChG chalcogenide.

CSB-M constant spectral bandwidth method.

DW dispersion wave.

EDFA Erbium-doped fiber amplifier.

EM electromagnetic.

FFT fast Fourier transform.

FROG frequency resolved optical gating.

FS frequency-shifted soliton.

GNLSE generalized nonlinear Schrodinger equation.

GVD group-velocity dispersion.

IR Infrared.

OCT optical coherence tomography.

OPO optical parametric oscillators.

P-M perturbative method.

PCF photonic crystal fibers.

QCL quantum cascade lasers.

RK4IP Runge-Kutta in the interaction picture.

SC supercontinuum.

SHG second harmonic generation.

SMF single-mode fiber.

SPM self-phase modulation.

SSFM split-step Fourier method.

SSFS soliton self-frequency shift.

SSFS$_r$ rate of soliton self-frequency shift per unit length.

TOD third-order dispersion.

TPA two-photon absorption.

XPM cross-phase modulation.

ZDW zero-dispersion wavelength.

List of Figures

Chapter 1

Introduction

In recent years, there has been much interest in developing broadband light sources suitable for mid-Infrared (IR) spectral region [1–7]. The mid-IR spectral region could be defined as the range of wavelengths, of electromagnetic (EM) waves, between 2 and 10 μm. The wavelength region between 2 and 5 μm, which is also known as "molecular fingerprint" region, is particularly important since a large number of molecules undergo strong vibrational transitions in this domain. Molecules of atmospheric constituents, such as water vapor (H_2O) have an absorption spectrum spanning between 2.5 and 3 μm with an absorption peak around 2.7 μm, carbon monoxide (CO) has strong absorption features around 2.3-2.4 μm, carbon dioxide (CO_2) absorbs around 2.7-2.8 μm, nitrogen dioxide (N_2O) also have several absorption features (see e.g. fig. 1.1).

Many applications would benefit from broadband mid-IR sources. For example, these sources can be used for molecular spectroscopy, chemical and biomolecular sensing, thermal and space-based terrestrial imaging, communications, materials processing, pollution monitoring and medical diagnosis. Therefore, it is strategically important to develop an efficient light source which spectrally covers this wavelength region in a single broadband pulse or by rapidly tuning the laser.

Mid-IR sources must satisfy a range of requirements to take full advantage of these

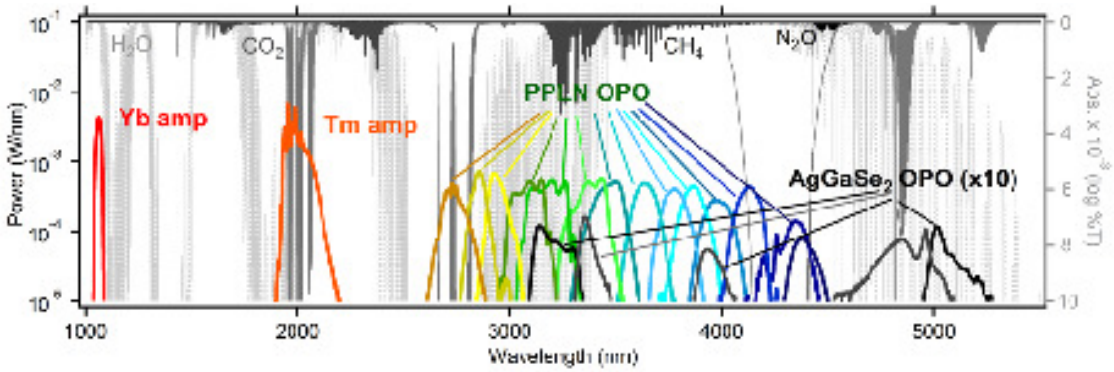

Figure 1.1: *Some of the available sources in the mid-IR regime (bottom axis) and the absorption specta for molecules of atmospheric constituents (top axis) [8].*

applications. For remote sensing applications, the output average power of the sources should be on the order of milliwatts or higher. However, pollution monitors may only require sources with power levels in the microwatt range. These sources should also be compact and have low production costs. For all the mentioned applications, the tunability of the source across part of the mid-IR spectrum is another important requirement. Spectroscopic applications may require tuning the operating wavelength of the source between several resonances and off the resonances to determine the actual absorption of materials (chemical or biological). Also, the power stability of sources is of paramount importance for spectroscopic applications as spectra are often taken in a differential mode to substract the background signal of omnipresent molecules. Finally, such sources must operate near room temperature. This is necessary to reduce the cost and size of the system.

The development of mid-IR light sources with performance comparable to sources in the near-IR regime traditionally was challenging. Much of the mid-IR spectrum is still inaccessible to conventional lasers due to the lack of suitable gain materials [9]. However, alternative technologies for the generation of mid-IR radiation have been proposed and developed with the goal of overcoming this limitation. Technologies based on quantum

cascade lasers (QCL)s, diode-pumped crystal and fiber lasers are now becoming available. The QCLs cannot at present be used to access the important 2-3 μm regime. The diode-pumped crystal include optical parametric oscillators (OPO). The OPOs achieve excellent wavelength tunability in mid-IR as shown in fig. 1.1, however, they require large-size lasers and high-precision alignment and are often pumped by expensive, high maintenance gas lasers. Such devices add to the complexity and cost, and increase the physical size of the overall system. On the other hand, the fiber laser has several unique properties, some of these properties are that the laser is free of alignment of bulk components and therefore very robust, less sensitive to the environment, and requires less maintenance. The properties are of high interest for many of the commercial and industry applications.

A common method used in fiber lasers is to dope the fiber with rare earth elements, e.g. ytterbium, erbium, and thulium to obtain lasing in discrete spectral windows in the mid-IR region [9, 10]. For lasing over broad spectral windows, an often applied strategy is to utilize nonlinear effects [11]. Among the nonlinear processes, soliton self-frequency shift (SSFS) and supercontinuum (SC) generation is receiving much interest because of its ability to generate new frequency components and spectra with broad spectral bandwidth.

1.1 Soliton self-frequency shift sources

A promising new way of developing mid-IR fiber sources is to exploit nonlinear wavelength shift via the SSFS effect [12, 13] triggered by a pulsed fiber laser operating at a wavelength at the transmission limit of silica glass [14]. The transmission window for fused silica stretches from $\sim$0.4 μm but not much further than $\sim$2 μm after which, the material absorption increases by orders of magnitude and creating an efficient nonlinear interaction becomes challenging [15, 16]. The SSFS originates from the stimulated Raman scattering and is, therefore, mainly dependent on the pulse energy density in the

fiber. This process takes place with short femtosecond pulses during their propagation in standard or specifically designed optical fibers with anomalous dispersion. It leads to a progressive shift of the central wavelength of the pulses towards longer wavelengths. Since the discovery of the SSFS in 1980 [12], several fiber designs were proposed with the goal of enhancing the rate of soliton self-frequency shift per unit length ($SSFS_r$) [17]. The parameters of the optical fiber that affects the have the most effect on the strength of SSFS are the chromatic dispersion, waveguide nonlinearity and fiber length. However, for the pulse source, the SSFS is mainly affected by the pump pulse duration and the peak power.

These sources are particularly interesting as they efficiently tune the central wavelength of a single pulse over a wide range while maintaining a significant portion of the pulse energy stored in the shifted soliton. There are many applications that could benefit from these sources such as frequency metrology, frequency comb sources [6], optical coherence tomography (OCT), etc.

1.2 Supercontinuum laser sources

SC laser sources are broadband lasers that cover continuous wide spectral regions. SC generation is an optical phenomenon of extreme spectral broadening of a laser spectrum which involves various nonlinear processes [11, 18]. The SC technology has great potential in fields where a single SC source can replace an array of lasers operating at different wavelengths. The SC field's potential is highlighted by its immense growth over the last ten years [19–21]. These sources have two major features: ultra-wide bandwidth where their bandwidths are usually as wide as a hundred nanometers or more and are of flexible spectral-coverage. The flexible-coverage range enables SC sources to be used in more applications with different spectral requirements.

Following the first observation of SC generation in bulk glass in the 1970s [22, 23],

the field began using optical telecom fibers [24, 25]. A large number of theoretical and experimental investigations have been conducted on the SC generation using different types of fibers. Very recently, much of the investigations have shifted from understanding the fundamentals to optimizing and lowering the power threshold requirements for a broadband SC generation. This requires designing the fibers in order to engineer their dispersion and nonlinearity profiles. Several approaches have been explored to lower the SC generation power threshold, for example by reducing the waveguide dimension [26–28] or by employing materials exhibiting high nonlinearity [29].

Nonlinearity in waveguides can be enhanced either by reducing the effective area of the mode, or by using materials with high Kerr nonlinearity (n_2). photonic crystal fibers (PCF) [21] and tapered fibers of uniform and non-uniform axial diameter profiles [30] are commonly used for reducing optical fiber dimensions and engineering the waveguide dispersion. Many publications focus on SSFS and SC generation in PCFs since it is easy to design their group-velocity dispersion (GVD) and possible to fabricate PCFs with long nonlinear interaction length. However, tapered fibers also show a large potential to become a competitor to PCFs [31] due to their simple manufacturing process [32, 33] and small fabrication loss. Low loss tapered fibers with sub-wavelength diameters (or microwires) have been successfully fabricated [34]. In silica, these fibers have enabled nonlinear processes such as SC generation and SSFS at low power thresholds [26, 35]. However, the nonlinearity in these fibers is ultimately limited by the index contrast of air and silica [28] and the transparency edge of silica lies at $\sim$2 μm.

The high mid-IR losses in silica have prompted the exploration of non-silica glass fibers for SSFS and SC fiber sources. The non-silica glass properties, and in particular tellurite [36–39], ZBLAN [40–42], and chalcogenide (ChG) [43–48] have been investigated by many researchers. The nonlinear properties are approximately the same for silica and ZBLAN [11], while ChG (As_2S_3 and As_2Se_3) can be as much as a factor of 200 and 1000 more nonlinear than silica depending on the content of sulfur (S) or selenium (Se),

respectively [49, 50]. The linear properties of the non-silica glass are also different than silica, and particularly the zero-dispersion wavelength (ZDW) which is located far in the mid-IR regime. Non-silica microstructured and tapered fibers have been designed to shift the ZDW to shorter wavelengths close to the central wavelengths of the available commercial laser sources, or even form two ZDWs in the optical spectrum [51–53]. The future of the fiber-based SC field seems to point to the development of cheap broadband SC sources which extend the SC spectrum into the mid-IR regime by using non-silica glass of high nonlinearities and/or low transmission loss in the mid-IR [37, 40–42] or to extend the SC spectrum into the deep-blue and ultraviolet with dispersion engineering [54–58].

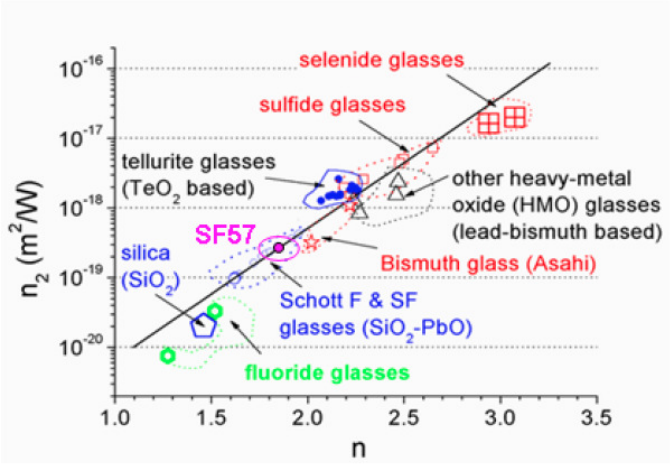

Figure 1.2: *Relation between the refractive index n and nonlinear refractive index n_2 for various types of glass [59].*

ChG As_2Se_3 fibers are excellent candidates for the generation of broadband mid-IR SC and tuning the SSFS over wide spectral bandwidth. This is because this glass exhibits a wide transmission window spanning from 1 up 12 μm [60], and has the largest ultrafast third order ($\chi^{(3)}$) nonlinear optical response (i.e. largest nonlinear refractive index n_2 (fig. 1.2)) among the non-silica glass and a good nonlinear figure of merit. For this,

As_2Se_3 fibers are useful in numerous applications [61]. Despite its wide transparency window, As_2Se_3 (non-silica glass in general as well) suffers from a small bandgap value [62]. This results in a poor transparency and a two-photon absorption (TPA) effects in the visible and IR wavelength (C-band) ranges, respectively [63]. However, both the Kerr nonlinearity (n_2 – related to the real part of $\chi^{(3)}$) and TPA (β_{TPA}– related to the imaginary part of $\chi^{(3)}$) are known to vary significantly across the C-band in this material. At high intensities, the TPA effects lead to the absorption of two photons of the same or different frequencies while only one photon is then being emitted [11, 64]. This phenomenon has shown limitation in several nonlinear processes including SSFS and SC generation in the C-band. On the other hand, since the Raman gain coefficient g_R, n_2 and TPA are different components of $\chi^{(3)}$ [65] which is inversely proportional to the fourth power of the bandgap value, the Raman gain coefficient and n_2 increases as moving towards shorter wavelengths. Therefore, it is of significant interest to study how the spectral bandwidth extent of the SC generation varies across the C and L-band which is indirectly related to the counteraction of the Raman gain, Kerr nonlinearity, and nonlinear absorption. Another obstacle for generating a broadband SC in ChG fibers is the absorption by fiber impurities, and in particular the hydroxyl (OH) band impurity [66].

1.3 Summary of thesis contribution

I provide in this thesis a study on the SSFS and SC generation in As_2Se_3 microwires.

Methods to design microwires for efficient wavelength conversion based on SSFS process

I contribute to the field of nonlinear optics by investigating the dynamics of SSFS in As_2Se_3 microwires both analytically and numerically. The thesis provides the optimum

launching pulse conditions and fiber parameters necessary to maximize the $SSFS_r$ in optical fibers. It also offers methods to design microwires with uniform diameters and a varying axial (non-uniform) diameter profiles in order to maximize the SSFS and the transfer of energy converted into longer wavelengths. The microwire designs are considered optimal for reducing soliton perturbations by third-order dispersion (TOD) effects that reduce the extent of soliton wavelength-shifting and shed the soliton energy into non-solitonic radiations [67].

SC generation in As_2Se_3 microwires

I also contribute to the field of nonlinear optics by investigating the SC generation in As_2Se_3 microwires both numerically and experimentally. I discuss the possible limitations of mid-IR SC generation in As_2Se_3 microwires. First, the thesis provides an investigation of the limitation of the TPA effects on generating a mid-IR SC generation in As_2Se_3 microwires by using a pump source in the C-band and provides a solution to avoid this effect. It also provides for the first time an analytical expression of the TPA spectrum of As_2Se_3 that spans from the visible up to the mid-IR wavelength range. Second, the thesis provides a numerical model to indicate the optimal pulse parameters and the optimum design of tapered fibers for a maximum bandwidth of SC generation in tapered fibers and presents the first demonstration of mid-IR SC generation in As_2Se_3 microwires.

1.4 Thesis content

To give a more detailed overview of the chapters in this thesis, a short description of each chapter is given in this section. The structure of the thesis is as follows:

In chapter 2, an introduction to nonlinear pulse propagation in As_2Se_3 optical fibers is presented. This chapter summarizes the basic theory of linear and nonlinear fiber optics with a focus on SSFS and SC generation.

In chapter 3, two methods are presented to optimize the design of non-uniform microwires to maximize the SSFS in microwires. The importance of the input soliton energy and the effect of the longitudinal confinement of the mode on the $SSFS_r$ are investigated. The SSFS is also investigated in uniform microwires to show the advantages of non-unifrom microwires in enhancing the $SSFS_r$.

In chapter 4, the effects of TPA on the SC generation are investigated. An analytical expression to calculate the full spectrum of TPA for As_2Se_3 is provided. An experimental system is presented to avoid the TPA effects, which generates a broadband SC spectrum using an As_2Se_3 microwire and a laser source at 1550 nm.

In chapter 5, a numerical model is presented to indicate the optimal pulse parameters and the optimum structure of tapered fiber for a maximum bandwidth of SC generation. The chapter also discusses the effects of the water vapor absorption on the energy carried in the SC spectrum, and the limitation by the absorption band of OH impurity for extending the SC spectrum in the mid-IR regime.

List of publications

Journal publications

Journal publication I

A. M. Al-kadry and M. Rochette. "Mid-infrared sources based on the soliton self-frequency shift". *J. Opt. Soc. Am. B* 29 (6 2012), pp. 1347–1355

Comments: This paper provides and analytical and numerical study of the SSFS in As_2Se_3 microwires.

A. Al-kadry: Theoretical development, paper preparation.

M. Rochette: Paper preparation, project supervision.

Journal publication II

A. Al-Kadry and M. Rochette. "Maximized Soliton Self-Frequency Shift in Non-Uniform Microwires by the Control of Third-Order Dispersion Perturbation". *J. Lightwave Technol.* 31.9 (2013), pp. 1462–1467

Comments: This paper provides a method to design microwires for a maximum $SSFS_r$.

A. Al-kadry: Theoretical development, paper preparation.

M. Rochette: Paper preparation, project supervision.

Journal publication III

A. Al-kadry, C. Baker, M. El Amraoui, Y. Messaddeq, and M. Rochette. "Broadband

supercontinuum generation in As2Se3 chalcogenide wires by avoiding the two-photon absorption effects". *Opt. Lett.* 38.7 (2013), pp. 1185–1187

Comments: This paper describes the effects of TPA on SC generation.

A. Al-kadry: Performed experiment, paper preparation.

C. Baker: Performed experiment.

M. El Amraoui: Provided As_2Se_3 fiber.

Y. Messaddeq: Provided As_2Se_3 fiber.

M. Rochette: Paper preparation, project supervision.

Other Journal publication

T. North, A. Al-kadry, and M. Rochette."Analysis of self-pulsating sources based on cascaded regeneration and soliton self-frequency shifting". (*Submitted to Journal of Selected Topics in Quantum Electronics*).

Conference publications

conference publication I

A. Al-kadry and M Rochette. "Mid-infrared sources based on the soliton self-frequency shift". In: *Proceedings of SPIE*. Vol. 8007. 2011, p. 80070D

Comments: This paper provides and analytical and numerical study of the SSFS in As_2Se_3 microwires.

A. Al-kadry: Theoretical development, paper preparation.

M. Rochette: paper preparation, project supervision.

conference publication II

A. Al-Kadry and M. Rochette. "Optimization of optical soliton self-frequency shifting towards the mid-infrared". In: *Fibre and Optical Passive Components (WFOPC), 2011 7th*

Workshop on. IEEE. 2011, pp. 1–4

Comments: This paper provides a method to design microwires for a maximum $SSFS_r$.

A. Al-kadry: Theoretical development, paper preparation.

M. Rochette: Paper preparation, project supervision.

conference publication III

A. Al-Kadry and M. Rochette. "Widely tunable soliton frequency shifting for mid-infrared applications". In: *Photonics Conference (PHO), 2011 IEEE*. IEEE. 2011, pp. 59–60

Comments: This paper provides an analytical and numerical description of SSFS to have a widely tunable wavelength conversion in As_2Se_3 mcirowires.

A. Al-kadry: Theoretical development, paper preparation.

M. Rochette: Paper preparation, project supervision.

conference publication IV

A. Al-kadry, C. Baker, M. El-Amraoui, Y. Messaddeq, and M. Rochette. "Broadband Supercontinuum in As2Se3 Wires by Suppression of Two-photon Absorption". In: *CLEO: Science and Innovations*. Optical Society of America. 2013

Comments: This paper describes the effects of TPA on SC generation.

A. Al-kadry: Performed experiment, paper preparation.

C. Baker: Performed experiment.

M. El Amraoui: Provided As_2Se_3 fiber.

Y. Messaddeq: Provided As_2Se_3 fiber.

M. Rochette: Paper preparation, project supervision.

Chapter 2

Pulse propagation in As_2Se_3 fibers

The interaction of light with matter has been extensively studied for decades. When light propagates in a medium, the EM field interacts with the atoms of the medium. Light causes atoms to oscillate, which in turn re-emits light that interferes with the original light. This means that the light experiences loss and dispersion. The latter effect occurs because different wavelength components travel at different velocities due to the spectral dependence of the refractive index. These effects are termed the linear response of the medium. If the intensity of the light is sufficiently high, the medium could respond also in a nonlinear way. In this case, the refractive index becomes intensity dependent (called the Kerr effect) which leads to the generation of light at new frequencies. Also, light can further interact with the molecular vibrations of the medium through the Raman effect. These effects (Raman and Kerr) are the basis for the many spectral broadening mechanisms we will investigate further in this chapter.

This chapter provides an introduction of the physics of the pulse propagation in As_2Se_3 fibers, so to make the thesis self-contained. An in-depth treatment is found in elsewhere, see e.g. on the book by Agrawal [11], the book on SC generation by Dudley [18] and the book on solitons in optical fibers by Hasegawa [75].

2.1 Optical propagation in As_2Se_3 fibers

Optical fibers are dielectric waveguides which represent a possible medium for the guided transmission of energy at optical frequencies. An EM field can be constrained in an optical fiber, by surrounding the core region with a lower refractive index cladding. When optical pulses propagate inside a fiber, the bound electrons regenerating the incoming fields are driven into harmonic and anharmonic motion which is manifested as complex changes in the pulse's shape and spectrum. Mathematically, the propagation of optical pulses in optical fibers is described by the wave equation obtained from Maxwell's equation. It is expressed as:

$$\nabla^2 E\,(r,t) - \frac{1}{c^2}\frac{\partial^2 E(r,t)}{\partial t^2} = \mu_o \frac{\partial^2}{\partial t^2}(P_L(r,t) + P_{NL}(r,t)) \tag{2.1}$$

P_L and P_{NL} are the linear and the nonlinear parts of the collection of the electric dipole moments (the induced polarization in the medium), and E is the electric field which can be mathematically described as

$$E(r,t) = \widehat{x}F(x,y)A(z,t)exp[i\beta_o z - \omega_o t], \tag{2.2}$$

F(x,y) is the transverse field distribution, A(z,t) is pulse envelope and $\beta_o = \beta_{\omega_o}$ the propagation constant at pulse center frequency ω_o, which specifies the phase change per unit length.

Equation (2.1) provides the general formalism for studying the linear and nonlinear effects in optical fibers. If a low-intensity optical pulses propagate along a fiber, the nonlinear polarization P_{NL}(r,t) term can be considered as a small perturbation to the total induced polarization in the medium and thus is neglected. In this case, the pulse propagate linearly in the medium.

2.2 Linear propagation

Linear impairments in optical fibers manifest independently of the pulse power. They result from the dependence of the refractive index n(ω) and the absorption on the frequency ω of incident EM field. n(ω) can be written in terms of the density of atoms N, the electron charge e and mass m, the oscillator strength f_{vo} of the transition from the atomic ground state o into the excited one v, the frequency ω_{vo}=(E_v-E_o)/$\hbar$ of this transition, and the width γ_v of the excited state:

$$n(\omega) = 1 + \frac{2\pi N e^2}{m} \sum_v \frac{f_{vo}}{\omega_{vo}^2 - \omega^2 - i\omega_{vo}\gamma_v} \tag{2.3}$$

n(ω)-1 is the response of a medium to the incoming EM field. The real part of eq. (2.3) gives the dispersion which optical pulses experience while propagating in optical fibers. This effect is manifested as a temporal spreading of the pulse. The imaginary part gives the absorption of the EM waves.

2.2.1 Chromatic dispersion

Chromatic dispersion is an important characteristic of optical materials. This detrimental effect is characterized by light of different wavelengths experiencing different refractive indices in the optical fiber and, accordingly, the different wavelengths travel at different speeds, c/n(ω), within the fiber. Dispersion originates from the frequency dependence of the response of electrons of As_2Se_3 (refractive index n(ω)) to EM field, and from the frequency dependence of the confinement of EM field by the fiber. These two components are known as material and waveguide dispersion, respectively. The wavelength dependence of the refractive index of bulk As_2Se_3 is given approximately by the Sellmeier equation as [76] (fig. 2.1):

$$n(\lambda) = (1 + \frac{0.2274\lambda^2}{(\lambda^2 - 508.05159)} + \frac{6.74238\lambda^2}{(\lambda^2 - 0.10545)})^{(1/2)}. \tag{2.4}$$

Equation (2.4) is valid for wavelengths far from resonances which is approximately between the wavelength range 1 and 12 µm.

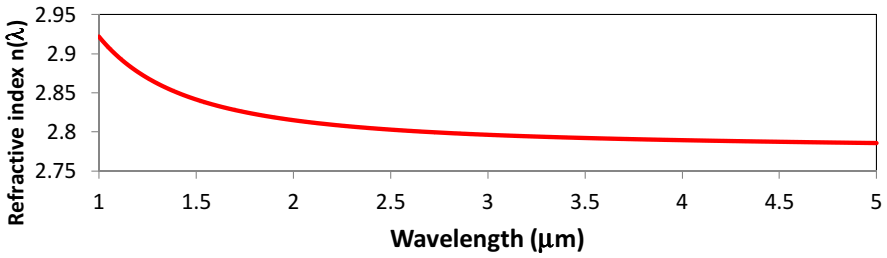

Figure 2.1: *The linear refractive index of As_2Se_3 calculated from eq.* (2.4) *as a function of wavelength λ.*

Chromatic dispersion is mathematically accounted for by Taylor expanding the propagation constant about the pulse center frequency ω_o:

$$\beta(\omega) = \beta_o + (\omega - \omega_o)\beta_1 + \frac{1}{2}(\omega - \omega_o)^2\beta_2 + \frac{1}{6}(\omega - \omega_o)^3\beta_3 + \cdots \tag{2.5}$$

where c is the speed of light in free space, and the β_m coefficients are given by

$$\beta_m = (\frac{d^m\beta_o}{d\omega^m})_{\omega-\omega_o}(m = 0, 1, 2, \dots). \tag{2.6}$$

The pulse envelope moves at the group velocity $v_g \equiv {}^1/_{\beta_1}$, while the effects of GVD in broadening pulses temporally are governed by β_2. The TOD distorts the symmetry of the pulse and the pulse shape exhibits an oscillatory structure near the trailing edge. Dispersion parameters β_m of third and higher order are called higher-order dispersion.

Either anomalous ($\beta_2 < 0$) or normal ($\beta_2 > 0$) dispersion characteristics can be possessed by fibers. The sign and magnitude of β_2 are important for most nonlinear processes in optical fibers. In the normal dispersion regime, the longer wavelength components of a pulse travels faster than its shorter wavelength components. The opposite is true for regions with anomalous dispersion. The crossing point between the two dispersion regimes is called the ZDW. At the ZDW, the material dispersion and the waveguide dispersion

cancel each other, and the GVD is zero. For A_2Se_3 fibers, the ZDW is centered at the wavelength of $\sim$7.2 μm [66, 77] and β_2 is positive in the range where the wavelength is less than ZDW and negative elsewhere (fig. 2.2) (For theoretical calculation of dispersion see the appendix).

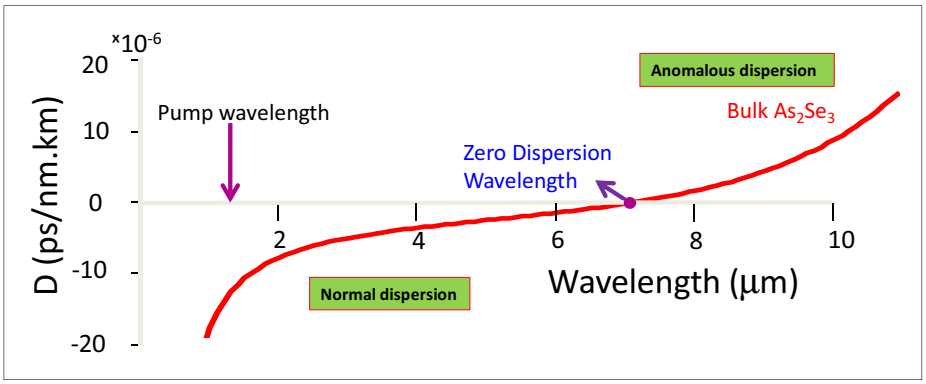

Figure 2.2: *The GVD spectrum of As_2Se_3 glass calculated as function of wavelength. The ZDW is located at around 7.2 µm.*

Efficient nonlinear frequency conversion requires long nonlinear interaction length between a medium and propagating pulses. The nonlinear interaction can thus be limited if pulses propagate with large magnitudes of β_2 (manifested as rapid temporal broadening of pulses), and accurate control of the dispersion is a clear prerequisite for efficient nonlinear processes.

2.2.2 As_2Se_3 tapered optical fibers

The tapered fiber is manufactured from a fiber [1] by the heat-brushing technique [32, 79], which means that a part of a 1 cm long of the fiber is heated up and pulled so that the diameter of the heated part can be decreased down to a micron and submicron scale. While pulling, the heater is moved along the fiber to provide a homogeneous waist with a length between 1 and 150 mm. The tapering stage is shown in fig. 2.3.

[1] Commercial fibers are available from Coractive [78]

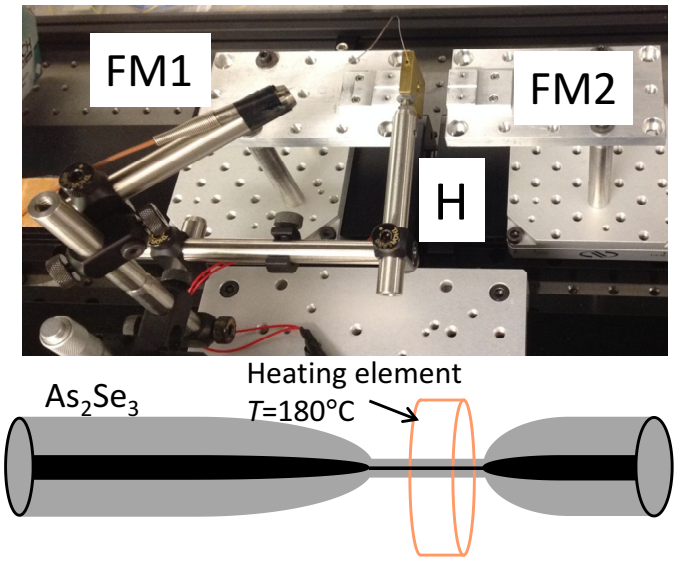

Figure 2.3: *A picture of the tapering stage used to heat part of the fiber at 180^o and stretch it to form a microwire; FM1 & FM2: Fiber mounts, H:Heater.*

ChG As_2Se_3 fibers consist of a core surrounded by a cladding with a lower refractive index. The diameters of the core and the cladding are ∼6 and 170 μm, respectively. The index difference is controlled by slightly changing the compound composition of AsSe and typically is ∼0.004 **3.(e.g. $As_{38}Se_{62}$ for cladding and $As_{39}Se_{61}$ for core [50])**. The small index difference results in a weak waveguide. The dispersion property of such fibers is thus comprised mostly of the material dispersion and a small amount of the waveguide dispersion.

When As_2Se_3 fibers are tapered down to diameters in micron range, a waveguide with a strong confinement develops between As_2Se_3 and its surrounding air [80]. Compared to As_2Se_3 fiber, the total dispersion is more significantly affected by the waveguide dispersion. By controlling the waveguide dispersion it is thus possible to create waveguides with properties very different from As_2Se_3 fibers.

The diameter of tapered fibers has a great wavelength dependence as the light distribution in the air and glass varies with wavelength. This enables a unique engineering of

the dispersion and nonlinear processes, which offers unprecedented control of nonlinear processes. In particular, the success of tapered fibers lies in the precise control of the ZDW through the change of the fiber diameter to match the wavelength of commercially available lasers.

Schematic structure of As_2Se_3 tapered optical fibers

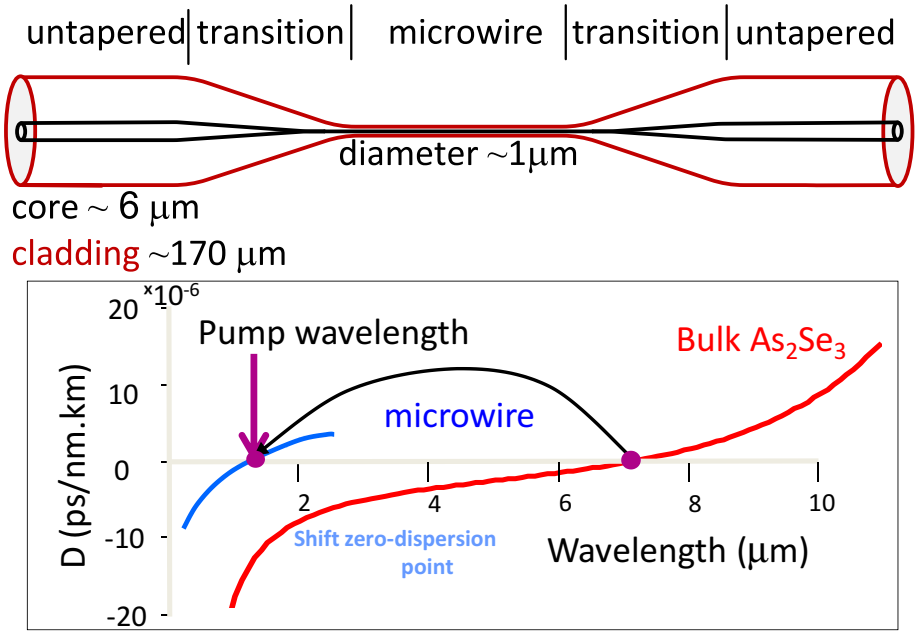

Figure 2.4: *A schematic structure of a tapered fiber. It shifts the ZDW of the As_2Se_3 glass to shorter wavelengths close to the available commercial laser sources.*

Tapered fiber consists of three sections: Untapered, transition, and microwire section as shown in fig. 2.4. In the untapered and transition sections, light is weekly guided by the core-cladding interface. Therefore most of the intensity is located in the core. In the microwire section, the light is strongly guided by the As_2Se_3-air interface. Since the microwire diameter is on the order of the light wavelength, an evanescent field appears in the air. The confinement of the light in microwires of diameters in the micron range

results in high intensity.

The ZDW of the As_2Se_3 material is located at 7.2 μm as it was mentioned before. However, the ZDW of the As_2Se_3 microwire is shifted to shorter wavelengths (fig. 2.4). Figure 2.5 shows that the smaller the diameter, the shorter is the ZDW. For a microwire with a diameter of 1.2 μm, the ZDW is at 1160 nm, where as 0.6 μm has two ZDWs: ZDW_1 and ZDW_2. ZDW_1 is located at 1160 nm and ZDW_2 at 2180 nm.

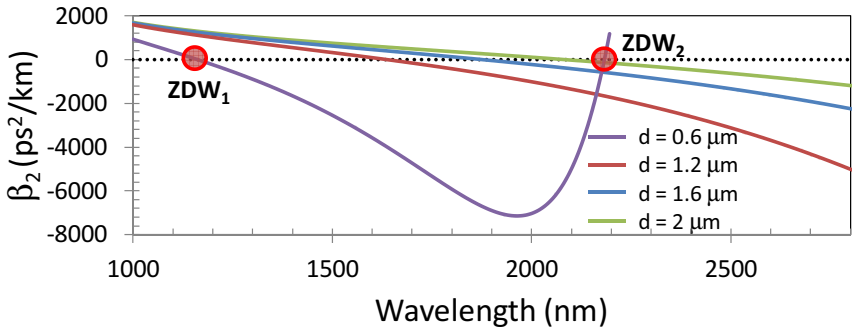

Figure 2.5: *The GVD spectrum of As_2Se_3 microwires calculated as function of wavelength. In a microwire, two ZDWs can exist: ZDW_1 and ZDW_2.*

These diameter-dependent dispersion variations not only changes the ZDWs, but also change other related linear properties, such as the condition for dispersion wave (DW) emissions during SSFS (described in Chapter 3). Therefore, tapering provide us with a tool to manipulate the linear properties of fibers and to optimize the conditions for avoiding the DW emissions.

Attenuation

In tapered fibers, there are three mechanisms to the total loss which can be categorized as intrinsic, extrinsic and radiative losses [77, 78, 81]. The intrinsic loss of As_2Se_3 is ~ 0.01 cm^{-1} in the range 1-12 μm (fig. 2.6), but increases towards the ultraviolet regime due to electronic resonances [78, 82]. Extrinsic losses arises generally from the presence

of impurities [83, 84] and OH ions dissolved in glass. The latter losses can be significant and limits the SSFS and SC generation processes [85, 86]. Therefore, their concentration should be reduced to a low level (one order of magnitude [87]) so that they contribute negligibly to the fiber loss. Hydroxyl (OH) group losses are also known to increase with decreasing core size as was investigated in PCF [88]. For this, tapered fibers are particularly exposed to water-related losses, where an overtone of OH bond absorption causes attenuation at 2.7μm [89, 90]. The limitation of the OH impurity to mid-IR SC generation is further discussed in Chapter 4. Radiative losses arises fundamentally from the geometry of tapered fibers which causes structural defects (diameter fluctuations) [91–93], bending losses, and defects at joints between fibers. Defects at joints arise from the mismatch of the mode field intensity distribution when coupling light into a fiber. Also, the guided modes can couple with the radiation modes in the transition region of the tapered fibers which leads to an extra losses. With careful design and fabrication, all of the radiative losses can be reduced [30, 34, 94].

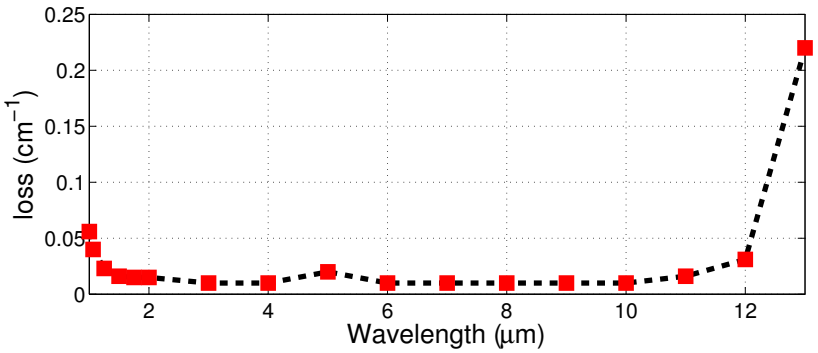

Figure 2.6: *The intrinsic loss spectrum of As_2Se_3 glass depicted as a function of wavelength. The transparency window spans from 1 to 12 μm [60].*

2.3 Nonlinear propagation

Under the influence of intense EM fields, the response of the polarization dipole to an optical excitation in a dielectric media becomes nonlinear. This case occurs when short optical pulses characterized with high peak power propagates in optical fibers. The total polarization induced by electric dipoles to an EM field is commonly represented by a Taylor series as:

$$P(r,t) = \epsilon_o \left(\left[P_L(r,t) \equiv \chi^{(1)} E(r,t) \right] + \left[P_{NL}(r,t) \equiv \chi^{(n)} E^n(r,t); n \geq 2 \right] \right) \tag{2.7}$$

where $\chi^{(n)}$ is the nth order susceptibility. This equation corresponds to the different possible responses a material can undergo when being exposed by different signal powers. Since the glass structure of As_2Se_3 inherently possesses an inversion symmetry, second-order and subsequent higher even-order electrical susceptibilities vanish, leaving the $\chi^{(3)}$ to be the first nonlinear induced polarization term that is responsible for nonlinear effects. Therefore, mentioning the nonlinear effects in As_2Se_3 fibers corresponds to some of the common nonlinear $\chi^{(3)}$ processes [11, 64]. This term gives rise to the Kerr effects and Raman Scattering.

When the intensity of the pulse is high enough to modulate the index of refraction of the material, a nonlinear Kerr effect takes place giving the refractive as:

$$n = n_o + \Delta n; \Delta n = n_2 |E|^2, \tag{2.8}$$

where $|E|^2$ is the optical intensity inside the fiber, and n_2 is the nonlinear refractive index which measures the nonlinearity of the fiber. The first term is the linear refractive index. n_2 can be measured and theoretically evaluated using several approaches [62]. Some of the theoretical methods used in calculating the linear refractive index and n_2 are presented later in the appendix.

A propagation equation which describes the influence of the linear and the $\chi^{(3)}$ nonlinear effects on the pulse envelope while propagating in a waveguide can be derived

from eq. (2.1). The equation assumes that the nonlinearity is small (the nonlinear induced polarization is treated as a small perturbation to the total induced polarization) and the spectral bandwidth of the pulse is less than 1/3 of the pulse carrier frequency [95]. This equation is known as the generalized nonlinear Schrodinger equation (GNLSE) [11] and is given in the retarded time frame $\tau = t - \beta_1 z$ as:

$$\begin{aligned}\frac{\partial A}{\partial z} &= i\sum_{n\geqslant 2}\frac{i^n\beta_n\left(z,\delta\right)\partial_\tau^n}{n!}A\left(z,\tau\right) - \frac{\alpha(\delta)}{2}A\left(z,\tau\right) \\ &+ i\gamma(\delta)\left(1+\frac{i}{\delta_o}\frac{\partial}{\partial t}\right)\left(A\left(z,\tau\right)\int_{-\infty}^{\infty}R\left(\tau^{'}\right)\left|A\left(z,\tau-\tau^{'}\right)\right|^2 d\tau^{'}\right).\end{aligned} \tag{2.9}$$

The first two terms on the right side describe the effects of dispersion and loss α, respectively. The term proportional to δ_o^{-1} is responsible for self-steepening, where δ is the frequency. $R(\tau)$ in the last term is the nonlinear response function. The convolution term of $R(\tau)$ with the field intensity $\left|A\left(z,\tau-\tau^{'}\right)\right|^2$ provides a full description of the effect of the shape of the Raman gain spectrum $g_R(\delta)$ in Raman response. The nonlinearities are quantified by the waveguide nonlinearity parameter:

$$\gamma = \frac{n_2\left(\delta\right)\delta}{cA_{eff}} + i\frac{\beta_{TPA}}{2A_{eff}}, \tag{2.10}$$

where n_2 is the material nonlinear parameter, c is the speed of light, β_{TPA} is the TPA coefficient, and A_{eff} is the effective mode area $A_{eff} = \left[\int\int|F(x,y)|^2dxdy\right]^2/\int\int|F(x,y)|^4dxdy$ [11]. The values of γ and A_{eff} at 2100 nm wavelength are depicted in fig. 2.7 as a function of microwire diameters. Also n_2 of As_2Se_3 is plotted as a function of wavelength (The values are obtained theoretically based on eq. (A.10)).

2.4 Two photon Absorption

Two photon absorption is the nonlinear process by which two photons, not necessarily of the same frequencies, are absorbed by the material. The two photons do not have

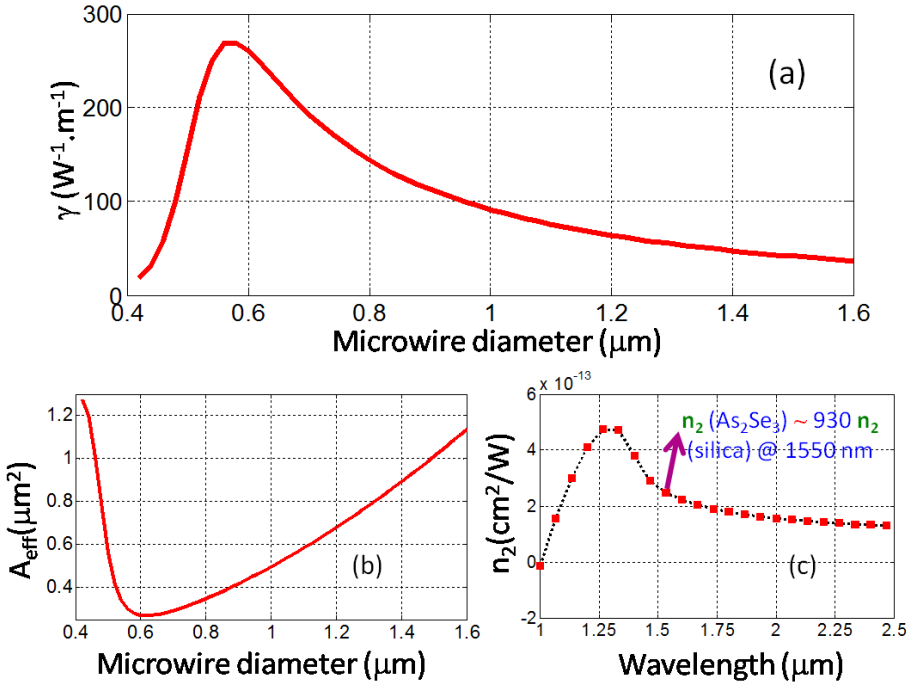

Figure 2.7: *Waveguide nonlinearity a), and effective mode area b) of As_2Se_3 at 2100 nm wavelength calculated numerically as a function of microwire diameters. c) The nonlinear refractive index as a function of wavelength calculated using eq.* (A.10).

enough energy to bridge the energy gap and complete the transition alone. Therefore, TPA is normally observed in the spectral region where the material is transparent. In this process, the first photon makes a transition to a virtual state between the upper and lower real states. If a second photon appears within the virtual lifetime of the state, a complete transition would occur. Otherwise, the first photon would fall back to the lower state and no absorption takes place. In order the TPA happen at a considerable rate, photons must be applied at a rate high enough that the probability of having two photons within the virtual lifetime is high. Because the virtual life time is so short, the photon flux must be high and therefore laser sources of high intensity are required.

In crystalline semiconductors, the TPA is calculated using models involving only two parabolic bands [96]. The TPA coefficient can be expressed as:

$$\beta_{TPA} = \frac{K\sqrt{E_p}}{n^2 E_g^3} F_2(\frac{2E_{ph}}{E_g}) cm/GW, \tag{2.11}$$

where K is chosen to best fit with experimental measurements, n is the linear refractive index curve, E_g is the energy gap, E_p=21 eV for As_2Se_3 (is material independent and related to the reciprocal lattice vector of the crystal), E_{ph} is the photon energy, and $F_2(2x) = (2x-1)^{3/2}/(2x)^5$ describes the dispersion of the TPA. Figure 2.8 shows the TPA of a semiconductor with a defined "sharp" band edges. The figure shows that no TPA exist for photons with energies less than half the E_g. However, this is not accurate for As_2Se_3 due to its amorphous structure.

The optical absorption of amorphous semiconductors is different from that of crystalline semiconductors due to the localized states present in the gap region of amorphous materials. Unlike crystalline semiconductors which are periodic [2], glasses lack translational symmetry. Therefore, the standard band structure calculations used for determin-

[2]Crystalline solids consist of atoms or molecules arranged in three dimensional arrays, where the structure has well defined symmetry and periodicity. Amorphous solids do not have the long range periodicity of their crystalline counterparts. The amorphous structure instead has disordered bond geometry.

ing electronic transport in crystalline materials cannot be applied to glasses. Any model must account for the random disorder which leads to localized states within the gap because the optical properties of the glass depend on the nature and density of those localized states.

For As_2Se_3, the band edges are not sharp, and TPA can still exist below the energy ratio of E_{ph}/E_g=0.5. The full spectrum of TPA is presented later in chapter 4.

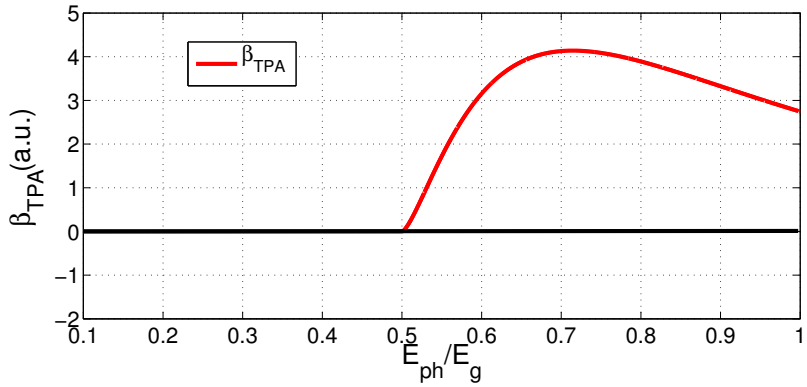

Figure 2.8: *TPA cruve of As_2Se_3 calculated from eq.* (2.11) *as a function of the ratio E_{ph}/E_g. E_{ph}:Photon energy, E_g: Band-gap energy.*

2.4.1 Numerical solutions

In general, the GNLSE has no analytic solutions except for some simplified cases. A numerical approach is therefore required to pulse-propagation problems in optical fibers. The GNLSE in this thesis is solved by the Runge-Kutta in the interaction picture (RK4IP) solver [97]. The implementation is detailed in the appendix. For SC generation, it is important to include a noise background in the simulations. This can be added by using the white Gaussian noise in Matlab. When comparing the numerical results to experiments, it is often convenient to show the power spectral density curves.

2.4.2 Stimulated Raman scattering

Raman scattering is a non-instantaneous $\chi^{(3)}$ process. When a photon travels in an optical fiber, the photon scatters by a molecule of the fiber and transfers a small fraction of energy to the molecule. As a result, this photon becomes a low frequency photon due to the energy loss. This process is called Raman scattering effect. The new low frequency component is called the Stokes wave [11]. The Raman scattering depends on the vibrational resonance frequency of the material molecules. In As_2Se_3, the resonance frequencies are overlapped with each other and form a relatively wide frequency range. The molecular vibrations of As_2Se_3 induced by an optical field can be described by a simple damped oscillator model [11, 95]

$$R(\tau) = (1 - f_R)\,\theta(\tau) + f_R h_R(\tau)\,\Theta(t) \tag{2.12}$$

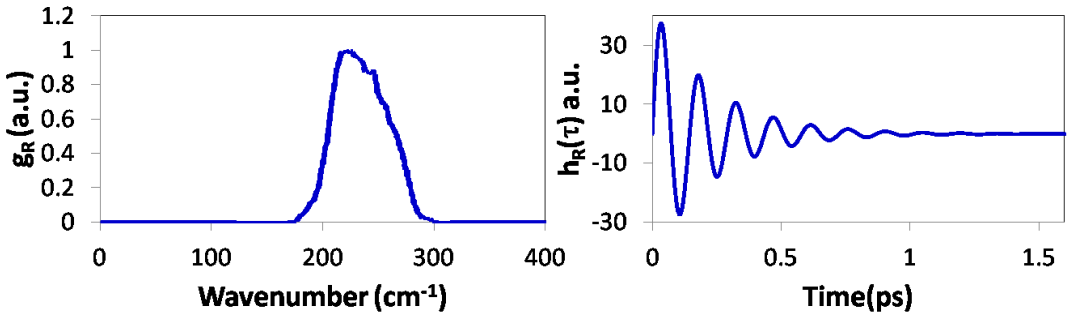

Figure 2.9: *a)The measured Raman gain spectrum [98], and b) the Raman nonlinear response calculated from eq.* (2.13) *depicted as a function of the wavenumber and response time, respectively.*

The molecular vibrations of As_2Se_3 induced by an optical field can to a fair approximation be described by a simple damped oscillator mode:

$$h_R(\tau) = \frac{\tau_1^2 + \tau_2^2}{\tau_2 \tau_2^2} exp\left(-\frac{\tau}{\tau_2}\right) sin\left(\frac{\tau}{\tau_1}\right). \tag{2.13}$$

with τ_1 =23 fs is the inverse phonon frequency and τ_2 =195 fs is the phonon life time or the inverse of the bandwidth of the Raman gain spectrum. Θ(t) is the unit step function. The nonlinear response function $R(\tau)$ comprises two responses: (1) the electronic response, which is assumed instantaneous and hence described by the delta function $\theta(t)$, and (2) the delayed Raman response $h_R(\tau)$ originating from photon-phonon interactions [95]. f_R represents the fractional contribution of the delayed Raman response and for As_2Se_3 is equal to 0.1 [45]. The Raman gain (i.e. gain obtained by a weak Stokes signal) is given by the imaginary part of $h_R(\tau)$ in the frequency domain. The measured Raman gain spectrum is shown in fig. 2.9. The Raman gain show a clear maximum at 230 cm^{-1} (6.9 THz). Equation (2.12) has been used extensively for modeling pulse propagation with good results [19] and was used in this thesis.

2.5 Solitons and solitonic effects

Solitons

In optical fibers with anomalous dispersion, the chirp from self-phase modulation (SPM) can be exactly compensated by dispersion. This leads to the formation of a nonlinear wave known as soliton. Solitons were first discovered in the early 1800s in the form of water waves [99]. The propagation of solitons in optical fibers was first considered in 1973 by Hasegawa and Tappert [100] and experimentally observed in 1980 by Mollenauer et al. [101]. Mathematically, solitons are exact solutions to the NLSE [101] following a sech profile. Since the dispersion is a linear effect and the SPM is a nonlinear effect, there is a peak power level (P_o) and a magnitude of β_2 for which the two effects cancel each other. The relation that represents the condition for soliton formation in optical fibers is given as:

$$N^2 = \frac{\gamma P_o T_o^2}{|\beta_2|} \tag{2.14}$$

where T_o is the pulse duration of a hyperbolic-secant pulse, and N is the soliton number. Fundamental solitons have N = 1 and propagate without any change in temporal or spectral shape. If the number N is larger than 1, pulses will be a higher order solitons which periodically return to their initial shape. The fundamental soliton shape is very stable and any pulse whose soliton number is between 0.5 and 1.5 will eventually evolve into a fundamental soliton [11]. In this case, pulses automatically adjust their shape to that of a fundamental soliton, possibly by dispersing excess energy. Solitons are similarly known to be stable under small perturbations, such as changes in its energy due to losses and gain [100, 102–104], as well as gradual changes in the fiber parameters (dispersion and nonlinearity) [105, 106]. The changes just need to be sufficiently slow for the soliton to adiabatically adjust its shape. In contrast, higher-order solitons (N$\geq$2) are not stable under perturbations, rather they undergo soliton fission that breaks the higher-order soliton into its fundamental soliton constituents [11, 107, 108].

Soliton self-frequency shift

For a soliton in the sub-picosecond range, its spectrum can be sufficiently broad for the short wavelength components of the soliton to act as a Raman amplifier for the long wavelength components [109]. This intra-pulse Raman scattering transfers energy from the blue to the red edge of the soliton. This phenomenon, called the soliton self-frequency shift, shifts the soliton to longer wavelengths [12, 13]. The magnitude of the SSFS depends strongly on the soliton duration, the GVD, and the Raman fraction to the nonlinear fraction.

The SSFS can be used to access spectral regions that are hard to reach with existing commercial lasers (see e.g. fig. 1.1). In chapter 3, I propose a mid-IR source based on the

SSFS using As_2Se_3 microwires. I present two methods developed to maximize the SSFS in optical fiber and attain the maximum possible energy at the output end of the fiber.

Dispersive wave generation and soliton spectral recoil

In the presence of higher-order dispersion, the soliton can transfer its energy into the normal dispersion regime to so called DW or non-solitonic radiation [110]. The transfer of energy from the soliton to the DW emissions requires a phase matching condition. This can occur when soliton propagates close to the ZDW of the fiber and its tail extends to the normal dispersion regime, so that the central frequency component of the soliton amplify its spectral tail [67, 111]. In the vicinity of the ZDW and due to the transfer of energy to the normal dispersion regime, a soliton shifting towards longer wavelengths slows down and the SSFS process cancels. This mechanism is known as a spectral recoil [112]. These mechanisms are depicted in fig. 2.10. The tapering of the fiber, which allows a precise control of the ZDW position, can thus provide a good tool to avoid the DW emissions and soliton recoil. Based on this phenomenon, I follow this approach in this thesis to extend the SSFS in microwires.

2.6 Supercontinuum generation

SC generation is an optical phenomenon which is based on a combination of multiple nonlinear effects (e.g. SPM, four-wave mixing, modulation instability, SSFS, cross-phase modulation, etc.) [11, 18, 113]. When a narrow-band beam with high power propagates through a nonlinear medium, various nonlinear effects are generated in the medium. All of these nonlinear effects are capable of generating new frequency components, resulting in broadening the narrow spectrum of original beam into a wide continuum spectrum, called SC.

In a SC source, the pump laser is an important component since different pump lasers

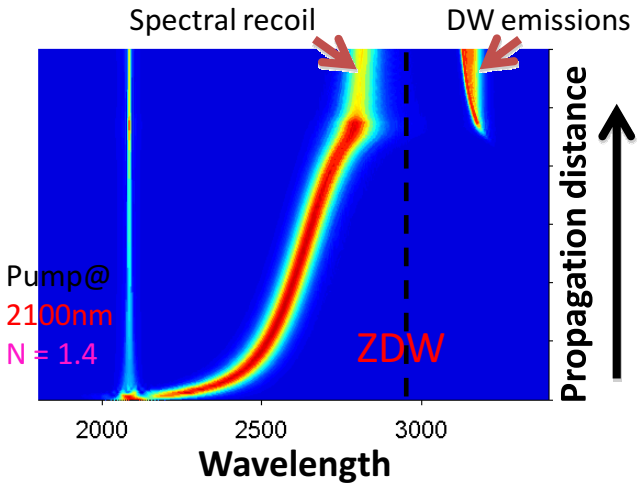

Figure 2.10: *Energy density plot shows a numerical calculation of the frequency shifting of a soliton towards longer wavelength. The soliton shifting stops close to the ZDW and transfers energy to the normal dispersion regime.*

(different pump wavelengths and pulse durations) generate SC spectra in different ways and thus have different results [19]. Besides the pump laser, the nonlinear fiber is another key component in SC generation since its nonlinearity to EM fields and its dispersion profile determine the extent of the SC broadening.

The dispersion profile plays a critical role in SC generation. The importance of dispersion, rather than nonlinearity, in influencing the dynamics of SC generation could be described by the experiment done in [19] while keeping the peak power and pulse duration at constant value. Three different regimes could be identified according to pumping wavelength.

Normal GVD pump wavelength: If the pump wavelength is far from the ZDW, the initial dynamics of SC are dominated by the interaction of SPM and normal GVD which gives approximately symmetric temporal and spectral properties. Because this leads to significant temporal broadening and rapid decrease of peak power in the beginning of propagation, the extent of nonlinear spectral broadening is necessarily limited.

Zero dispersion pump wavelength: When the pump pulses are launched close to the ZDW of the nonlinear media, the propagation of ultrashort pulses in optical fibers near the ZDW allows for relatively long interaction lengths with high peak intensities, which can result in dramatic nonlinear effects.

Anomalous GVD pump wavelength: For pump wavelengths exceeding ZDW, the soliton dynamics play an important role. Specifically, the spectral and temporal SC characteristics exhibit signatures of soliton fission. In this regime, the higher-order solitons undergo an initial period of spectral broadening and temporal compression, followed by soliton fission. The characteristic length scale over which the soliton fission occurs is given by $L_{fiss} = L_D/N$, where $L_D = T_0^2/\beta_2$ is the dispersion length. Soliton fission manifests itself as the higher order soliton pulse breaks up into N distinct fundamental soliton components as shown in fig. 2.11. The process occurs due to higher-order dispersion and stimulated Raman scattering. The initial propagation of these fundamental solitons is associated with the generation of DW spectral components through resonant transfer of energy across the ZDW. As the solitons continue propagating, the result is a continuous shift to longer wavelengths through the Raman self-frequency shift. Finally, the generated Raman soliton broaden temporally and stops shifting and the spectral components of the SC spectrum couple through cross phase modulation to generate additional frequency components and make the structure of the SC spectrum more complex.

The first observation of SC generation was reported in 1970s by Alfano and Shapiro in bulk material [23]. After this discovery, numerous theoretical and experimental investigations of the SC generation was made in different pumping regimes while using PCF, single mode fibers, tapered fibers, etc [18]. While few nano-joule pulse energies are required for high nonlinear interactions in optical fibers, these pulse energies could be high enough to cause damage to the fiber endface with extended exposure and to several applications.

The development of tapered fibers has allowed for nonlinear processes to occur with

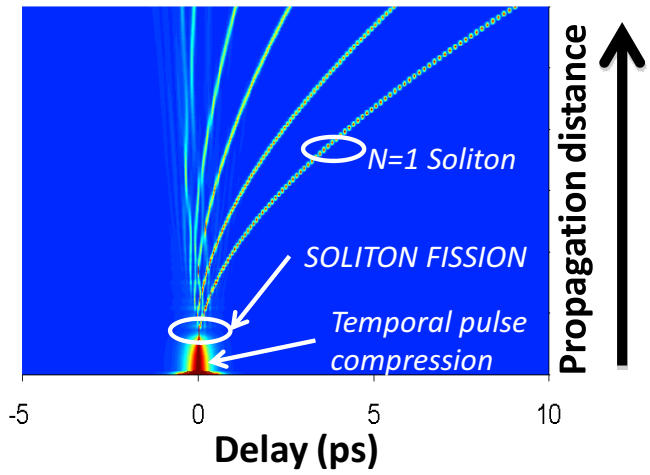

Figure 2.11: *The soliton fission of a higher-order soliton calculated numerically when propagating along a microwire in the anomalous dispersion regime of a fiber.*

relatively low pulse energies. The strong confinement results both in a large effective nonlinearity and in appropriate dispersion characteristics that allow for dramatic spectral broadening of laser pulses.

Chapter 3

Mid-infared Soliton Self-frequency Shift in As_2Se_3 microwires

In this chapter, I present the work of SSFS in two types of As_2Se_3 microwires; uniform and non-uniform microwires. The SSFS in uniform microwires is studied numerically by solving the GNLSE. For non-uniform microwires, I propose two methods to design these microwires with a goal set to maximize the SSFS process in microwires. Compared to the available methods in the literature [114], the first method improves the efficiency of SSFS, i.e. $SSFS_r$. I refer to this method as constant spectral bandwidth method (CSB-M). This work was published in [68] (journal publication I). The second method improves the efficiency further SSFS and maximizes the SSFS process and was published in [69] (journal publication II). I refer to this method as perturbative method (P-M). The CSB-M is tested in an As_2Se_3 microwire coated with a polymer by using a pump source at 2100 nm, while the P-M is tested in As_2Se_3-air microwire with a pump centered at 2000 nm wavelength. Later in the chapter, a comparison between the two methods is made.

3.1 Introduction

Since the first discovery of SSFS in 1986 by Mitschke et al. in a polarization maintaining single mode fiber [107], the SSFS was then investigated in different fiber profiles with a goal of maximizing the wavelength shift per unit length [115–120]. This includes, for example, highly nonlinear fibers [115], tapered [116] and untapered [117, 118] microstructured optical fibers, bandgap hollow fibers [119, 121–125], and tapered single mode fibers [120] (A review can be found in [17]). SSFS can be generated in fibers but requires high energy density (pulse energy of few nano joules) to induce a substantial frequency conversion. Unfortunately, this pulse energy is too high for any in vivo application in human tissue (requires only a sub-nanojoule pulse energy for diagnostic purposes). The use of microstructured [126] and tapered optical fibers has enhanced the waveguide nonlinearity (γ) and thus reduced the amount of energy E_o required to generate input solitons through $E_o \propto 1/\gamma$ [100]. In addition, the microstructured and tapered optical fiber profiles have allowed the tailoring of GVD over a wide spectral range [127]. This has opened the prospect of realizing SSFS at low input powers [117], in short fiber lengths [116, 120], and at different pump wavelengths [118, 128–130]. Furthermore, the recent advancement of PCF fabrication [131] and the tapering technique [132] is promising in maximizing the $SSFS_r$. All the mentioned features allow for the building of a compact, tunable, mid-IR source that can operate for long duration without being damaged or damaging biological samples.

In spite of tuning the soliton wavelength over hundreds of nanometers [129], the transmission window of silica glass between 300 nm and 2200 nm limits the wavelength conversion towards the mid-IR. Non-silica glass can serve for the purpose of SSFS in the mid-IR due to their wide transparency window and their nonlinear characteristics as was discussed in Chapter 2. Several theoretical studies have been performed on the SSFS in non-silica glass fibers, such as fibers based on ZBLAN [133] and tellurite [133], sulfide

[134]. However, As_2Se_3 offers one of the strongest glass nonlinearities among non-silica glass [98] and can thus be considered optimal for a wide SSFS.

A soliton launched in a uniform microwire with a pump wavelength lying between ZDW_1 and ZDW_2 may experience SSFS but remains limited in its overall wavelength-shift by the spectral position of ZDW_2. Near the ZDWs, the soliton is strongly perturbed by the TOD which broadens its pulse width and leads to the generation of resonant DW emissions in the normal dispersion region [67]. The soliton perturbation manifests as an extreme deceleration in the $SSFS_r$ [135].

In this chapter, I present methods to optimize the diameter profiles of both uniform and non-uniform microwires with the purpose of maximizing the SSFS in optical fibers. The methods are tested in microwires made of As_2Se_3, which are the optimal host materials for a maximum SSFS. For the uniform microwire, the optimal diameter profile is the one in which an incident soliton acquires a large waveguide nonlinearity and undergoes wide spectral shifting. The designed uniform microwire presented here could potentially shift the central wavelength of a soliton over 600 nm after propagation through a 20 cm length.

Tapered PCFs with axially non-uniform diameter have been proposed by Jude et. al. [114] to extend the long-wavelength limit of uniform PCFs [116], increase further their waveguide nonlinearity, and reduce power requirements for SSFS. This is achieved by shifting the ZDW_2 to longer wavelengths, which is enabled by increasing the tapered PCF diameter. As the soliton enters this designed PCF, the diameter increases gradually along the soliton path such that the soliton experiences the highest possible waveguide nonlinearity and an appropriate level of GVD to avoid DW emissions. The diameter profile was determined by imposing a minimum value on the GVD that a soliton can experience during its self-frequency shifting. However, I have found that this method does not provide the maximum possible SSFS in microwires. A *fundamental* soliton (eq. (2.14)) experiencing the highest possible waveguide nonlinearity does not necessarily lead to

the maximum SSFS. Besides, an increase in the input soliton energy ($1<N\leq1.4$), with the purpose of extending the wavelength shift along the microwire profile, leads to an exponential growth of DW emissions [67] along the propagation path and thus a significant reduction in the soliton energy. Losses experienced by the soliton slow down the $SSFS_r$ and prevent the soliton from large wavelength shifts. I follow an alternative approach where I divide the non-uniform microwire into two segments and optimize the $SSFS_r$ in each segment. I show that the optimization of the selection of the first segment and the design of the second segment enables an improvement in SSFS and energy conservation of the soliton in non-uniform microwires.

3.2 SSFS in uniform microwire

For the study of the SSFS in uniform, and non-uniform microwires designed by the CSB-M, As_2Se_3 microwire is assumed to be coated with a protective polymer which improves its mechanical strength and insulate it from the surrounding environment.

The protective polymer considered in the model has a refractive index similar to Polymethyl methacrylate (PMMA) polymer and is considered transparent in the mid-IR. In practice, PMMA has an attenuation of ∼4.3 dB/cm at 2100 nm [136] and thus partially absorbs the propagating mode from the evanescent wave. However, this loss is a specific characteristic of PMMA and instead, I keep the model more general by simulating results of an ideal case with a negligibly lossy polymer. Polymers with optical and mechanical properties compatible with the hybrid microwire fabrication are available but with better transparency in the mid-IR than PMMA [137]. The linear refractive indices of As_2Se_3 and the polymer ($n_{As_2Se_3}$=2.79, $n_{polymer}$=1.46) are calculated at a wavelength 2100 nm by using the Cauchy relation $n^2(\lambda) = A + {}^{B}/_{\lambda^2} + {}^{C}/_{\lambda^4}$, where A, B, and C are the Cauchy coefficients given for As_2Se_3 [50] and the polymer as: A = 7.56, B = 1.03 μm^2, and C =

0.12 μm^4, and A = 2.149, B = 0.028 μm^2, and C = -0.002 μm^4, respectively[1]. The large index contrast between As_2Se_3 and polymer allows more than 96% of mode power to propagate in As_2Se_3 while only 4% propagate in the polymer (see fig. A.2). Since the attenuation of As_2Se_3 is typically between 0.0015-0.0020 dB/cm in the mid-infrared [138] and only a small ratio of the evanescent field is propagating in the polymer, all losses are neglected along the considered microwire length.

3.2.1 Design of uniform microwire

To investigate the potential of the As_2Se_3-polymer microwires in generating SSFS, the soliton shifting is studied in a uniform microwire with 20 cm length and a diameter of 0.97 μm using pump pulses centered at a wavelength of 2100 nm. The diameter profile remains constant at 0.97 μm along the possible spectral shift range. The schematic diagram of the uniform microwire and its dispersion profile are shown in fig. 3.1. The uniform microwire is located between two ideally [139] adiabatic transition regions. The dispersion profile contains two ZDW points: ZDW_1 and ZDW_2 at 1760 nm and 2940 nm, respectively. The microwire parameters chosen are based on two criteria imposed here on the diameter of uniform microwire in order to achieve a wide soliton shifting. First, the soliton must acquire large waveguide nonlinearity at the pump wavelength as it enters the microwire. Second, the two zero dispersion wavelengths, ZDW_1 and ZDW_2 must be widely spaced such that the soliton occurs in the anomalous dispersion regime and undergoes a wide spectral shifting along the microwire length before reaching the ZDW_2.

[1]Note: For the fiber used in the photonics group at McGill University, I found later that the linear refractive index provided in eq. (2.3) describes more accurately the linear properties of As_2Se_3.

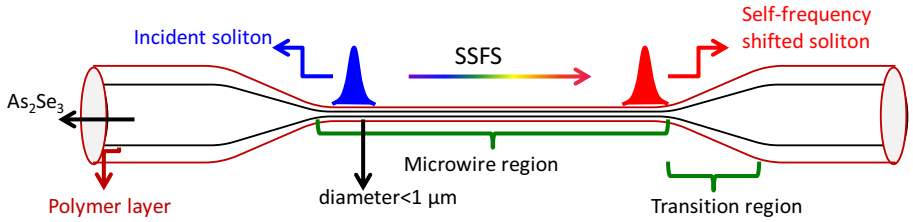

(a)

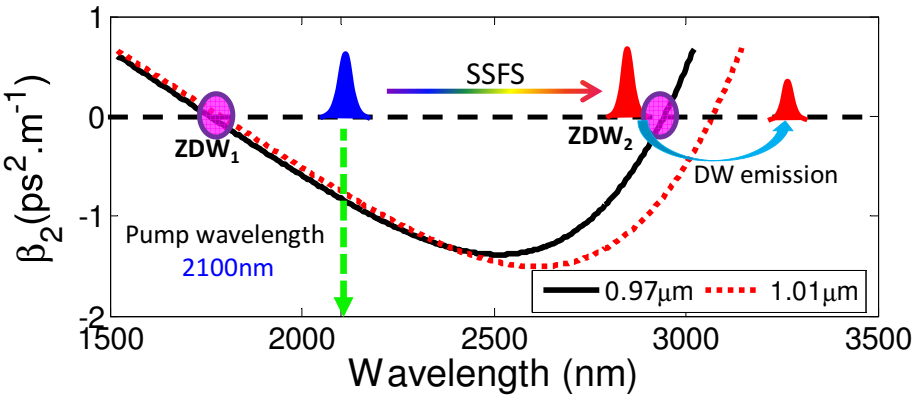

(b)

Figure 3.1: *a) The schematic diagram of a uniform microwire with 0.97 µm diameter. b) The dispersion profile of uniform microwire with diameters of 0.97 µm (black-curve) and 1.01 µm (red-dotted-curve).*

3.2.2 Numerical simulation

I perform complete simulations for SSFS in As_2Se_3-polymer microwires by using the GNLSE eq. (2.9) and solve it with an input sech pulse centered at a wavelength of 2100 nm, $A(z=0,\tau) = \sqrt{P_o}\,sech\,(\tau/\tau_o)$, with τ_o =29 fs and a varying input peak power P_o. The peak power values correspond to solitons with orders of N varying between N=1 and 1.4. For N>1.4, the conversion efficiency from the pump sech pulse into the soliton pulse declines gradually. A strong portion of the pump pulse is shed as non-solitonic (dispersive) emissions leading the fundamental soliton to generate at a broad pulse duration (eq. (3.3)). The generation of the fundamental soliton at a broad pulse duration leads to a slow $SSFS_r$ [13] which manifests as a reduced output soliton wavelength-shift.

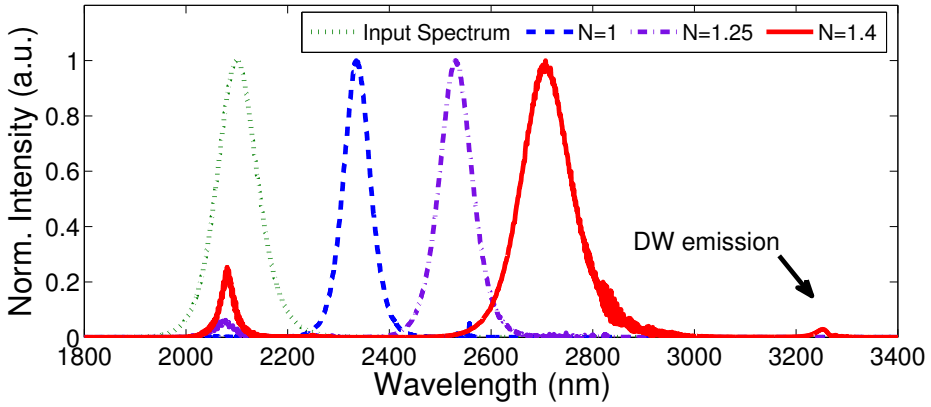

Figure 3.2: *SSFS after propagation through a uniform microwire for soliton orders N=1, N=1.25, and N=1.4. The results are calculated numerically. The length of the As_2Se_3-polymer microwire used is 20 cm with 0.97 µm diameter.*

In fig. 3.2, I depict the wavelength shifting of solitons with input peak powers of 22 W, 34 W and 43 W, which correspond to soliton order N of 1, 1.25 and 1.4, respectively. From the figure, the fundamental soliton (i.e. N=1) undergoes a wavelength shift of 320 nm. The small relative wavelength-shift is due to the large magnitudes of GVD values the soliton experiences along the spectral shifting length. However, at higher powers the

amount of wavelength shift increases. For instance, a soliton with N=1.4 red-shifts to a maximum output wavelength of 2715 nm (615 nm of SSFS). At this wavelength, the soliton overlaps the ZDW_2 and sheds energy in the normal dispersion regime.

To avoid DW emissions and extend the limit of output soliton wavelength, larger anomalous dispersion window is required. For this purpose, two approaches can be followed in controlling the anomalous dispersion window:

1. The use of uniform microwires with diameters larger than 0.97 μm. For this approach, the ZDW_2 is located at longer wavelengths and thus provides a larger anomalous dispersion window as shown in fig. 3.1(b). Nonetheless, the soliton in this case experiences smaller waveguide nonlinearity and larger magnitudes of GVD which manifests as a shorter output wavelength-shift.

2. Gradual increase of the diameter size along the propagation length leading to a non-uniform microwire. These microwires maintain a high waveguide nonlinearity along the soliton propagation path and avoid DW emissions. These microwires are desired and are suitable to maximize the $SSFS_r$.

3.3 SSFS in non-uniform microwire

3.3.1 Schematic structure of non-uniform microwire

Figure 3.3(a) shows the schematic of a tapered fiber. The non-uniform microwire consists of a uniform segment and a taper segment. In the uniform segment, the diameter remains fixed at constant diameter value, which allows the input soliton to spectrally shift until it reaches wavelengths near the ZDW_2. The increase of the diameter along the taper segment serves to shift the ZDW_2 to longer wavelengths at the rate of the SSFS. This allows a soliton to shift over wide spectral range in the anomalous dispersion region without DW emissions. In the rest of this chapter, I explain the methods to optimize SSFS

in each segment which leads to the maximum possible wavelength shift in non-uniform microwires.

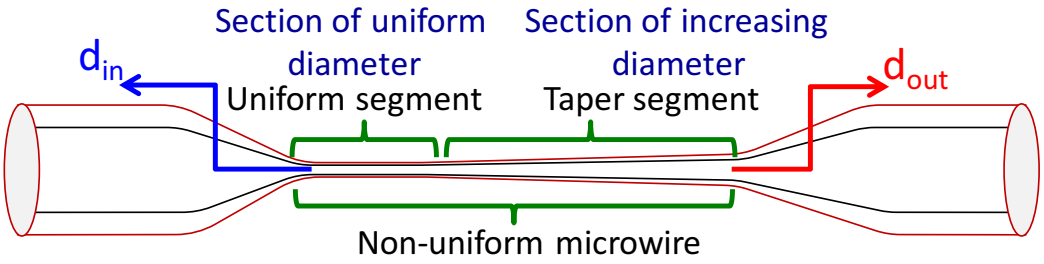

Figure 3.3: *A schematic of the non-uniform As_2Se_3-polymer microwire. The microwire consists of a uniform and a taper segments.*

3.4 Design method of non-uniform microwire based on adiabatic approximation theory (CSB-M)

Judge et. al. have developed a method to design non-uniform tapered PCFs for a specific input soliton energy [114]. As a soliton enters this PCF, the diameter increases gradually along the fiber length such that the soliton experiences the highest possible waveguide nonlinearity and an appropriate level of GVD to avoid DW emissions. The uniform segment is chosen such that the soliton experiences the highest possible waveguide nonilnearity without impinging the ZDWs, and thus avoid DW emissions. This is a weak point in the proposed design, since this does not (as I will show later) lead to the highest SSFS for a *fundamental* soliton. When selecting the optimal diameter for the highest $SSFS_r$, other parameters including the soliton energy, and GVD profile must be considered. The problem also arises when there is a trial to enhance the SSFS by increasing the input soliton energy. Because the rate of the diameter profile follows the $SSFS_r$, any change in the input energy leads soliton to overlap the ZDW_2 along the spectral shift length and

thus transfers its energy to DW emissions. The growth of DW emissions slows down the SSFS and reduces the output energy radiating at the soliton frequencies.

In what follows, I am going first to carry out calculations under the adiabatic approximation theory, which will provide an analytical expression of the $SSFS_r$. The expression is used to determine the $SSFS_r$ in uniform segments with different diameters. To provide a full description of the SSFS in non-uniform microwires, I am then going to numerically solve the GNLSE and obtain the output wavelengths of the frequency-shifted soliton.

3.4.1 Theoretical basis of the design method

Design of the uniform segment

The starting point in optimizing the design of non-uniform microwires consists in selecting the diameter of uniform segment leading to the highest $SSFS_r$. To achieve this, I investigate first the self-frequency shift of *fundamental* soliton using the adiabatic theory.

The adiabatic approximation is based on the assumption that while a fundamental soliton undergoes a frequency-shift, its evolution is weakly perturbed by the higher-order dispersion and nonlinear effects. Because of the stability of fundamental solitons far from ZDWs, the higher-order dispersion effects ($\beta_{n\geq 3}$=0) and the nonlinear dispersive effects (self-steepening and stimulated Raman scattering) can be treated as perturbations and thus neglected from eq. (2.9). In this case, the soliton propagation is adiabatic (i.e. no radiation scattering) and the $SSFS_r$ can be estimated by analytically solving eq. (2.9) with $n = 2$ and neglecting the derivative term.

Gordon [13] was the first to give a theoretical description of the SSFS based on the adiabatic approximation. He predicted the $SSFS_r$ to be inversely proportional to the fourth power of the soliton temporal width. This is under the assumption the soliton spectrum is still narrow compared to the Raman spectrum width (fig. 2.9(a)). For duration less than the period of molecular oscillation, Hermann et. al. [140] showed a change in the behavior

of soliton-shift in which it becomes inversely proportional to soliton duration. Recently, a rearrangement of the Gordon equation was provided by Judge et. al. [114] to include the actual Raman gain spectrum in the analytic expression. The theory is used as it is less time consuming than solving the GNLSE and provides an approximate estimation of the frequency-shift a soliton undergoes per unit length.

Since the priority in this section is to optimize the diameter profile of the uniform segment, I use the adiabatic theory to provide only a qualitative estimation of the $SSFS_r$. The $SSFS_r$ can be written as [141]:

$$\frac{d\bar{\delta}}{dz} = -\frac{\left|\beta_2\left(\bar{\delta}\right)\right|}{\tau_s^3\left(\bar{\delta}\right)}\frac{f_R}{1-f_R}R\left(\tau_s\left(\bar{\delta}\right)\right) \tag{3.1}$$

where $R[\tau_s\left(\bar{\delta}\right)]$, shown in fig. 3.4, is the dimensionless spectral response function containing the effect of the shape of the Raman gain spectrum $g_R(\delta)$, given as

$$R\left(\tau_s\left(\bar{\delta}\right)\right) = \frac{\pi^2\tau_s^4\left(\bar{\delta}\right)}{6}\int_0^\infty \frac{d\delta}{2\pi}\frac{g_R(\delta)\delta^3}{sinh^2(\pi\tau_s\delta/2)}. \tag{3.2}$$

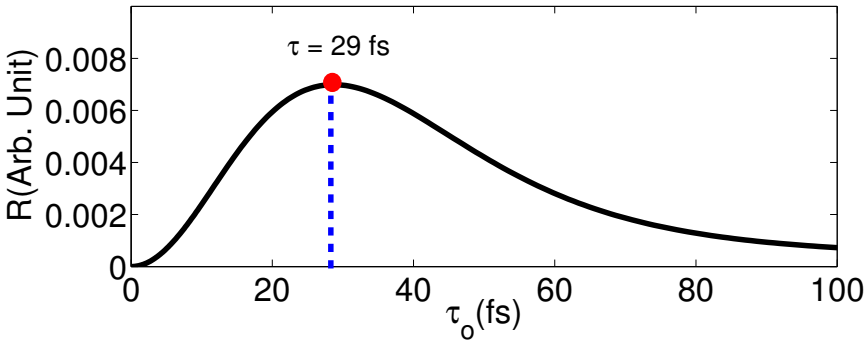

Figure 3.4: *The spectral response function of As_2Se_3 microwire calculated for a 0.88 μm diameter. The function is calculated from eq.* (3.2) *peaks at pulse width of 29 fs.*

For the ultrashort pulse duration (the rate of SSFS is not changing as the fourth power of soliton duration) considered in this study, the investigation shows that the spectral response function $R[\tau_s\left(\bar{\delta}\right)]$ plays a minor role in determining the $SSFS_r$. From eq. (3.4) I

found that the ratio of $\frac{\gamma^3}{8|\beta_2|^2}$ has a greater influence on the rate of the SSFS than the pulse duration. In other words, the choice of the fiber "microwire diameter" and the spectral position of the soliton has a greater influence on the rate of the SSFS compared to the input soliton duration.

For As_2Se_3-polymer microwires, the dependence of this function on the evolution of the pulse duration along a uniform section peaks at τ_m= 29 fs. In eq. (3.2), the Raman gain spectrum is calculated from $g_R(\delta) = 16\pi n_2 f_R Im[h_R(\tau)]/3\lambda_o$ [65] where $Im[h_R(\tau)]$ is the imaginary part of the Fourier transform of $h_R(\tau)$. The nonlinear refractive index (n_2) of As_2Se_3 is taken equal to $n_2 = 1.1 \times 10^{-17} m/W$ at the 2100 nm pump wavelength [50].

For a fundamental soliton, with N=1, the evolution of the pulse width $\tau_s(\bar{\delta})$ as a function of the soliton center frequency $(\bar{\delta})$ is written based on eq. (2.14) as [11]:

$$\tau_s(\bar{\delta}) = 2\frac{|\beta_2(\bar{\delta})|}{\gamma(\bar{\delta})\, E(\bar{\delta})}. \tag{3.3}$$

By substituting eq. (3.3) in eq. (3.1), the $SSFS_r$ is:

$$\frac{d\bar{\delta}}{dz} = -\frac{\gamma^3(\bar{\delta})\, E^3(\bar{\delta})}{8\,|\beta_2(\bar{\delta})|^2}\frac{f_R}{1-f_R} R\left(\tau_s(\bar{\delta})\right). \tag{3.4}$$

The equation shows that the $SSFS_r$ depends on the soliton energy along the microwire. This illustrates the importance of DW emissions suppression along the taper segment in enhancing the overall $SSFS_r$. However, at the pump wavelength, eq. (3.4) is rewritten as:

$$\frac{d\bar{\delta}}{dz} = -\frac{\gamma^3(\delta_o)\, E^3(\delta_o)}{8\,|\beta_2(\delta_o)|^2}\frac{f_R}{1-f_R} R\left(\tau_s(\delta_o)\right), \tag{3.5}$$

where $\gamma(\delta_o)$, and $\beta_2(\delta_o)$ are the waveguide nonlinearity and the GVD parameters at the pump wavelength, respectively. For a specific input soliton width $\tau_s(\delta_o)$, the $R(\tau_s(\delta_o))$ parameter is constant. Therefore, the $SSFS_r$ increases as the $\kappa = \gamma^3(\delta_o)E^3(\delta_o)/8|\beta_2(\delta_o)|^2$ ratio increases. By calculating the ratio values (κ) for *fundamental* solitons incident at uniform

segments with different diameter scaling (d), I select the diameter of the uniform segment that leads to the highest $SSFS_r$.

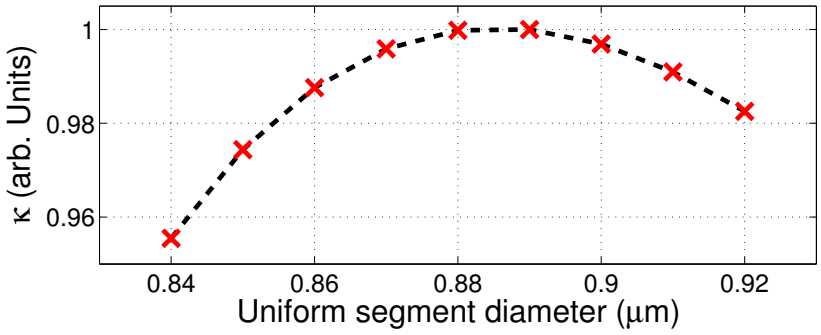

(a)

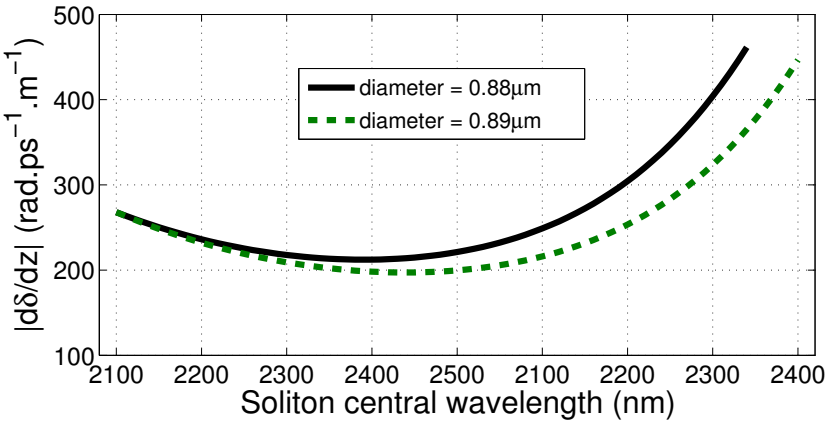

(b)

Figure 3.5: *a) The coefficient (κ) calculated as a function of uniform segment diameters of As_2Se_3-polymer microwire. The value is normalized to the maximum among coefficient values. b) The $SSFS_r$ given in eq.* (3.4) *for two uniform segment diameters: 0.88 and 0.89 μm.*

Figure 3.5(a) depicts the normalized ratio (κ) values for fundamental solitons incident at uniform segments with diameter values ranging from 0.82 to 0.9 μm. The fundamental solitons correspond to same input pulse width τ_s (δ_o), same pump frequency δ_o but different input energies to maintain N=1. It shows that the highest rate of fundamental soliton

shift is achieved in uniform segments with diameters of 0.88 and 0.89 μm. However, solving numerically eq. (3.4), as depicted in fig. 3.5(b), shows that the diameter of 0.88 μm provides higher rate of shift along the segment length. Therefore, based on the adiabatic theory, the non-uniform profile optimal for an input fundamental soliton consists of a uniform segment of 0.88 μm diameter. The length of the uniform segment required for the soliton to shift from the pump wavelength to wavelengths near ZDW_2 is determined numerically using the GNLSE.

Design of the taper segment

The taper segment has to be designed such that the soliton does not transfer energy into normal dispersion region as it shifts in the vicinity of ZDW_2. Therefore, the rate of increase of the diameter along the propagation length must follow the $SSFS_r$.

Dictated by the phase matching condition, the transfer of energy from the soliton to the DW emissions occurs at a specific frequency. The phase matching condition arises from the equality of the soliton and DW emissions propagation constant expressed in Taylor expansion. However, in the vicinity of the ZDW, the soliton propagation is mainly influenced by the TOD, and thus the Taylor expansion can be truncated at the third-order term (n=3 of eq. (2.9)). In this situation, the spectral separation ($\Delta\Omega$) between the soliton and the DW emissions is approximated as [67]:

$$\Delta\Omega = \bar{\delta} - \delta_{DW} = 3\frac{\beta_2\left(\bar{\delta}\right)}{\beta_3\left(\bar{\delta}\right)} = \Delta\bar{\delta} + \delta_{ZDW_2} - \delta_{DW} \tag{3.6}$$

where $\bar{\delta}$ is the soliton instantaneous central frequency, δ_{DW} is the DW resonance frequency, δ_{ZDW_2} is frequency corresponding to the ZDW_2, and $\beta_2\left(\bar{\delta}\right)$ and $\beta_3\left(\bar{\delta}\right)$ are the GVD and TOD parameters at $\bar{\delta}$, respectively.

The approach proposed by Judge et. al. [114] and that proposed here to avoid DW emissions can be explained using eq. (3.6) as:

1. GVD-threshold approach:

$$|\Delta\Omega|_{min} = 3\frac{\left(\left|\beta_2\left(\bar{\delta}\right)\right|_{min} \equiv \text{GVD}\right)}{\left|\beta_3\left(\bar{\delta}\right)\right|} \tag{3.7}$$

For the approach proposed by Judge et. al. [114], setting a threshold on the GVD values near ZDW_2 $\left(\left|\beta_2\left(\bar{\delta}\right)\right|_{min}\right)$ keeps the soliton at a spectral separation equal to $|\Delta\Omega|_{min}$. The GVD threshold is determined numerically by propagating a soliton in the uniform segment and corresponds to the GVD of DW emissions (Eqs. (20-21) in [114]). In this case, the soliton acquires a single value of $\left|\beta_2\left(\bar{\delta}\right)\right|_{min}$ along the spectral shift in the taper segment as shown in fig. 3.4(a) (blue-curve).

2. CSB-threshold approach:

$$|\Delta\Omega|_{min} = \left(\left|\Delta\bar{\delta}\right|_{min} \equiv \text{CSB}\right) + \left|\delta_{ZDW_2} - \delta_{DW}\right| \tag{3.8}$$

In the presented approach, I employ a threshold on the spectral separation of the center wavelength of the red-shifted soliton from the ZDW_2 ($\text{CSB} = \left|\Delta\bar{\delta}\right|_{min} = \overline{\delta} - \delta_{ZDW_2}$). The value of $\left|\Delta\bar{\delta}\right|_{min}$ is obtained at the soliton center wavelength where the red-shifted soliton in the uniform segment initiate DW emissions.

In the two approaches the incident soliton acts differently along the taper segment, which leads to different results at the fiber output. According to eq. (3.6), a constant spectral separation from the ZDW_2 of microwires with different diameters corresponds to different values of $\beta_2\left(\bar{\delta}\right)$. Following this approach, the dispersion profile the soliton center wavelength experiences in the non-uniform microwire is depicted in fig. 3.6(a) (green-curve).

From (eq. (3.7) and eq. (3.8)), the magnitude of $\left|\Delta\bar{\delta}\right|_{min}$ and $\left|\beta_2\left(\bar{\delta}\right)\right|_{min}$ required to avoid DW emissions has to be adjusted with the input soliton order. This is because an increase in the input soliton-order increases also its spectral bandwidth. In this case, the red-shifted soliton has to remain at a larger spectral distant to avoid the overlap with ZDW_2 as shown in fig. 3.6(b). The same applies to the GVD-threshold ($\left|\beta_2\left(\bar{\delta}\right)\right|_{min}$). This

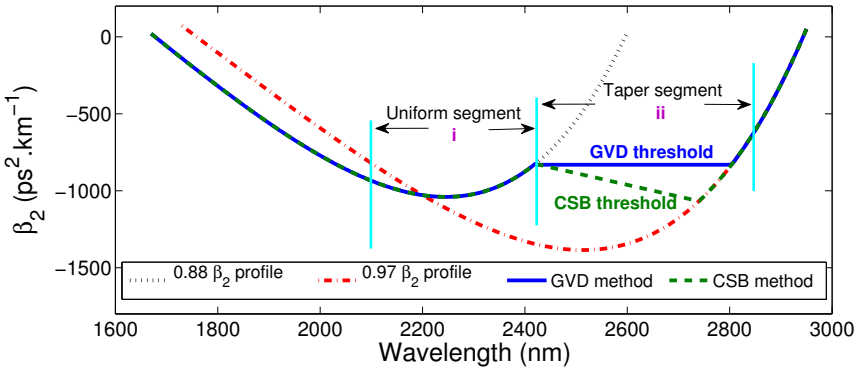

(a)

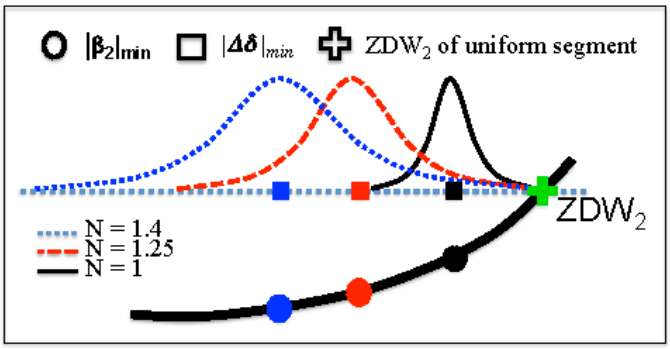

(b)

Figure 3.6: *a) The dispersion profile along the propagation path of non-uniform As_2Se_3-polymer microwires designed using the threshold conditions: GVD ($\left|\beta_2\left(\bar{\delta}\right)\right|_{min}$ in eq. (3.7); blue-curve) and CSB ($\left|\Delta\bar{\delta}\right|_{min}$ in eq. (3.8); green-curve). b) A schematic diagram of the spectral separation and magnitude of GVD threshold required to avoid DW emissions for red-shifted solitons generated from soliton of N=1, 1.25, and 1.4.*

is manifested in non-uniform microwires as a change in the rate of diameter increase per unit length.

3.4.2 Numerical investigation of the design method

To determine the optimum diameter profile for maximum wavelength-shift and transfer of energy towards longer wavelengths, the SSFS is investigated in non-uniform microwire profiles for soliton orders varying between N=1 and 1.4. The non-uniform microwires are designed specifically for each soliton order. The uniform segment of all non-uniform microwires is chosen based on the presented approach with a diameter of 0.88 μm. For the taper segment, the GVD and CSB threshold conditions are used in order to determine the influence of each condition on the characteristics of output spectra.

In fig. 3.7(a), the output soliton wavelengths from non-uniform microwires of taper segment designed with GVD conditions are shown for different input soliton orders. Figure 3.7(b) shows the corresponding ratio of the output energy radiating at the soliton frequencies (E_s/E_t), where E_s is the soliton energy and E_t is the total output energy including the soliton and DW energy.

Figure 3.8 shows the output soliton wavelengths obtained from non-uniform microwires of taper segments designed with CSB condition, and the ratio of the output energy radiated from the red-shifted solitons. From fig. 3.7(a) and fig. 3.8(a), the input soliton order and threshold conditions can be extracted for maximum wavelength-shift and soliton energy. Then from fig. 3.7(b) and fig. 3.8(b), the corresponding ratio of the output soliton energy can be obtained.

Comparing these two sets of graphs shows that soliton behavior differs when using either the rule of minimum GVD or the rule of minimum CSB to design taper segments. From fig. 3.7(a) and fig. 3.8(a), it can be concluded that the values of input soliton orders and the magnitudes of GVD and CSB conditions that enables a maximum wavelength-shift are different. In fig. 3.7(a), the maximum wavelength-shift is 2760 nm, obtained

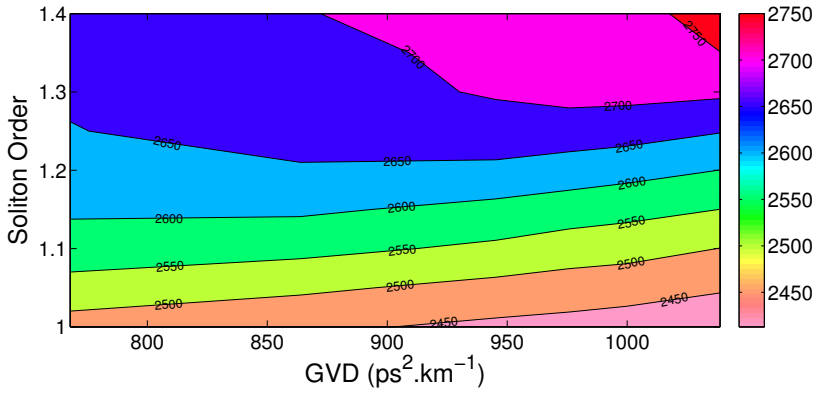

(a)

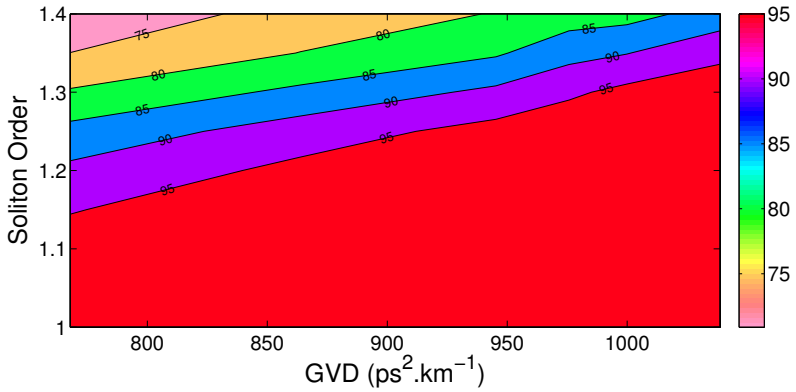

(b)

Figure 3.7: *The contour plot of the a) output wavelength-shift and b) percentage of remaining energy contained in the frequency shifted soliton obtained using GVD threshold conditions appropriate to input soliton orders varying between N = 1 and 1.4*

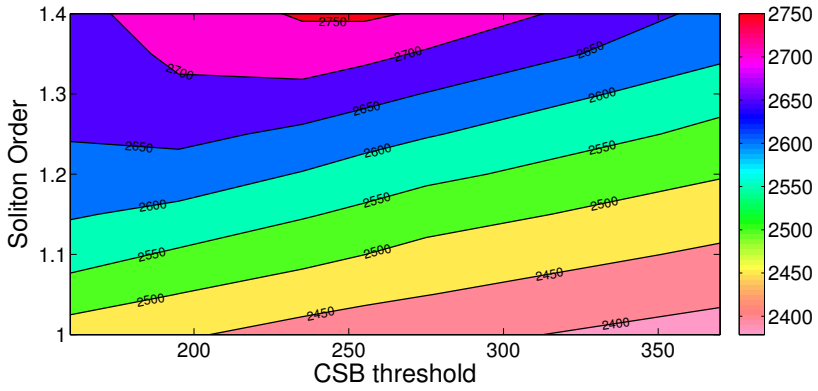

(a)

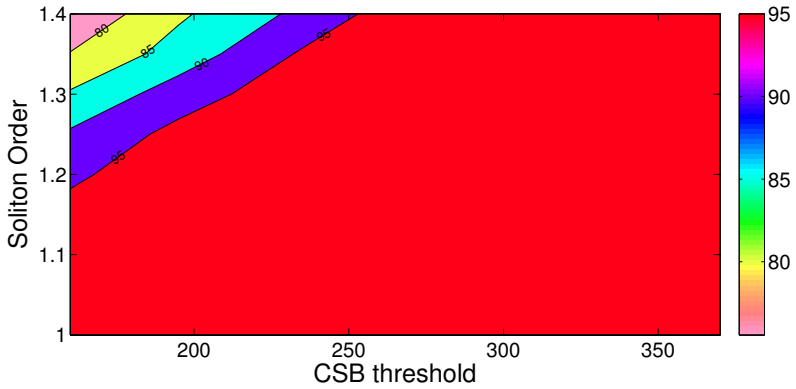

(b)

Figure 3.8: *The contour plot of the a) output wavelength-shift and b) percentage of remaining energy contained in the frequency shifted soliton obtained using CSB threshold conditions appropriate to input soliton orders varying between N = 1 and 1.4.*

for input soliton of order N=1.4 propagating in taper segments designed with a GVD threshold appropriate for N=1.4. While from fig. 3.8(a), it can be seen that the maximum wavelength-shift is obtained when a soliton of order N=1.4 propagates in a taper segment designed with a CSB condition appropriate for N=1.25. The output soliton wavelength is similar to that obtained in fig. 3.7(a).

For the output soliton wavelengths chosen from fig. 3.7(a) and fig. 3.8(a), fig. 3.7(b) and fig. 3.8(b) indicate that $\backsim$87% and 95% of output energy would be emitted at soliton frequencies, respectively. Therefore, the results reveal that the approach presented in this thesis to optimize the taper segment provides an enhancement of 8% in comparison to that proposed Judge et. al. [114].

In fig. 3.9(a), I present the soliton spectra generated at the non-uniform microwires output for the two maximum output wavelength-shift values chosen in fig. 3.7(a) and fig. 3.8(a). The results are obtained numerically using the input pulse parameters: a sech pulse shape of N=1.4, peak power = 22 W (1.21 pJ), and τ_o = 29 fs. By comparison, it can be seen that the two spectra are centered at the same wavelength, i.e. 2760 nm but with a reduced DW emissions in the profile proposed in here. The microwire profiles leading to fig. 3.9(a) are shown in fig. 3.9(b) as a function of the soliton propagation length. The diameter of the two optimum microwires considered here increase gradually from 0.88 μm, i.e. the value chosen from the adiabatic theory, along a 20 cm microwire length. The difference between the two microwires is the length of the uniform segment and the rate of increase of the diameter per unit of propagation length. From a practical point of view, using pulses of duration longer than 29 fs lead to reduced DW spectral feature at the output of the two microwires. This is due to the decrease of the $SSFS_r$ with the increase of pulse duration [13]. In contrast, a reduction in the pulse duration causes significant emissions of DW due to an increased overlap of the soliton spectrum with ZDW_2. The figure shows also the microwire profile designed based on [114] where the fundamental soliton acquires the maximum possible waveguide nonlinearity as it

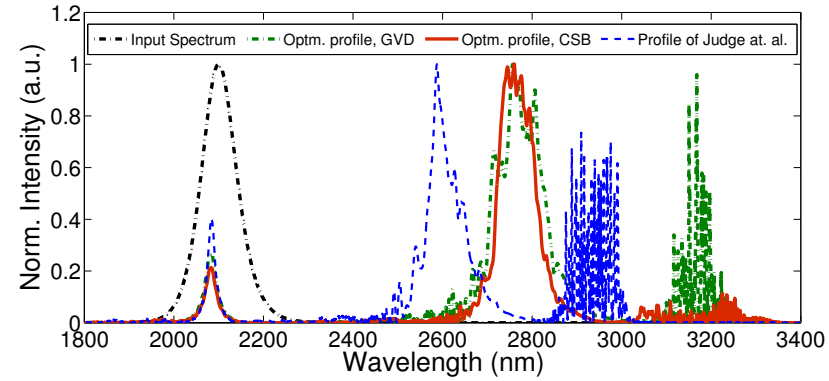

(a)

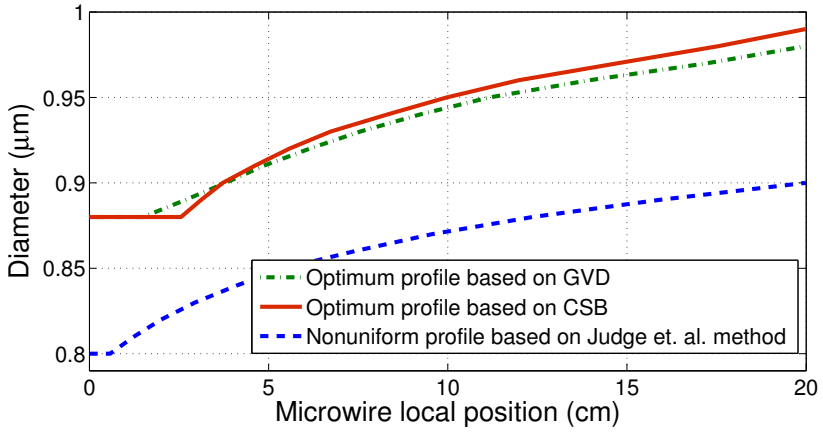

(b)

Figure 3.9: *a) The maximum wavelength-shift obtained for a soliton with N=1.4 in non-uniform microwires designed with: GVD condition appropriate for N=1.4 (Green-curve), and: CSB condition appropriate for N=1.25 (red-curve) b) Optimum non-uniform microwire profiles designed based on GVD- (Green dashed-dotted curve) and CSB- (red-curve) threshold conditions with a uniform segment based on the approach proposed above, and optimum profiles designed based on [114] (blue dashed-curve).*

enters the microwire, but with no overlap with the ZDWs. However, the rate of increase of the diameter profile follows the rate of SSFS of N=1.4 in order to reduce the DW emissions. The corresponding output spectra from this profile is shown in fig. 3.9(a) (blue dashed-curve).

3.4.3 Comparison of SSFS in uniform and non-uniform microwires

To illustrate the enhancement between using a uniform and non-uniform microwire, I show in fig. 3.10 the maximum wavelength shifts received after the propagation of input solitons with N varying from 1 to 1.4 for constant input pulse duration of 29 fs. I bring the attention here that the energy required to generate solitons in the non-uniform microwires is much less than that required in uniform microwires. From the figure, the wavelength shifts change continuously as the soliton order, i.e. input peak power, is changed for each soliton order. A dramatic increase in the magnitude of the output wavelength-shift occurs when the non-uniform microwires are used as a hosting media for soliton shifting. This is because soliton experiences a higher waveguide nonlinearity along non-uniform microwires.

3.5 Design method of non-uniform microwire based on perturbation theory (P-M)

After further investigation, I have found that the threshold approaches proposed by Judge et. al. [114] and in the CSB-M are not optimal for designing the taper segment as they do not account for the change of soliton temporal duration and that of the TOD along the taper segment.

In the P-M, the TOD is controlled in the uniform segment and in the taper segment by a normalized parameter ϵ. This parameter is a function of the varying diameter of

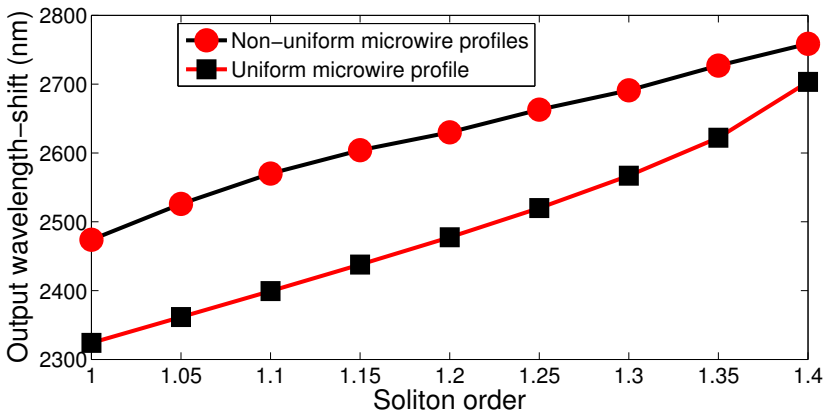

Figure 3.10: *Wavelength-shift vs. input soliton-order generated from microwires with uniform (red data) & non-uniform (black data) diameter profiles. The input soliton order varies between N=1 and 1.4. The non-uniform microwire profiles are designed based on CSB threshold conditions.*

the non-uniform microwire and the soliton local duration. This provides a different broadening rate of the microwire diameter than the one proposed by Judge et. al. and in the CSB-M, leading to an increased red-shift in the SSFS. Further description of the uniform and the taper segment design is provided in the next section.

3.5.1 Theoretical basis of the design method

To maximize the SSFS, the approach followed relies on minimizing the soliton perturbation by TOD while taking into account the change of the soliton local duration along the propagation path. The soliton perturbation by TOD effect has been extensively examined both numerically [110, 142] and analytically [67, 143–147]. Theoretical studies reveal that soliton propagation in the presence of TOD is possible if the strength of TOD is sufficiently small, and that the $SSFS_r$ decreases by the TOD perturbation. The TOD perturbation is adequately described by a normalized parameter ϵ. The parameter is analytically obtained from the normalized nonlinear Schrodinger equation given as [11]:

$$\begin{aligned}\frac{\partial U}{\partial \xi}+i\frac{(\text{sign}\,(\beta_2))}{2}\partial_\tau^2 U\,(\xi,\tau)-iN^2U\,(\xi,\tau)\,|U\,(\xi,\tau)|^2\\ =\text{sign}\,(\beta_3)\,\frac{\epsilon}{6}\partial_\tau^3 U\,(\xi,\tau)\end{aligned} \tag{3.9}$$

where ξ, τ, N and ϵ are dimensionless variables given as:

$$\xi=\frac{z}{L_D},\ \tau=\frac{t-z/v_g}{\tau_o},\ N^2=\frac{\gamma P_o\tau_o^2}{|\beta_2|}\text{ and }\epsilon=\frac{|\beta_3|}{|\beta_2|\,\tau_o}. \tag{3.10}$$

Here, $L_D=\tau_o^2/|\beta_2|$ is the GVD length, τ_o and P_o represent the temporal duration of the input pulse and the threshold peak power to generate a fundamental soliton, respectively, N is the soliton order, $\beta_n=d^n\beta/d\omega^n$ is the nth order chromatic dispersion parameter of the fiber where β is mode propagation constant, ξ is the distance along the microwire measured in units of L_D, τ is the characteristic time in the reference frame moving with the group velocity (v_g), and γ is the waveguide nonlinear parameter of the microwire.

The temporal duration evolution $\tau_s(\bar{\delta},d_l)$ of a fundamental soliton (N=1) experiencing SSFS is written as [11]:

$$\tau_s\left(\bar{\delta},d_l\right)=2\frac{\left|\beta_2\left(\bar{\delta},d_l\right)\right|}{\gamma\left(\bar{\delta},d_l\right)E_s\left(\bar{\delta},d_l\right)}, \tag{3.11}$$

where $\bar{\delta}$ is the local central frequency of wavelength-shifting soliton, and d_l is the local diameter of the microwire. According to the conservation law of photon number, the energy of wavelength-shifting soliton can be approximated by: $E_s(\bar{\delta},d_l)=E_o\gamma(\bar{\delta},d_l)/\gamma_o$. E_o and γ_o are the input soliton energy and waveguide nonlinear parameter at the pump wavelength, respectively, $\gamma\left(\bar{\delta},d_l\right)=n_2(\bar{\delta})\bar{\delta}/cA_{\text{eff}}(\bar{\delta},d_l)$ where n_2 is the material nonlinear parameter and A_{eff} is the effective mode area.

By substituting $\tau_s(\bar{\delta},d_l)$ into eq. (3.10), the normalized $\epsilon(\bar{\delta},d_l)$ parameter is written as:

$$\epsilon\equiv\epsilon\left(\bar{\delta},d_l\right)=\frac{\left|\beta_3\left(\bar{\delta},d_l\right)\right|E_o\gamma^2\left(\bar{\delta},d_l\right)}{2\left|\beta_2\left(\bar{\delta},d_l\right)\right|^2\gamma_o}. \tag{3.12}$$

This expression of ϵ is used to design non-uniform microwires. *The diameter profile of these microwires is optimized such that a wavelength-shifting soliton tolerates from the pump wavelength to the output wavelength-shift a magnitude of ϵ less or equal a threshold level*. In this study, I find that a level of 0.1 provides a good approximation for the optimization of SSFS in the non-uniform microwires. The assumption of the threshold value as 0.1 is illustrated later in the numerical simulation section.

For the uniform segment of the non-uniform microwire, the diameter is selected such that an incident soliton acquires at its central frequency (δ_o) an $\epsilon_o \equiv \epsilon(\delta_o) \approx 0.1$. This corresponds to a weak perturbation by TOD at the pump wavelength which leads to avoiding DW emissions at shorter wavelengths in the normal dispersion regime.

For the taper segment, the diameter is increased such that the soliton acquires at its local central frequency only ϵ-values close to 0.1.

Design of the uniform segment

To exemplify the presented method, a design of non-uniform As_2Se_3 microwire is proposed for a pump wavelength at the upper transmission wavelength of silica (i.e. 2000 nm). The input soliton to the microwire is assumed to be of a duration of τ_{fwhm}=50 fs and the microwire length is limited to 10 cm. To give a thorough discussion, the design of the microwire is explained firstly based on the analytical expression of eq. (3.12) and then investigated through numerical simulation.

Figure 3.11(a) depicts the ϵ_o values obtained using eq. (3.12) for a 50 fs fundamental soliton at the pump wavelength λ_o=2000 nm for different uniform segment diameters. From the figure, the closest value of ϵ_o=0.1 is obtained from a uniform segment diameter of 0.65 μm.

Figure 3.11(b) shows the ϵ-curve (blue-dashed) and the anomalous β_2-curve (dotted-green) as a function of anomalous dispersion wavelengths for a uniform segment of 0.65 μm diameter. The ϵ-curve increases asymptotically close to ZDWs while it exhibits

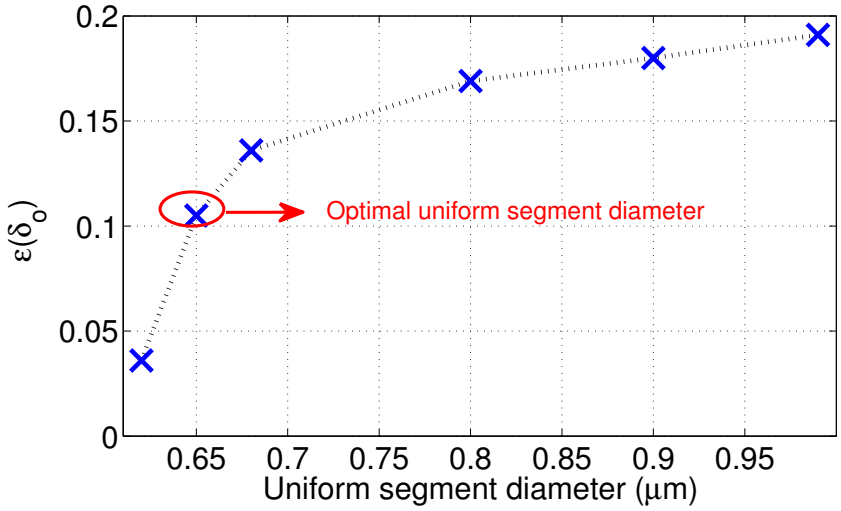

(a)

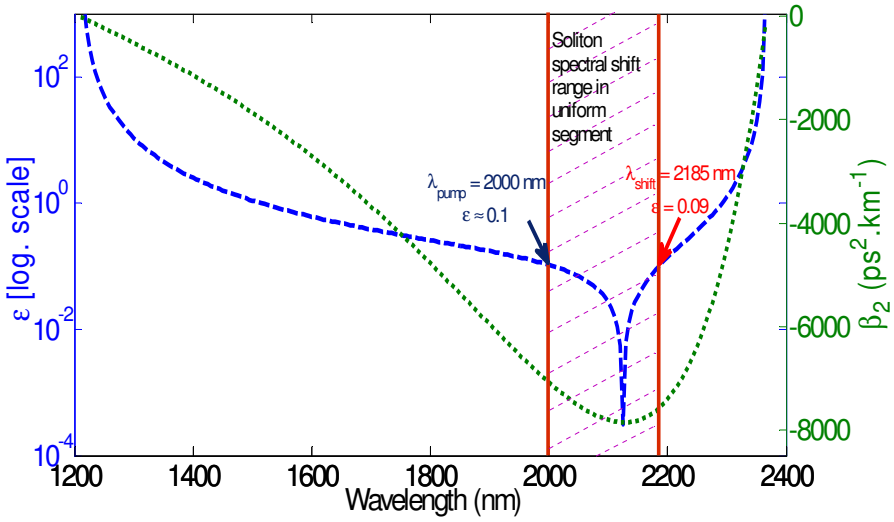

(b)

Figure 3.11: *In a), the dimensionless variable ϵ as a function of uniform segment diameter. In b), the dimensionless variable ϵ and the GVD curve as a function of wavelength for a uniform segment diameter of 0.65 µm.*

a minimum value at the peak magnitude of the β_2 curve. For a fundamental soliton of N=1 pumped at a wavelength of 2000 nm, the figure shows that an optimal $SSFS_r$ in the uniform segment is achieved when the soliton is spectrally maintained between 2000 nm and 2185 nm. Over this wavelength range, the wavelength-shifting soliton acquires ϵ-values below 0.1 and thus remains slightly perturbed by TOD. Beyond 2185 nm, the soliton is transferred into the taper segment to maintain $\epsilon \leq 0.1$. In the taper segment, the diameter increases along the propagation path of the wavelength-shifting soliton such that the ZDW_2 shifts away from the soliton towards longer wavelengths.

Design of the taper segment

The design of the taper segment is determined by dividing the segment into infinitesimally short subsegments as shown in fig. 3.12. Each subsegment induces a wavelength-shift of the soliton's central wavelength such that the wavelength-shifting soliton exhibits ϵ-values below or equal to 0.1 and thus remains weakly perturbed by TOD. Figure 3.13(a) shows the ϵ spectra (dashed-dotted) of several subsegment diameters (d=0.65-0.85 μm) determined for a soliton of 50 fs. The pink solid-curve shows the ϵ-values tolerated by a wavelength-shifting soliton along the non-uniform microwire. In the taper segment, the wavelength shifting soliton acquires only ϵ-values close to 0.1 depicted as a line in the figure.

The GVD profiles of a few selected microwire subsegments (d=0.65-0.85 μm) are shown in fig. 3.13(b). The dispersion profile of the uniform segment (d=0.65 μm) is shown in red solid-curve while those of the subsegments are shown as blue dashed-dotted curves. The pink solid-curve depicts the GVD values experienced by the wavelength-shifting soliton along the non-uniform microwire length.

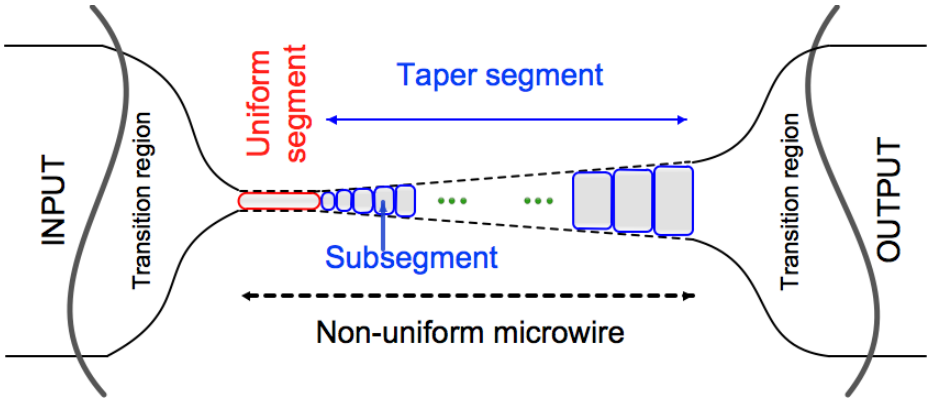

Figure 3.12: *Schematic structure of a tapered fiber with non-uniform microwire. The non-uniform microwire consists of a uniform and a taper segment. The taper segment is subdivided into uniform subsegments. Each subsegment induces a finite wavelength-shift on a propagating soliton.*

3.5.2 Numerical investigation of the design method

Design of the uniform Segment

To investigate the validity of the proposed method in optimizing the non-uniform microwire profile, the SSFS is studied in several non-uniform As_2Se_3 microwire profiles comprising uniform segments with diameters ranging from 0.60 to 0.99 μm as previously depicted in fig. 3.11(a). In each uniform segment, the launching energies required to generate a fundamental soliton of N=1 are different due to the dependence of $\beta_2(\delta_o)$ and $\gamma(\delta_o)$ on uniform segment diameter.

To generate the SSFS spectrum at the output of the non-uniform microwire, the GNLSE [95] is numerically solved using a sech pulse centered at wavelength of 2000 nm, $A(z = 0, \tau) = \sqrt{P_o}\,\mathrm{sech}(2ln(1+\sqrt{2})\tau/\tau_{\mathrm{fwhm}})$, with τ_{fwhm}=50 fs and an input peak power P_o. The GNLSE is numerically solved using the RK4IP [97] with a local error threshold of 10^{-5}. The pulse is discretized into 2^{15} samples with a temporal window of width 256 ps. The higher-order dispersion terms are included up to 9th order. For the material parameters

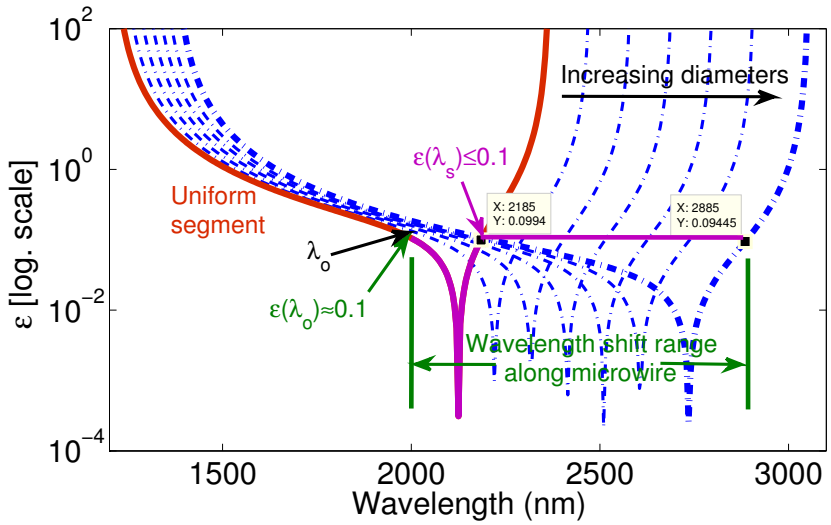

(a)

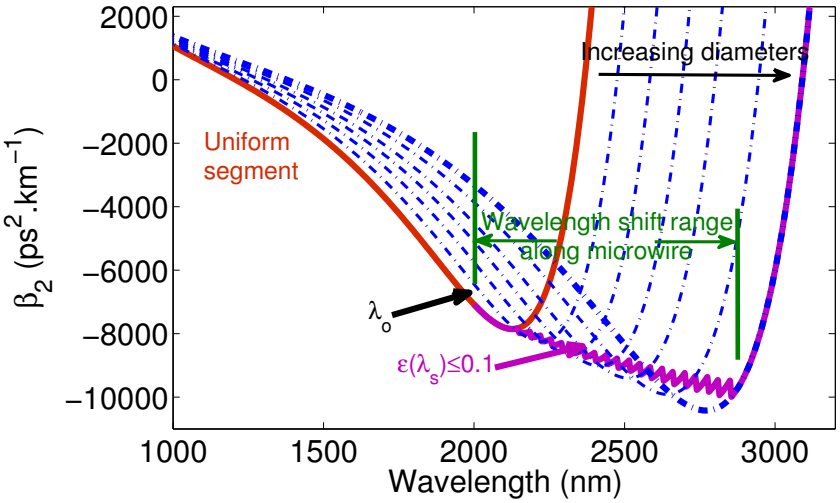

(b)

Figure 3.13: *a) The $\epsilon(\bar{\delta})$ values of the anomalous wavelengths for different subsegment diameters (0.65-0.85 µm) obtained using eq.* (3.12)*. b) The GVD profiles for the subsegments (blue dashed-dotted) of the taper segment designed based on the ϵ-threshold condition. The pink solid-curve depicts the GVD values experienced at the central frequency of a wavelength-shifting soliton in the non-uniform microwire profile. λ_s: instantaneous soliton central wavelength. λ_o: pump wavelength.*

of bulk As_2Se_3, $n_2 = 2 \times 10^{-17} m^2/W$ and f_R=0.1 [50] are used with τ_1=23 fs and τ_2=195 fs parameters chosen [68] to best fit with the experimental measurements of the Raman gain spectrum in As_2Se_3.

Figure 3.14 depicts the soliton central output wavelengths obtained at the end of a 10 cm non-uniform microwires length. The soliton wavelength is the center of mass wavelength of the generated SSFS spectrum. In each non-uniform microwire profile, the rate of increase of the diameter along the microwire length is different due to the difference of the input physical parameters of incident solitons. The results show that the maximum output wavelength-shift is obtained for non-uniform microwire with a uniform segment of 0.65 μm diameter. This illustrates the analytical predictions depicted in fig. 3.14(a) of 0.65 μm being the optimal diameter value for a soliton pumped at 2000 nm with 50 fs pulse width.

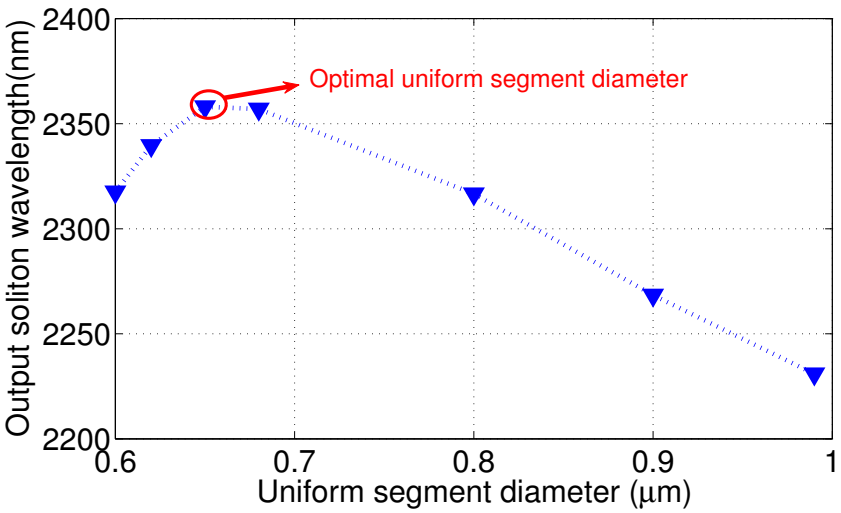

Figure 3.14: *Output soliton wavelengths from non-uniform microwires for an input soliton of N=1. Symbols represent the wavelength at the output end of non-uniform microwires designed with different uniform segment diameters. The uniform segment diameters varies between 0.60 µm and 0.99 µm. The maximum output soliton wavelength (2358 nm) is obtained from the microwire of uniform segment diameter of 0.65 µm.*

For non-uniform microwires of uniform segments with diameters smaller than 0.65 μm, incident fundamental solitons exhibit lower magnitudes of $\beta_2(\delta_o)$ at 2000 nm and thus, requires smaller input energies to satisfy the condition for N=1. This manifest as shorter output wavelength shifts. For diameters smaller than 0.60 μm, input soliton impinge the ZDWs of uniform segment which results also in shorter output wavelength shifts. However, for uniform segments with diameters larger than 0.65 μm, the $SSFS_r$ decreases as the wavelength-shifting soliton experiences larger magnitudes of $|\beta_2(\bar{\delta})|$ and smaller magnitudes of $|\gamma(\bar{\delta})|$ values along the propagation path.

Design of the taper Segment

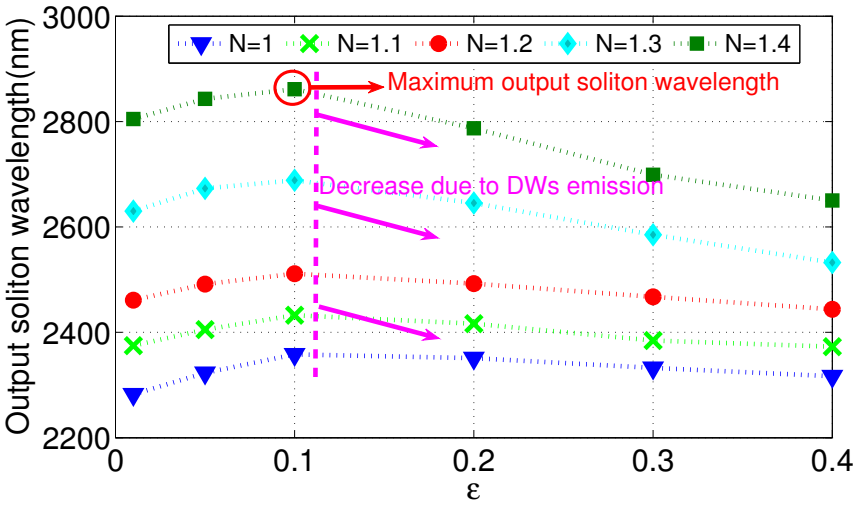

Figure 3.15: *Output soliton wavelengths from non-uniform microwires for input solitons of N varying between 1 and 1.4. Symbols represent the wavelength at the output end of non-uniform microwires designed using ϵ-threshold condition that varies between 0.01 and 0.4. The maximum output soliton wavelength (2860 nm) is obtained from the microwire that is designed using ϵ=0.1.*

To investigate the influence of the taper segment profile on the dynamics of the SSFS,

the wavelength-shifting of a soliton is numerically studied in non-uniform microwire profiles designed with a uniform segment diameter of 0.65 μm but with different taper segments. The taper segments are designed using different ϵ-threshold conditions that varies from 0.01 to 0.4.

Figure 3.15 depicts the output wavelength-shifts for a 50 fs input soliton with a varying input peak powers. The peak power values correspond to N varying between 1 and 1.4. Each symbol in the figure corresponds to the central wavelength of a wavelength-shifted soliton at the output end of a microwire profile. The profiles are designed specifically for each soliton order, where eq. (3.12) is multiplied by (2N-1) to accommodate to the change of soliton order. From the figure, the output soliton wavelengths from microwire profiles determined using ϵ=0.1 are longer compared to the results obtained from microwires of ϵ levels smaller or larger than 0.1. For ϵ<0.1, the wavelength-shifting soliton exhibits large magnitudes of GVD along the propagation path which leads to a rapid broadening of its duration. Since the $SSFS_r$ is inversely proportional to pulse duration, the soliton undergoes a shorter wavelength-shift range along the microwire length. For non-uniform profiles designed using ϵ>0.1, the soliton shifts closer to ZDW_2 and transfers its energy to DW. This reduces the energy density of the wavelength-shifting soliton and broadens its duration.

To illustrate the influence of DW emissions on decreasing the $SSFS_r$ for ϵ>0.1, fig. 3.16 depicts the spectral density of the wavelength-shifting of N=1.4 soliton in two non-uniform microwire profiles designed with ϵ=0.1(a) and 0.4(b). Figure 3.16 (a) shows no sign of DW emissions, while a significant fraction of energy is transferred into DW emissions in case (b). The reduction in the DW emissions and the optimal dispersion- and nonlinearity- profiles of the non-uniform microwire in case (a) manifest as the most wavelength-shifted soliton at the output of the microwire. The output soltion wavelength of the two cases are: 2860 nm, and 2650 nm respectively.

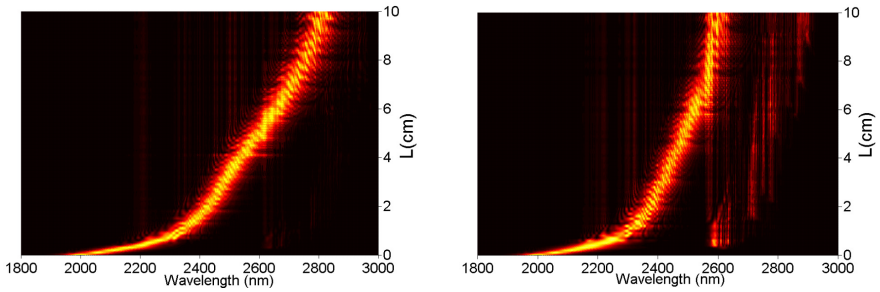

Figure 3.16: *Spectral energy density versus propagation length of soliton shifting with N=1.4 and input pulse width of 50 fs. Microwires considered are non-uniform and designed using the ϵ-threshold conditions of: (a) ϵ=0.1, and (b) ϵ=0.4. Output soliton wavelength of cases (a-b) are: 2860 nm, and 2650 nm, respectively.*

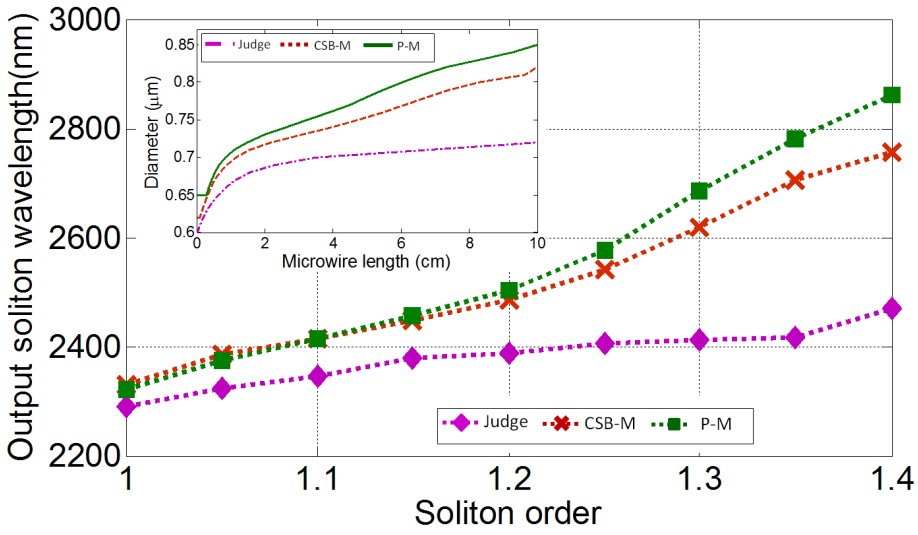

Figure 3.17: *Output soliton wavelengths from non-uniform microwires for input solitons of N varying between 1 and 1.4. Symbols represent the wavelength at the output end of non-uniform microwires designed using methods of: [114] (diamond), [68] (cross), and ϵ-threshold condition (square). Inset: Non-uniform microwire profile based on [114] (dotted-dashed), [68] (dashed), and ϵ-threshold condition (solid).*

3.5.3 Comparison of SSFS in non-uniform microwires designed by the two methods

To show the wavelength-shift improvements provided by the proposed method in comparison to previous ones[68, 114], fig. 3.17 depicts the output wavelength-shifts for input solitons with N varying from 1 to 1.4. The numerical solutions correspond to three non-uniform microwire profiles designed based on: [114] (pink-diamond), [68] (red-cross), and ϵ-threshold condition (green-square). From the figure, the output wavelength-shifts in the proposed non-uniform microwire profile are longer compared to the results obtained using previous methods. The inset of fig. 3.17 shows the corresponding non-uniform microwire profiles based on [114] (dotted-dashed), [68] (dashed) and the proposed method (solid).

3.6 Summary and Conclusion

In this chapter, I presented two methods to design non-uniform microwires which enhance the SSFS in optical fibers.

In the CSB-M [68], the central wavelength of a soliton is kept at a wavelength separation with respect to the ZDW_2 that is above or equal to a threshold value in the taper segment (eq. (3.5)). The uniform segment is chosen based on an analytical expression (eq. (3.6)) that ensures the highest $SSFS_r$ in the uniform segment. I found that the selection of a transverse dimension of the uniform segment in non-uniform microwires has a dramatic impact in the wavelength shift.

In the P-M [69], I included the change of the soliton pulse duration and the TOD value along the soliton propagation length in a non-uniform microwire. The microwire profile avoids DW emissions and maximizes the SSFS. The method ensures that the soliton is constantly exposed to the optimal ϵ values (i.e., TOD perturbation) during its propagation

along the microwire. The ϵ value which leads to a maximum SSFS was shown to be 0.1. The results reveal a wavelength-shift of 860 nm in a microwire length as short as 10 cm.

Numerical simulations were carried out for solitons that were propagated in uniform and non-uniform microwires with varying input peak power values corresponding to soliton orders between N =1 and 1.4. The numerical results showed that despite the increase of input peak power values, the soliton energy is preserved at the output end of the designed microwires. This has illustrates the proposed approach's usefulness in suppressing the DW emissions of input solitons with $N > 1$ and in tuning the output soliton wavelength.

Using contour plots, I demonstrated a non-uniform microwire profile based on the CSB-M that maximizes the output soliton wavelength and preserves the soliton energy along the propagation length. Numerical results were compared to those from microwires designed by previous approaches. The non-uniform microwire profile allows a 29 fs input soliton with power varying from 21 to 41 W (1.21 to 2.37 pJ) to reach a maximum output wavelength shift of 650 nm. I showed the ability to tune the output soliton wavelength with more than 95% of the total output energy radiating at the soliton frequencies. I compared the output soliton wavelengths with the ones from a uniform microwire to illustrate the advancement of using non-uniform microwires in maximizing the extent of the soliton wavelength shift in the mid-IR.

Chapter 4

Broadband supercontinuum generation in As_2Se_3 microwires by avoiding the two-photon absorption effects

In this chapter, I generate a SC extending from 1260 to 2200 nm using a 10 cm long As_2Se_3 microwire from a pump at a wavelength of 1550 nm. I also provide analytical expression to calculate the TPA full spectrum of As_2Se_3. This spectrum could be inserted in a numerical simulator to compare the calculated SC to experiments with better precision. Also, values of the TPA coefficient could be extracted from the calculated spectrum. The work was published in [70] (iournal publication III). In As_2Se_3, several nonlinear processes were found to be limited by the TPA effect when pumping with sources with a central wavelength at 1550 nm. To avoid TPA, pump pulses at λ_p =1550 nm were self-frequency shifted towards longer wavelength before nonlinear propagation through the As_2Se_3 microwire. The spectral broadening is examined using a pump spectrum that contains a frequency-shifted soliton (FS) centered at 1775 nm in the anomalous dispersion regime of an As_2Se_3 microwire.

4.1 Introduction

Over the past decade, there has been much interest in the generation of SC with broad spectral bandwidth [19, 20, 148]. Broadband SC sources have found many applications in diverse fields [24] including multiwavelength and tunable sources [149], frequency metrology [150], OCT [151], biomedical technologies [152–154] and molecular spectroscopy [155–157]. The amount of spectral broadening depends on the fiber type, pulse duration, and pulse energies used. The use of tapered fibers has reduced the need for high power and allowed for SC generation over short lengths.

ChG glasses such as As_2S_3 and As_2Se_3 are excellent candidates for broadband SC generation due to their high nonlinearity. Tapering ChG fibers has led to efficient SC generation by shifting the ZDW from the mid-IR to the operating wavelengths of available commercial laser sources. A SC covering an octave wavelength bandwidth was generated using As_2S_3 microwires from pulses energies of 77 pJ (peak power=824 W) [47]. However, As_2Se_3 is among the optimal materials for SC generation at low peak powers as it possesses a larger nonlinear refractive index, i.e. up to 1000x that of silica and ∼4x that of As_2S_3 [158]. The tapering of As_2Se_3 fiber to subwavelength dimensions have yielded microwires with waveguide nonlinearities of γ =60 $W^{-1}.m^{-1}$ [80] and later reaching as high as γ =176 $W^{-1}.m^{-1}$ [159]. Using such ChG microwires, a SC spanning from 1450 nm to 1650 nm (-20 dB bandwidth) was achieved at pulse energies of only 2.2 pJ (peak power=7.8 W) [160].

TPA is an unavoidable absorption process in As_2Se_3 that is small but non-negligible at a wavelength of 1550 nm and decreases with increasing wavelength [161, 162]. TPA has been shown to limit the efficiency of nonlinear processes including SC generation [160], guided-wave switching [163], Raman gain amplification [164], intrapulse Raman Scattering [147] and parametric processes [165]. Quantitatively, the nonlinear absorption (β_{TPA}) for As_2Se_3 as shown in fig. 4.1 drops by a factor of 5 and becomes negligible when

the pump wavelength (λ_p) is shifted from 1550 nm (β_{TPA}=0.14 cm/GW) to 1775 nm (β_{TPA}=0.028 cm/GW) (The numerical Matlab code of the TPA absorption curve is provided in the appendix). Therefore, the efficiency of the nonlinear processes could be enhanced by pumping As_2Se_3 at ∼1775 nm wavelength where the Kerr nonlinear response is free from a significant TPA.

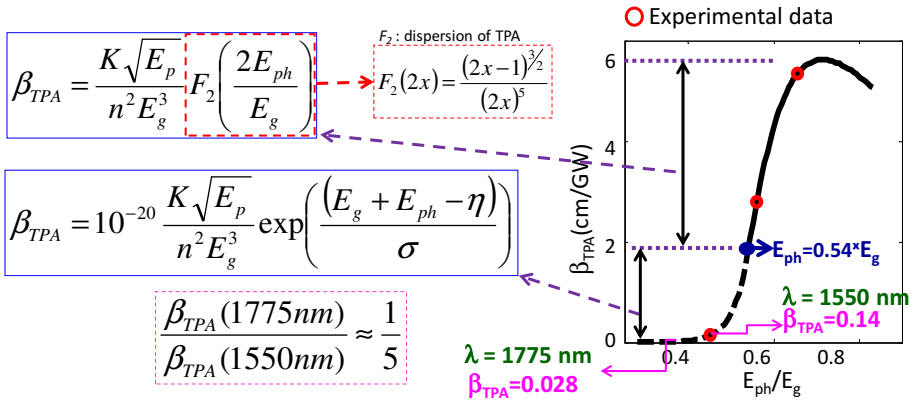

Figure 4.1: *Calculated (solid [161], dashed [166]) and experimental data (dots [49, 162]) of TPA spectrum of As_2Se_3 as a function of normalized energy (E_{ph}/E_g). E_{ph}: Photon energy; E_g: Energy gap.*

One of the interesting nonlinear effects which has been used to shift pump sources towards longer wavelengths is the SSFS. The SSFS is a consequence of the intrapulse Raman scattering, in which short wavelengths of a soliton spectrum amplify longer ones. The SSFS was demonstrated and investigated in various fiber types [17, 68].

4.2 Experimental setup

The experimental setup for the generation of SC spectrum is shown in fig. 4.2. Pump pulses are launched from a mode-locked Er doped fiber laser. The pulses have a hyperbolic secant shape and a duration of 260 fs at a repetition rate of 20 MHz (Autocorrelation

trace is shown in fig. 4.3(a)). The central wavelength and the average power of the laser are 1550 nm and 4.5 mW, respectively. The laser pulses are sent to a 4 dB attenuator and a 3 m long segment of a standard single mode fiber (SMF1) to temporally broaden the pulses and avoid strong nonlinear effects in SMF1 and subsequent amplification stage. Without the attenuator, the pump pulses spectrally broaden beyond the gain bandwidth of the Erbium-doped fiber amplifier (EDFA) (1525-1570 nm).

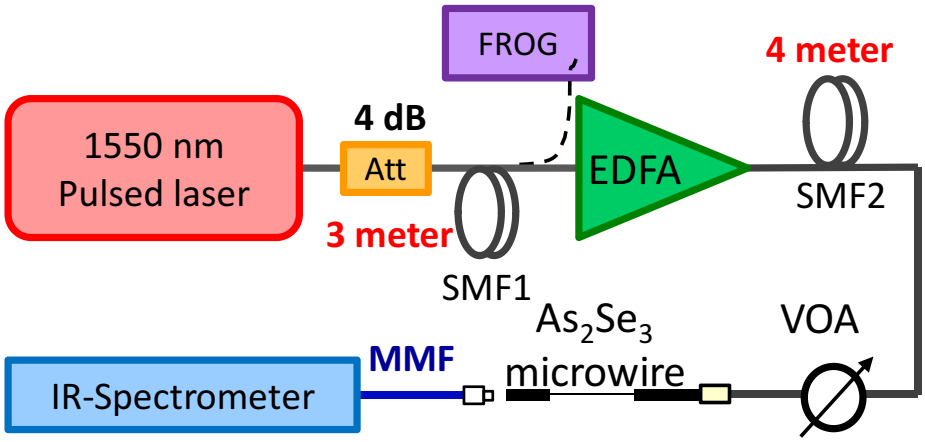

Figure 4.2: *Experimental setup for SC generation. Att: Attenuator; SMF: single-mode fiber; FROG: Frequency-resolved-optical-gating; EDFA: Er-doped fiber amplifier; VOA: Variable optical attenuator; MMF: Multimode fiber.*

Figure 4.3(b) shows the temporal- (solid line) and phase-profiles (dashed line) of the pump pulses at the input side of the EDFA measured by a second harmonic generation (SHG) frequency resolved optical gating (FROG) system. Figure 4.3(c) shows the spectrum which is broadened by SPM and the corresponding spectral phase. The pulses from SMF1 are then amplified using an EDFA of 8 m long Erbium-doped fiber with a residual normal dispersion of 35 fs/nm.

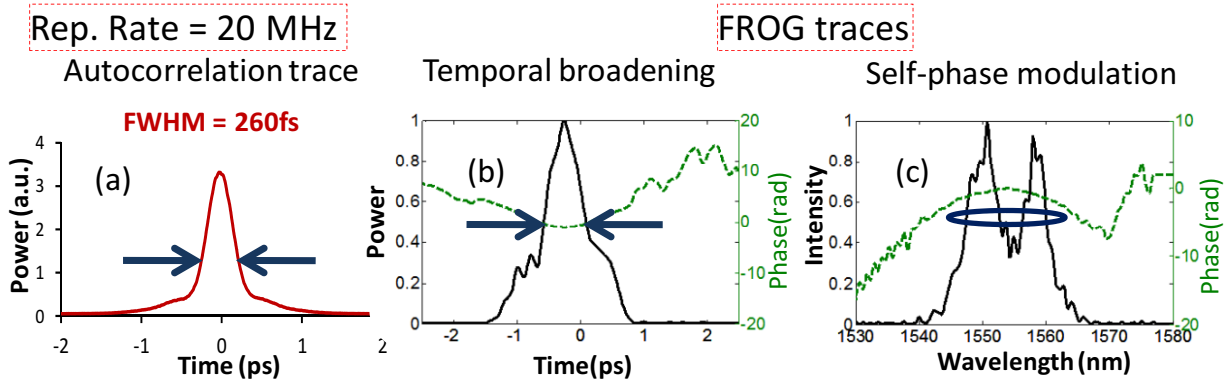

Figure 4.3: *a) Autocorrelation trace of mode-locked laser, b) Temporal- and c) spectral- profiles of the mode-locked laser pulses after SMF1.*

4.3 Generation of frequency shifted soliton in SMF

At the output end of the EDFA, the FS is generated using a 4 m long of SMF2. Along the SMF2, the pulses undergo a soliton fission which leads to the generation of a FS centered at 1775 nm. The wavelength of the FS could also be tuned by varying the gain provided by the EDFA. For the spectrum shown in fig. 4.4, the soliton contains 1.12 nJ which is about 75% of the amplified pulse power while the rest radiates as a residual pump power. From the time-bandwidth product ($\delta\tau * \delta v$=0.315), the soliton duration at the full width half-maximum is approximately 92 fs while the peak power is of 15.8 kW. The power of the output spectrum is controlled by a variable optical attenuator and then coupled to the ChG fiber to generate a SC.

4.4 Fabrication of As_2Se_3 microwire

The ChG fiber used for this experiment has a core/cladding diameter of 6/170 μm, numerical aperture of $\sim$0.2 and a linear loss of about 0.6 dB/m at a wavelength of 1550 nm.

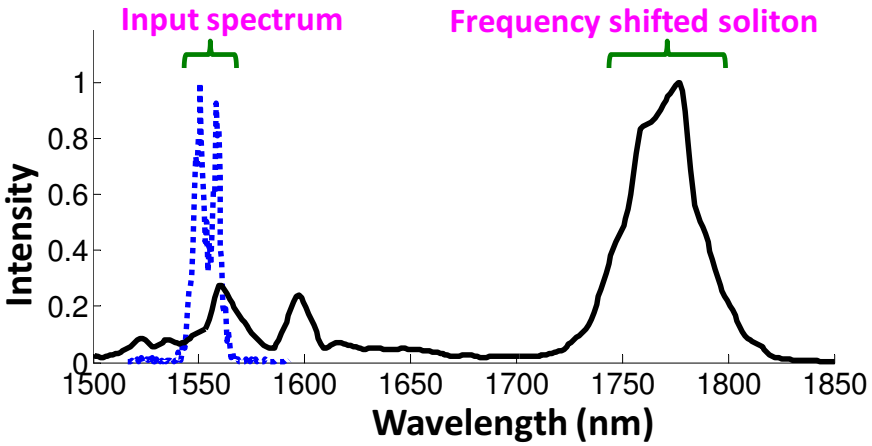

Figure 4.4: *Pulse spectrum after SMF2. Pulses initially at 1550 nm experienced SSFS up to 1775 nm.*

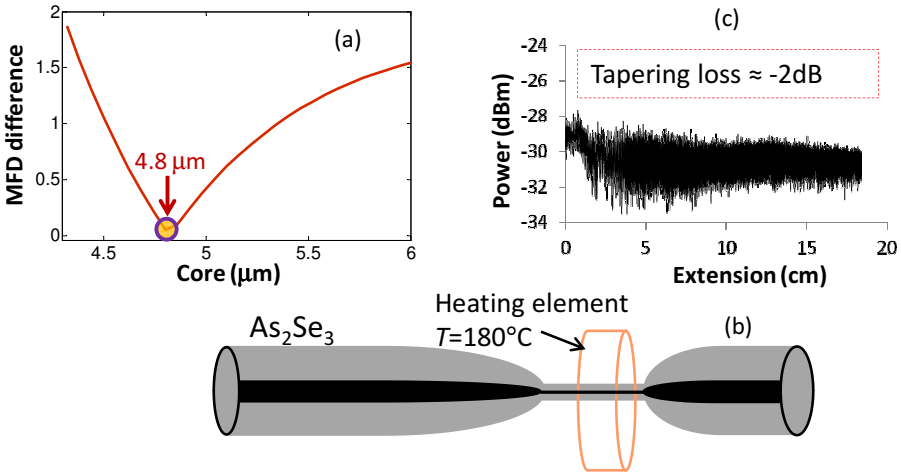

Figure 4.5: *a) MFD difference between SMF and As_2Se_3 fiber b) tapered fiber and c) tapering loss.*

The fiber is firstly pre-tapered to a core diameter of 4.8 μm to match the mode field distribution (MFD) in a SMF made of silica. The MFD difference between that in a SMF and As_2Se_3 fiber is shown in (fig. 4.5(a)) as a function of the As_2Se_3 core diameter. Using the tapering process described in [167], the central part of the fiber is heated to 180^o and subsequently tapered into 10 cm long microwire with a uniform diameter of $\sim$1.28 μm (fig. 4.5(b)). The value of the diameter is estimated and no real measurement was made to assure the actual diameter. However, the microwire diameter could be measured with a scanning electron microscope. The untapered input-side of the taper is connected permanently to SMF using UV epoxy (fig. 4.6) whereas the output-side is polished and butt-coupled to a mid-IR compatible multimode fiber leading to a calibrated spectrometer. The coupling loss at the input-side of the taper and the tapering loss are estimated to be $\sim$3 dB and $\sim$2 dB (fig. 4.5(c)), respectively. Figure 4.7(a) depicts the various parts of the tapered fiber. A 9 cm long input segment of the ChG fiber is left untapered. It is left untapered to compensate for the anomalous dispersion accumulated by the attenuated pump pulses on their way toward the ChG fiber.

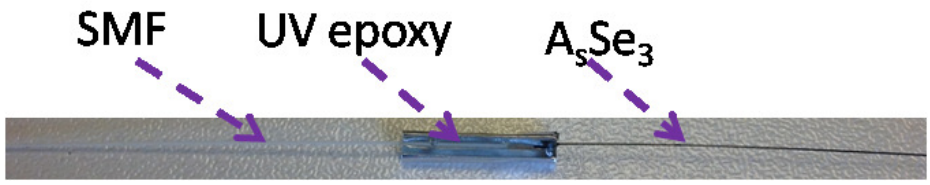

Figure 4.6: *The ChG fiber used for this experiment coupled with SMF by using UV epoxy.*

Figure 4.7(b & c) shows the calculated GVD and the waveguide nonlinearity versus wavelength for a 1.28 μm diameter As_2Se_3 microwire. The ZDW of the microwire is $\sim$1730 nm. At the 1775 nm wavelength, the GVD, mode effective area, and waveguide nonlinear parameter are β_2=-102 ps^2/km, A_{eff}=0.8 μm^2 , and γ=72.2 $W^{-1}.m^{-1}$, respectively.

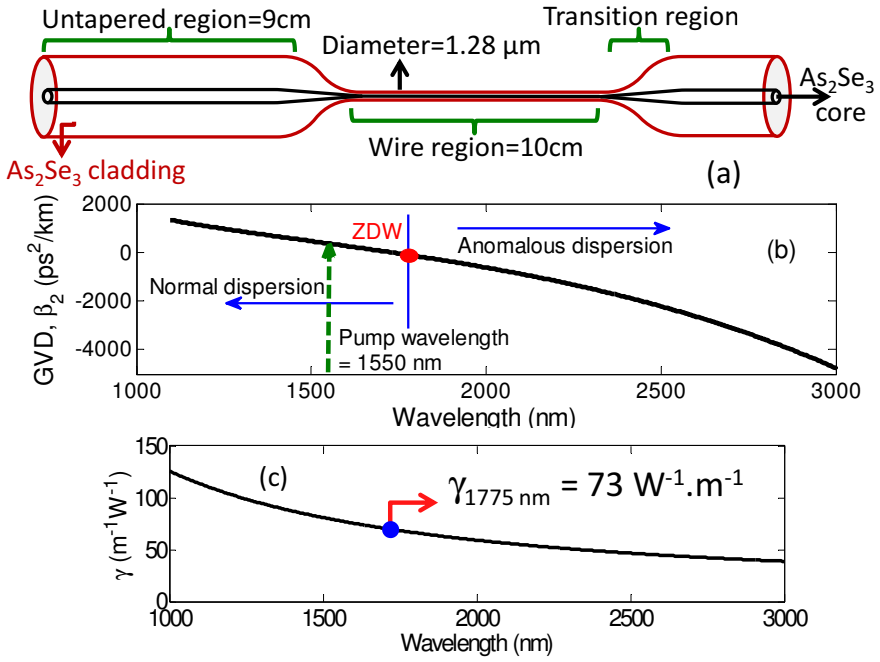

Figure 4.7: *a) Schematic of a tapered fiber with a microwire region of a subwavelength diameter. b) Calculated dispersion and c) waveguide nonlinearity of the microwire with a diameter of 1.28 µ m.*

4.5 Experimental results

Figure 4.8 shows the SC generated by the taper as a function of the launched pulse energy. The energy values depicted in the figure take into consideration the coupling loss. At a pulse energy of 6.3 pJ (corresponding to a soliton of order 25.2 with a duration of 335 fs, and a fission length of 14.5 mm) the -20 dB bandwidth is as large as 940 nm (1260-2200 nm). On the short wavelength side of the spectra, DW emissions appear at power levels above 1.5 pJ, while the SSFS process extends the long wavelength side of the spectra. The short wavelength edge of the generated SC is formed due to the cross-phase modulation (XPM) between the frequency-shifted soliton and the DW. The long wavelength edge of the SC saturates at 2200 nm as the soliton undergoing SSFS experiences

a large magnitude of dispersion. The temporal duration of the soliton broadens and the $SSFS_r$ decreases. With the given parameters, a close matching between the measured and numerically calculated spectra are obtained as shown in the figure.

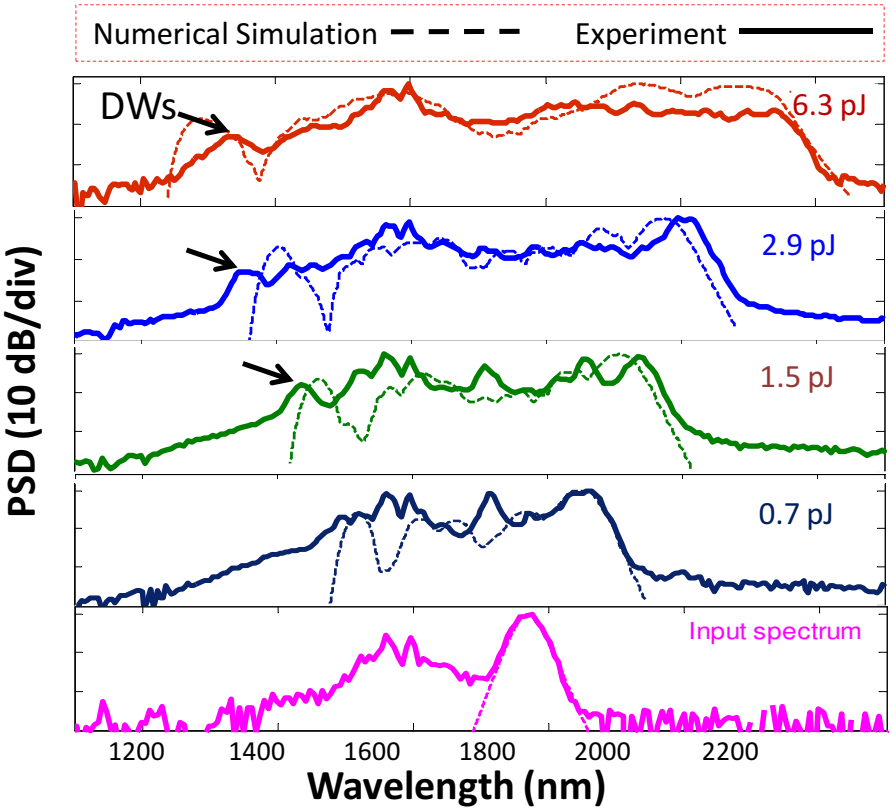

Figure 4.8: *SC spectrum of the tapered fiber measured at increasing pulse energies; DWs: dispersive wave emissions. The measured (solid) and simulated (dashed) SC spectra are depicted with a 10 dB/div.*

The numerical results are based on solving the GNLSE using the RK4IP. The numerical simulation incorporates the whole structure of the taper and takes into consideration the higher-order dispersion terms up to 9th order. The contribution of self steepening and delayed Raman response is included with f_R =0.1, τ_1=23 fs and τ_2=195 fs chosen to best fit with the experimental measurements [168] of the Raman gain spectrum in

As_2Se_3. The $\beta_2(\lambda)$, $\gamma(\lambda)$, $A_{\text{eff}}(\lambda)$, and TPA(λ) curves are also included. For the TPA curve of fig. 4.1(a), the parabolic change of values (solid) are determined by [161]:

$$\beta_{TPA_a} = \frac{K\sqrt{E_p}}{n^2 E_g^3} F_2(\frac{2E_{ph}}{E_g})\text{cm/GW},$$

while the dashed curve follows the Urbach rule [1] [166] and is obtained in this work by:

$$\beta_{TPA_b} = 10^{-20}\frac{K\sqrt{E_p}}{n^2 E_g^3} exp((E_g + E_{ph} - \eta)/\sigma)\text{cm/GW},$$

where the fitting parameters, K =1220 (material independent constant) η =0.12381 eV [2] and σ =0.0625 eV are chosen to best fit with experimental data of [162], E_p =21 eV (material independent for most direct bandgap semiconductors), E_g =1.78 eV, n is the linear refractive index curve, and $F_2(2x) = (2x-1)^{3/2}/(2x)^5$.

4.6 Influence of TPA on SC generation

To demonstrate the effect of TPA on the spectral broadening, the SC generation is numerically studied for different pump wavelengths (1550 and 1775 nm) together with different microwire diameters (1.02 and 1.28 μm). Incident pulses with the same parameters as given above are now assumed to be propagating only in a 10 cm long microwire and are freely-chirped. Figure 4.9(a) shows the results obtained from pulses at λ_p=1775 nm propagating in a diameter of 1.28 μm, while fig. 4.9(b) shows the ones obtained from pulses of the same pulse energy but at λ_p =1550 nm and propagating in a diameter of 1.02 μm. The diameter of 1.02 μm is chosen in order to have the 1550 nm pump at the same spectral separation from the ZDW as in the case of fig. 4.9(a). The SC spectra are obtained with the TPA being included (solid) and not included (dashed) in the GNLSE. The results reveal that at a pulse energy of 6.3 pJ, the TPA substantially limits the extent

[1] An exponential increase of absorption with photon energy

[2] Urbach energy and is dependent on the thermodynamic temperature, boltzmann constant and a fitting parameter which determines the slope of the Urbach tail

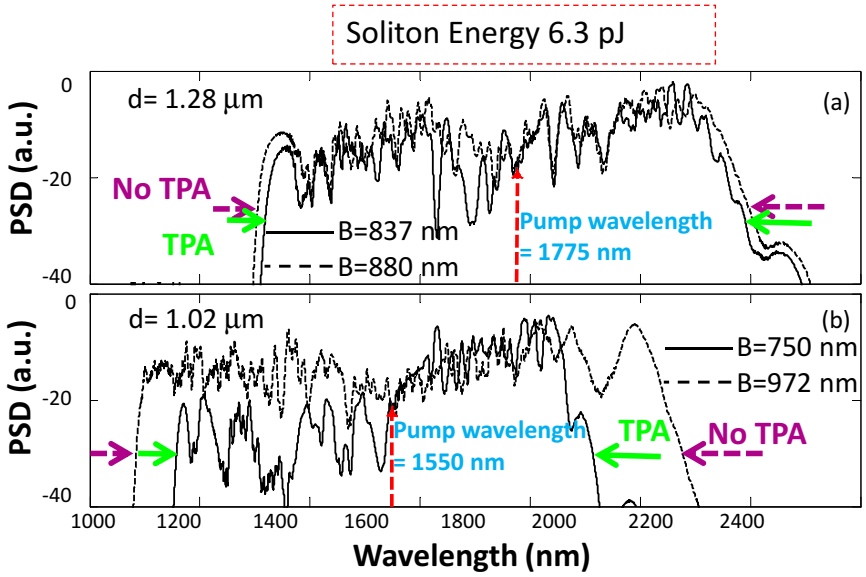

Figure 4.9: *SC spectra obtained numerically including TPA (solid) and not including TPA (dashed). In (a), λ_p=1775 nm in a microwire of d=1.28 µm. In (b), λ_p=1550 nm in a microwire of d=1.02 µm. All simulations are made with pulses of pulse energy of 6.3 pJ. B: Bandwidth at -20 dB; d: microwire diameter.*

of spectral broadening in As_2Se_3 at λ_p=1550 nm (B=750 nm), while having a minor influence at λ_p=1775 nm (B=837 nm). The difference in the spectral broadening are due to the higher value of TPA coefficient at λ_p=1550 nm and the smaller A_{eff} in d=1.02 μm.

4.7 Tunability of SC generation using SSFS

By varying the wavelength of the FS, a quantitative change in the spectra is observed. Figure 4.10 shows the spectral bandwidth for the SC spectra generated using FS at 1675 nm, 1740 nm, and 1775 nm wavelengths. As one would expect, the soliton with a wavelength lying in the anomalous dispersion generates the broadest spectrum.

In fig. 4.11, the SC generated at a pulse energy of 6.3 pJ is depicted for the three soliton wavelengths. The figure shows also the spectral broadening using the mode-locked laser

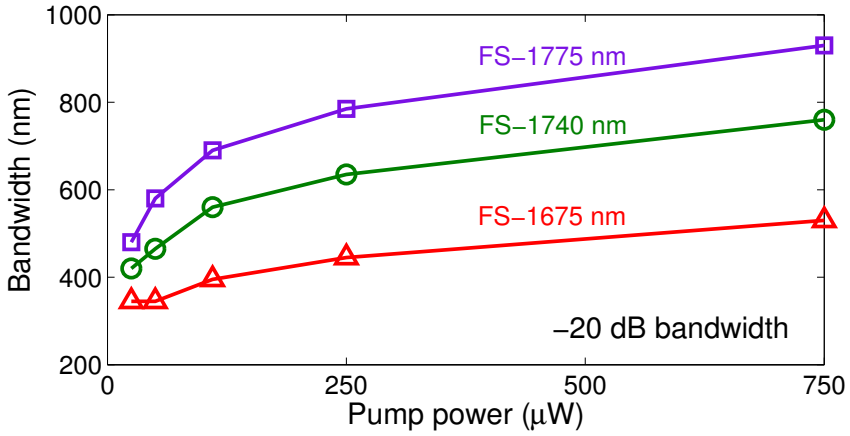

Figure 4.10: *Spectral broadening above the -20 dB level obtained using FSs centered at 1675 nm, 1740 nm, and 1775 nm.*

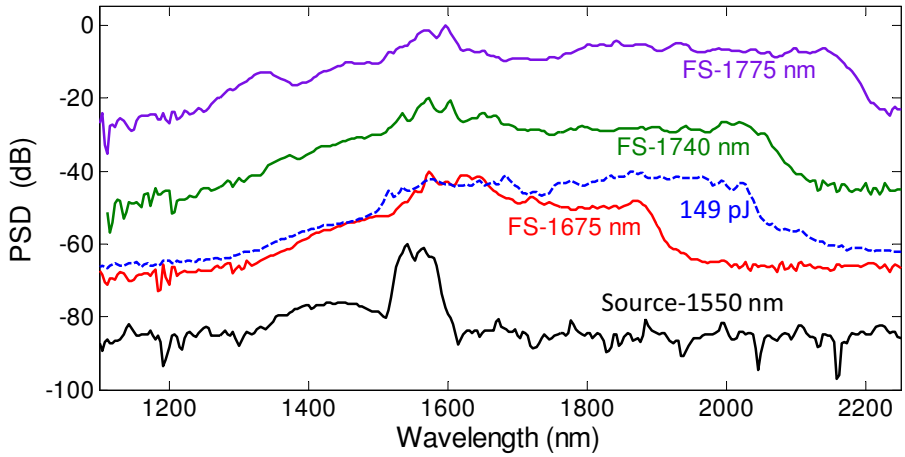

Figure 4.11: *SC generated at a pump energy of 6.3 pJ (solid-line) from solitons at 1550 nm, 1675 nm, 1740 nm, and 1775 nm. SC generated at a pump energy of 149 pJ (dashed-line) from soliton at 1675 nm. The measured continuum spectra are depicted with an offset of 20 dB.*

source. Pumping the microwire in the normal dispersion using the FS -1675 nm prevents efficient spectral broadening. However, at high pump power levels (149 pJ), where the spectral broadening is dominated by SPM, a SC is observed with a flat distribution of energy (dashed-line).

4.8 Summary and conclusion

In this chapter, I have discussed the demonstration of a broadband SC generation in a As_2Se_3 microwire spanning from 1260 nm to 2200 nm by avoiding the TPA effects. Using the SSFS process, the pump wavelength at 1550 nm is tuned toward longer wavelengths to avoid the TPA effects, thereby enhancing SC generation. Such a SC source is also an attractive option to extend the SC generation in the mid-IR and to build a broad, tunable SC source.

Chapter 5

Optimization of As_2Se_3 tapered fibers for mid-infrared supercontinuum generation and influence of water vapor absorption

5.1 Introduction

After the successful demonstration of light generation in the visible and infrared wavelength range, the design of SC sources has shifted to the mid-IR due to the many promising applications in this wavelength range [1]. Current mid-IR SC sources have been demonstrated in different media including planar waveguides [169, 170], bulk crystals [171], and optical fibers [9]. In contrast to other SC sources, the fiber-based SC source exhibits attractive features in terms of beam quality, robustness, compactness, and pump power requirements [20]. Demonstrations of mid-IR fiber SC have been reported with different host materials such as chalcogenides [172, 173], bismuth [174] germanate-glass [175], fluoride [41, 176], and tellurite [37, 177, 178]. Nonetheless, pump sources with pulse

energies at the milli- and nano- Joule levels are required to achieve an octave spectral broadening in such fibers. At low pump power conditions, ChG fibers based on selenium (As_2Se_3) are particularly attractive for generating a broadband SC over short fiber length due to their large n_2 value that is $\sim$930 times that of silica [49], and their wide transparency window that spreads from 1 μm to 12 μm [78]. The ZDW of As_2Se_3 fibers was shifted from the mid-IR down to the central wavelength of the available pump laser by tapering As_2Se_3 fibers into microwires with a diameter in the micron range [80], or by optimizing the design of PCFs [179]. In As_2Se_3 mcirowires [68], as was shown in chapter 4, limitations of TPA on SC generation were discussed, and a SC spectrum was expanded to a wavelength of 2200 nm.

Tapered fibers of As_2Se_3 are attractive for generating a mid-IR SC using low pulse energy sources, due to their high waveguide nonlinearity ($\gamma_{As_2Se_3wire} > 3 \times 10^5 \gamma_{SMF}$). However, the pump pulse characteristics (energy and duration) and the structure of the tapered fiber significantly influence the extent of SC spectral broadening. The pulse parameters depend on the lengths of the untapered and transition regions of a tapered fiber, and on the length of SMF when it is connected to a tapered fiber as shown in fig. 5.1(a). The position of the input pulse relative to the microwire ZDW is also critical for achieving a wide spectral broadening. This is because the magnitude of dispersion increases rapidly to large values as the pump wavelength is detuned from the wavelength of zero-dispersion. Figure 5.1(b) shows a comparison of the dispersion profile of the ChGs As_2Se_3 and As_2S_3 microwires of same ZDW. In the anomalous dispersion, for instance, the large magnitude of dispersion influence the solitonic propagation dynamics which rapidly increases their temporal duration and stops their shifting to longer wavelengths. Therefore, the generation of a mid-IR SC at low pulse energy with the maximum possible bandwidth requires optimization of the whole structure of the tapered fiber. Mid-IR SC sources of low power are ideal for many applications including gas sensing [180], and physical therapy [181].

In this chapter, I present an As_2Se_3 microwire that is capable of generating a mid-IR SC at a pulse energy of only E_p = 124 pJ, using a Tm-doped mode-locked fiber laser. The SC spectrum covers a range of 1400-2810 nm (25 dB) and 1500-2480 nm (10 dB). To achieve this spectral broadening at a low pulse energy level, I first develop a numerical model which indicates the optimal pulse parameters and the optimum structure of the tapered fiber, i.e. dispersion profile and lengths of the different parts of the tapered fiber, that maximizes the bandwidth of SC generation. In the numerical model, the whole structure of the tapered fiber is considered while connected to a SMF made of silica. All the fiber parameters, i.e. dispersion, Kerr nonlinearity index, effective mode area, are implemented as a function of wavelength and diameter. This is necessary due to the broad spectral coverage by the SC spectrum and the dependence of the fiber parameters on the diameter of the tapered fiber which varies along the light propagation path. It is also important to include SMF in the model as it imposes a chirp on the pulse and broadens the spectrum at high input pulse energies. Second, I experimentally generate a SC from the designed tapered fiber and compare it with numerical simulations to validate the numerical model. Finally, I investigate the influence of water vapor absorption on the generated spectrum originated from an open air propagation between the fiber and the spectrometer, and inside the spectrometer.

5.2 Experimental setup

Figure 5.1(a) shows a schematic of the SC source. The pump laser is a Tm-doped mode-locked laser emitting pulses with a duration of 800 fs, an energy up to 180 pJ, at a repetition rate of 30 MHz, and centered at a wavelength of 1940 nm. A variable optical attenuator inserted before the As_2Se_3 tapered fiber controls the pulse energy delivered to the input of the microwire.

The As_2Se_3 tapered fiber is prepared from an As_2Se_3 fiber similar to the one presented

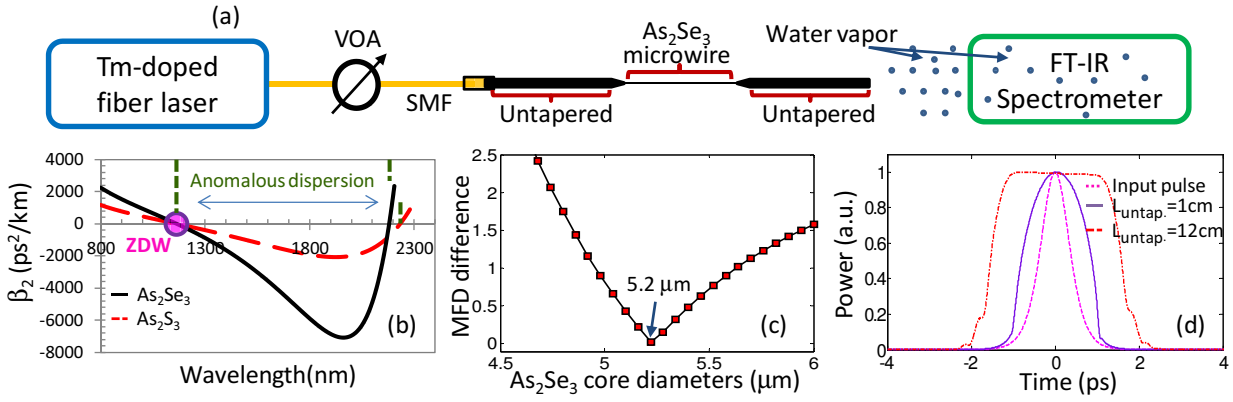

Figure 5.1: *a) Experimental setup for SC generation. VOA: Variable optical attenuator. b) Dispersion profiles of As_2Se_3 and As_2S_3 wires of same ZDW. c) Mode-field distribution difference between As_2Se_3 and SMF. d) Temporal profile of pulses input to: SMF (dashed), As_2Se_3 wire with 1 cm (solid) and 12 cm (dashed-dotted) untapered lengths.*

in chapter 2 & 4. The fiber is first pre-tapered to a core diameter of 5.2 μm to match the MFD in a SMF made of silica (Figure 5.1(c)). The MFD is calculated by: MFD $=$ $d(0.65 + (1.619/V^{3.5}) + (2.879/V^6)); V = \pi d\sqrt{n_{core}^2 - n_{cladding}^2}/\lambda$, where d, V, and n are the fiber diameter, V-number, and linear refractive index, respectively. One of the end-face is polished and coupled to a SMF. The Fresnel reflection, mode-mismatching, and the degree of alignment at the SMF-As_2Se_3 interface induces a measured coupling loss of 1.6 dB. Using the tapering process described in [167], a 1 cm long section in the central part of the fiber is heated and stretched into a 10 cm long microwire, resulting in a tapering loss of 2 dB. The fabricated tapered fiber thus consists of an untapered input section, a transition region, a microwire section which is connected to an untapered output section through another transition region. The output end of the fiber is polished and left unconnected. The SC spectrum generated by the microwire travels through an open-air path before reaching a Fourier Transform Infrared Spectrometer (FT-IR). The FT-IR is purged with dry nitrogen to reduce the concentration of the H_2O molecules

in the air. However, even after purging the relative humidity (RH) remains 30 % inside the FT-IR (the value is good enough to sustain the beam splitter from damage) through which the spectrum travels on a path of ∼1 m. In addition, the spectrum travels ∼0.25 m on an unpurged path length from the fiber to the FT-IR, in which the RH is 70 %.

5.3 Numerical simulation

Efficient SC generation in the microwire requires precise control of the GVD profile. It also requires optimization of the temporal properties of the pump pulses at the microwire input (fig. 5.1(d)), which strongly depend on the lengths of the SMF fiber, untapered input section and transition region of the As_2Se_3 fiber. As a result, numerical simulations of SC generation are first performed by solving the GNLSE, using the RK4IP, to optimize the output spectrum for a single experiment. Due to the shot-to-shot spectral fluctuations in the input spectra, an ensemble of 20 simulations are carried with different initial random noise seeds for each input pulse. The mean spectrum of this ensemble is also averaged using a bandwidth resolution which is comparable to laboratory measurements to mimic the finite spectrometer spectral resolution.

Figure 5.2(a) shows the numerically calculated SC bandwidth as a function of untapered input section lengths and wire diameters. In the numerical simulation, a sech pulse profile is assumed to propagate a path of 270 cm along a SMF, through variable untapered input section lengths, 2.54 cm transition regions (both sides of the microwire) to satisfy adiabatic conditions, a 10 cm microwire, and a 1 cm untapered output section. The pulse is discretized into 2^{14} samples with a temporal window width of 64 ps. The higher-order dispersion terms are included up to 9th order. The contribution of self steepening and delayed Raman response is included with f_R =0.1, τ_1=23 fs and τ_2=195 fs are chosen to best fit with the experimental measurements [168] of the Raman gain spectrum in As_2Se_3. TPA (λ) [69], loss $\alpha(\lambda)$, Kerr nonlinearity index $n_2(\lambda)$ [182], and effective mode

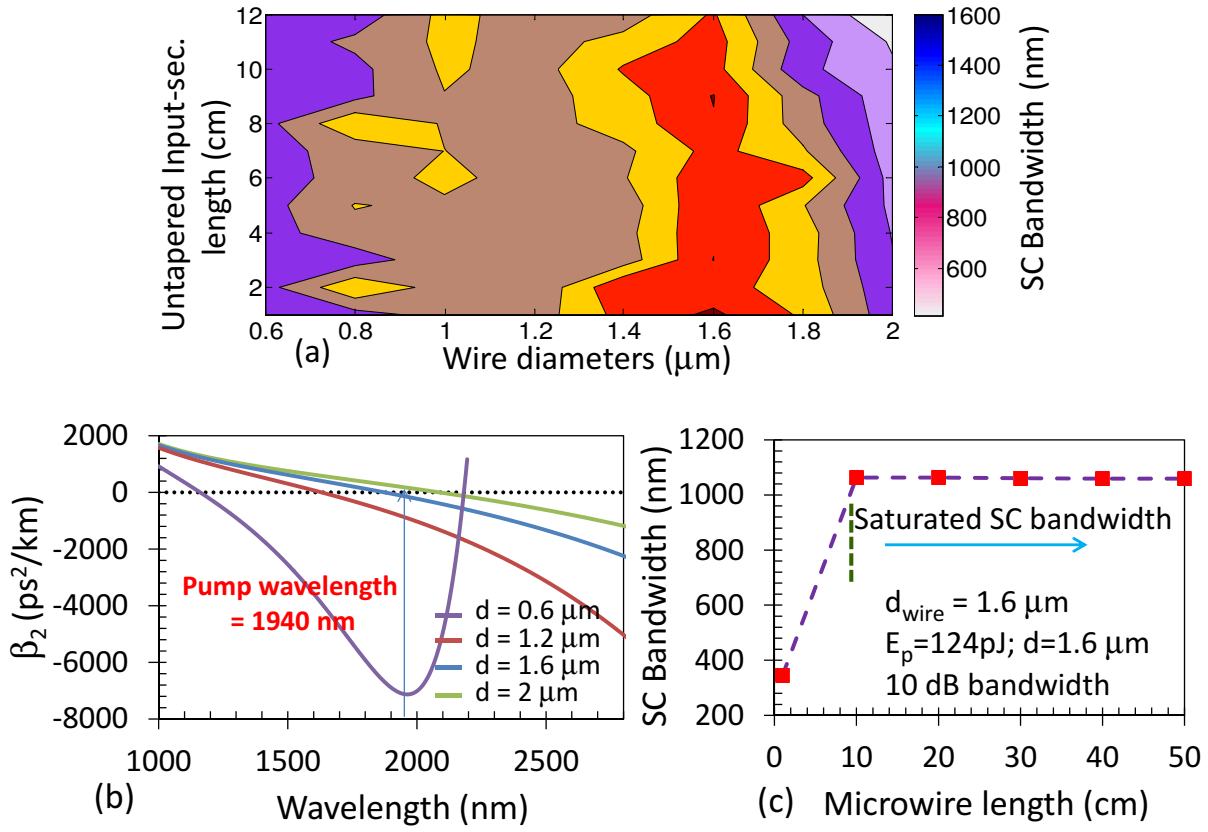

Figure 5.2: *a) Calculated SC bandwidths as the microwire diameters and lengths of the untapered input section of As_2Se_3 fiber are changed. The length of the microwires is 10 cm. b) Calculated waveguide dispersion for As_2Se_3 microwires with diameters of values between 0.6 µm and 2 µm. c) Calculated SC bandwidths as the microwire length is changed.*

area $A_{eff}(\lambda)$ curves are also included. From the figure, the maximum spectral broadening is achieved for a 1 cm long untapered input section length and a diameter of 1.6 μm. Figure 5.1(c) shows the pulses input to: SMF fiber (dashed), and microwire section with 1 cm (solid) and 12 cm (dashed-dotted) untapered section lengths. Figure 5.2(b) shows the calculated GVD versus wavelength for several As_2Se_3 microwire diameters. For the 1.6 μm microwire diameter, the pump pulse lies close to ZDW ($\sim$1850 nm) in the anomalous dispersion regime with β_2 = -15.6 ps^2/km, A_{eff} = 1.25 μm^2 and γ = 35.6 $W^{-1}m^{-1}$. This pump condition is ideal to achieve maximum spectral broadening [33]. Figure 5.2(c) shows that no further spectral broadening of SC is obtained in a microwire with a diameter of 1.6 µm, despite the increase of the microwire length longer than 10 cm.

In fig. 5.3(a), the SC bandwidth is depicted as a function of the input pulse energy and the untapered length. The figure shows that the SC increases as the pulse energy increases. The maximum SC bandwidth is achieved for the combination of E_p=620 pJ and untapered length of 1 cm. However, the SC bandwidth decreases as the untapered section length increases and for pulse energies larger that 620 pJ. Figure 5.3(b and c) shows the spectral and temporal evolution of the pulse along the SMF and the untapered section with E_p=620 pJ and E_p=1110 pJ. For E_p=1110 pJ (soliton order N=2.5), the pulse undergoes a soliton fission in SMF and split into two solitons, which both then undergo a *walk-off effect* in the untapered section. This effect spreads the energy over a long time window, and thus lower the pulse energy density entering the microwire.

5.4 Experimental results

Figure 5.4(a) shows the experimental results of SC generation as a function of microwire diameters, all of which have a 1 cm long untapered input section. The SC spectra are generated using the maximum pulse energy of the Tm-doped laser. The maximum spectral broadening is obtained with a 1.6 μm microwire diameter. This confirms the numerical

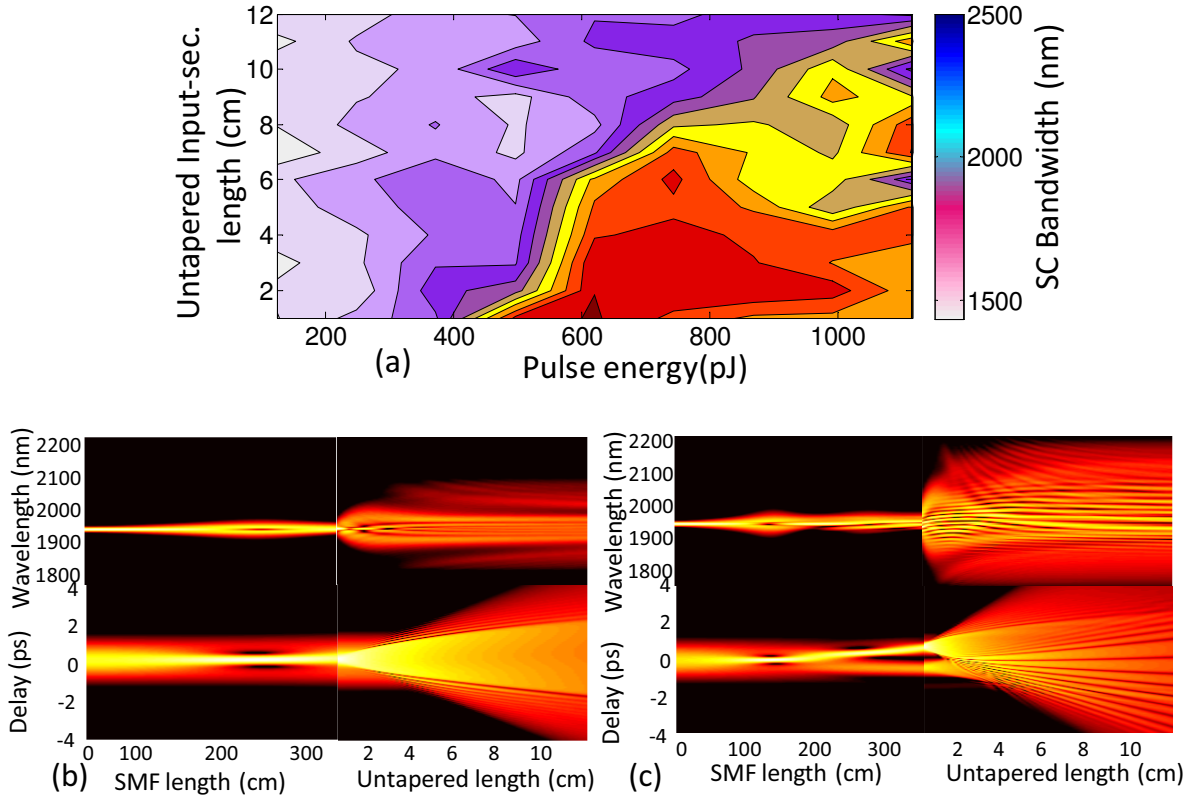

Figure 5.3: *a) Calculated SC bandwidths as the pulse energies and lengths of the untapered input section of As_2Se_3 fiber are changed. The length and diameter of the wire are 10 cm and 1.6 µm, respectively. Spectral and temporal evolution of the pulse with: b) E_p=620 pJ and c) E_p=1110 pJ along the SMF and untapered section.*

calculations of the SC generation in fig. 5.4(a). For the 0.6 μm and 1.2 μm microwire diameters, the pump experiences large magnitudes of GVD, which results in an increased temporal pulse broadening, and thus less output spectral broadening compared to that obtained with a 1.6 μm microwire diameter. For the 2 μm microwire diameter, the less spectral broadening is referred to the smaller γ of this diameter compared to a 1.6 μm microwire diameter, and for pumping in the normal dispersion regime. In fig. 5.4(b), the SC spectra generated from the 1.6 μm microwire diameter are depicted as a function of the launched pulse energy. The pulse energy values depicted in the figure take into consideration the coupling loss. At the pulse energy E_p = 124 pJ, the spectrum covers a spectral bandwidth from 1400 nm to 2810 nm wavelengths at a level 25 dB below the peak value. The long wavelength edge of the generated spectrum is limited by the absorption of OH impurity [89, 90] in the fiber. Also, the dip in the spectrum beyond 2500 nm is attributed to the water vapor absorption in the atmosphere [183, 184] while traversing the 1.25 m path length inside the FT-IR and between the fiber and the FT-IR.

Figure 5.5(a) shows the intensity of three types of absorption bands: the atmospheric water vapor at RH = 30 % and 70 %; OH contamination in the As_2Se_3 fiber (OH concentration $\sim$6 ppm [90, 185]); and intrinsic losses of As_2Se_3 at the wavelengths of interest. The water vapor absorption band spans from 2400 nm to 3000 nm wavelengths. The OH impurity has a peak value at 2900 nm and spans from 2600 nm to 3500 nm wavelengths.

5.5 Influence of OH impurity and H_2O on SC generation

To demonstrate the effect of water vaper absorption on spectral broadening, the SC generation is numerically studied as shown in fig. 5.6 while including the three losses (dashed line), intrinsic and OH impurity losses (dashed-dotted line), and only intrinsic loss (dotted line) in the GNLSE. The calculated spectra are obtained for the 1.6 μm microwire diameter and from pulses of E_p = 124 pJ, and travels on a path of 0.25 m

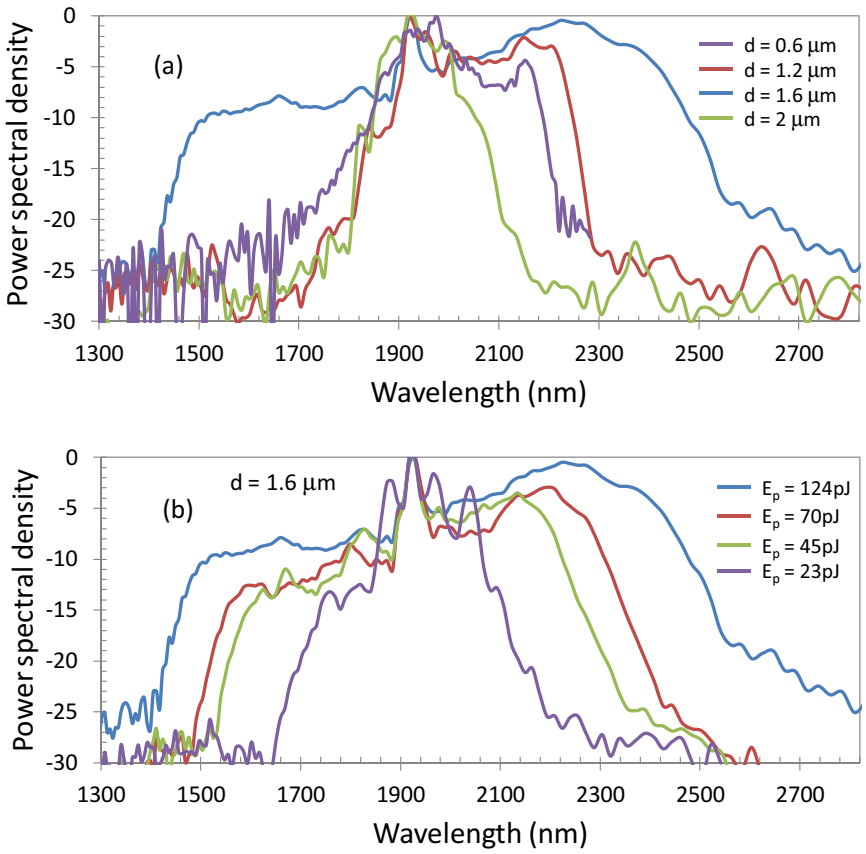

Figure 5.4: *Experimentally generated SC spectra for several As_2Se_3 microwire diameters and source energy values (microwire length = 10 cm, untapered input section length = 1 cm). a) microwire diameters vary between 0.6 µm and 2 µm. b) Launched pulse energy increase up to the maximum pulse energy delivered by the Tm-doped source.*

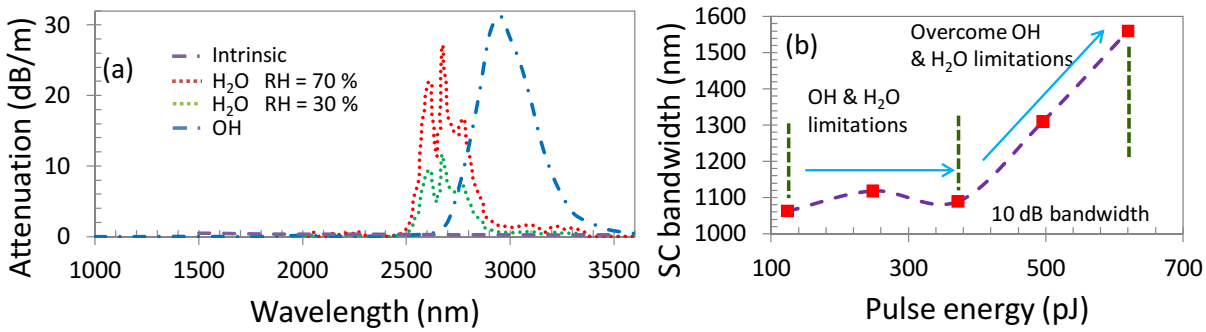

Figure 5.5: *Measured attenuation curves as a function of wavelength for OH impurity (dashed-dotted line), water vapor (dotted line), and As_2Se_3 material (dashed line). b) Calculated SC bandwidths as the pulse energy increases above the maximum source pulse energy.*

unpurged and 1 m purged lengths. Numerical simulations fit the measured spectrum when all losses are included and indicate that by eliminating the water vapor absorption, the spectrum carries larger energy at wavelengths beyond 2500 nm. The results also reveal that OH is not significantly affecting the SC bandwidth at the source energy level. However, purification methods of As_2Se_3 are now available to reduce the concentration of OH impurity [185].

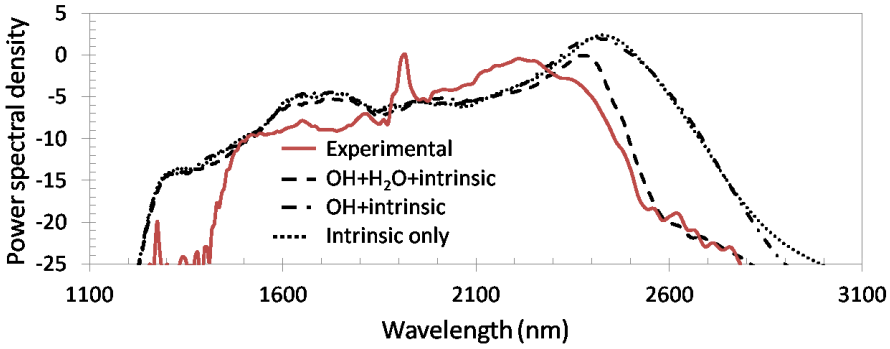

Figure 5.6: *Measured (solid-line) and calculated SC spectra for a 1.6 µm microwire diameter and from pulse energy of 124 pJ while including in the GNLSE the three losses; water vapor and intrinsic losses; and intrisic loss only.*

The long wavelength edge of the SC spectrum can be extended further to the mid-glsir regime, and overcome OH impurity band, by using laser sources of higher pulse energy as shown in fig. 5.7 and fig. 5.5(b), or sources operating at longer wavelengths. For biomedical applications that require radiation emission at wavelengths beyond 2500 nm, the fiber could be placed close to the examined tissue or in a dry environment and thus avoid the influence of water vapor absorption.

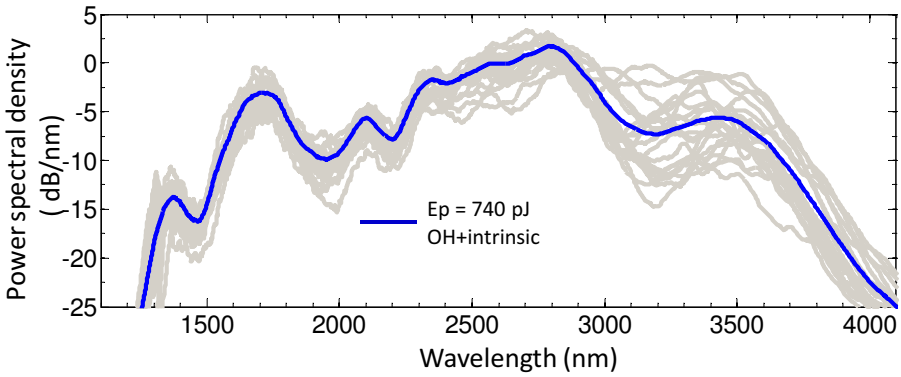

Figure 5.7: *Calculated SC spectra for a 1.6 µm microwire diameter and from pulse energy of 740 pJ while including in the GNLSE the OH and intrisic losses. The blue curve is the mean of 20 simulations of pulses with random noise.*

5.6 Summary and conclusion

In this chapter, I have presented a numerical to optimize the pulse parameters and the design of tapered fibers to maximize the bandwidth of SC generation in As_2Se_3 microwires. I have also depicted the demonstration of a SC generation in the mid-IR regime using an As_2Se_3 microwire by pumping with pulses of low energy from a Tm-doped fiber laser operating at 1940 nm. The generated spectrum covers a spectral bandwidth region spanning from 1400 nm to 2810 nm. By eliminating the atmospheric water vapor absorption, the spectrum carry more energy at the long wavelength edge. Increasing the pump pulse

energy overcome the OH impurity absorption band and extends the generation of SC further to the mid-IR wavelengths.

Chapter 6

Conclusion

In this thesis, I have presented a research on the SSFS and SC generation in As_2Se_3 microwires. I summarize the research work as follows:

In chapter 3, an analytical description of the soliton dynamics in As_2Se_3 microwires was presented. The importance of the input soliton energy along with the effect of the longitudinal confinement of the mode on the $SSFS_r$ were investigated. These descriptions were very helpful as they were used in optimizing the non-uniform microwire profiles. I found that a wide soliton wavelength-shift requires an optimization in the soliton input parameters and the fiber parameters. For this reason, an investigation of the SSFS in uniform and non-uniform microwires was conducted.

The optimum uniform microwire design was chosen such that soliton undergoes the maximum possible wavelength shift along a certain microwire length. However, this fiber limits the extent of wavelength-shift by its long ZDW. Consequently, research on non-uniform microwires was conducted to avoid this limitation.

Two methods to design non-uniform microwires were presented, which lead to a large soliton wavelength-shift and allow wide wavelength tuning while preserving the soliton energy from any perturbations.

In the first method which I referred to it as CSB-M, the wavelength-shifting soliton

was controlled such that it remains at a fixed spectral separation from the ZDW along the propagation path in a non-uniform microwire. The simulation results revealed the advantages of using non-uniform microwires to increase the wavelength shift in comparison with uniform microwires [68].

In the second method which I referred to it as P-M, the change of the soliton temporal duration and that of the TOD along the non-uniform microwire was considered. This designed microwire allowed a higher rate of $SSFS_r$ which manifests as wavelength shift of 860 nm in only 10 cm of microwire length [69].

In chapter 4, a broadband SC spectrum spanning from 1260 to 2200 nm using a 10 cm long As_2Se_3 microwire pumped at a wavelength of 1550 nm was presented. Such a wide SC in As_2Se_3 was obtained by avoiding the effects of TPA normally observed at a wavelength of 1550 nm. For this purpose, analytical expression of the full TPA spectrum from the visible to mid-IR wavelength range was presented. The pump soliton was initially self-frequency shifted toward longer wavelength by means of the Raman effect in standard silica fiber before being launched into the ChG microwire for spectral broadening. The presented scheme can be used in generating a tunable SC source in the mid-IR wavelength regime.

In chapter 5, a numerical model was developed to indicate the optimal pulse parameters and the optimum structure of tapered fiber for a maximum bandwidth of SC generation. A demonstration of a mid-infrared SC source based on a As_2Se_3 microwire and a thulium-doped fiber laser was presented. A SC spectrum extending from 1400 nm to 2810 nm is generated in a 10 cm long As_2Se_3 microwire from low-energy pulses of 124 pJ. The chapter also discussed the effects of the water vapor absorption on the energy carried in the SC spectrum, and the limitation by the absorption band of OH impurity for extending the SC spectrum in the mid-IR regime.

Future Perspective

In future, the SSFS could be experimentally demonstrated in both uniform and non-uniform As_2Se_3 microwires by using a femtosecond mid-IR pulsed source. The pulse duration should be short enough to induce a significant wavelength conversion. Non-uniform microwire should help reducing the power requirements to reach a given wavelength conversion in comparison to uniform microwire. To achieve this, first, pulses of the pump source should be compressed down to a temporal duration of a sub-hundred femtosecond by optical wavebreaking or soliton-self compression [11].

For SC generation, As_2Se_3 fiber must be treated first by one of the available purification methods to reduce the absorption band of OH impurity. This allows the SC spectrum to expand further to the mid-IR without being limited or attenuated. A more powerful source and shorter pulse duration could be used other than the one presented in this thesis. This allows the SC spectrum to expand further in the mid-IR regime and with a higher degree of coherency. A microwire with an all-normal-dispersion regime could also be fabricated to generate a SC with a high coherence, bandwidth, and power stability. These spectra could be used in spectroscopy applications. To assure the power stability of the SC spectra, a real-time measurement of the inherent fluctuations of the generated SC spectra could be made by using a dispersive time stretching technique [186]. The advantages of using As_2Se_3 non-uniform microwires for SC generation could also be investigated. Another research topic to be investigated is to generate a broadband SC in the mid-IR regime using an As_2Se_3 microwire coated with a polymer. The use of a more compact picosecond and nonsecond sources other than femtosecond sources could also be investigated in generating SC to reduce the size of the overall system [187–189].

Appendix A

Modeling tapered fibres

A.1 Implementing and solving the GNLSE

In this appendix, I provide information on modeling the pulse propagation in tapered fibres. This mainly corresponds to introducing a diameter (d) dependence on all fiber parameters in the GNLSE. In addition, for simulating a broadband spectra, it is necessary to include the frequency dependence of all the fiber parameters, this includes fiber losses α, dispersion β, waveguide nonlinearity γ, TPA β_{TPA}, and effective mode area A_{eff}. I provide also a summary of some of the available theoretical calculations for the nonlinear refractive index n_2 and recommend a one which gives values that matches the available experimental measurements for As_2Se_3 glass [50].

A.1.1 The interaction picture implementation

The GNLSE in this thesis is solved using the RK4IP method that is faster and more accurate than the split-step Fourier method (SSFM). The SSFM has been traditionally used to solve the GNLSE (see e.g. [11] for explanation about the implementation of this method). The RK4IP method works by expressing the GNLSE as:

$$\frac{\partial A\left(z,\tau\right)}{\partial z}=\left(\widehat{D}+\widehat{N}\right)A\left(z,\tau\right), \tag{A.1}$$

where $\widehat{D}$ and $\widehat{N}$ are the dispersive and nonlinear operators, respectively,

$$\begin{aligned}&\widehat{D}=i\sum_{n\geqslant 2}\frac{i^{n}\beta_{n}\partial_{\tau}^{n}}{n!}A\left(z,\tau\right);\\&\widehat{N}A\left(z,\tau\right)=i\gamma(\delta)\left(1+\frac{i}{\delta_{o}}\frac{\partial}{\partial t}\right)\left(A\left(z,\tau\right)\int_{-\infty}^{\infty}R\left(\tau^{'}\right)\left|A\left(z,\tau-\tau^{'}\right)\right|^{2}d\tau^{'}\right).\end{aligned} \tag{A.2}$$

The RK4IP method explicitly gives the pulse envelope at A(z+h,τ) from calculated with a RK4IP solver. In the time domain the RK4IP scheme can be stated as follows [190]:

$$\begin{aligned}&\widehat{A}_{I}=F^{-1}\left[exp\left(\frac{h}{2}\widehat{D}\right)\widehat{A}\left(z,\omega\right)\right]\\&k_{1}=F^{-1}\left[exp\left(\frac{h}{2}\widehat{D}\right)F\left[h\widehat{N}\widehat{A}\left(z,\tau\right)\right]\right]\\&k_{2}=h\widehat{N}\left(\widehat{A}_{I}+k_{1}/2\right)\\&k_{3}=h\widehat{N}\left(\widehat{A}_{I}+k_{2}/2\right)\\&k_{4}=F^{-1}\left[h\widehat{N}\left(exp\left(\frac{h}{2}\widehat{D}\right)F\left(\widehat{A}_{I}+k_{3}\right)\right)\right]\\&\widehat{A}\left(z+h,\tau\right)=F^{-1}\left[exp\left(\frac{h}{2}\widehat{D}\right)\left[\widehat{A}_{I}+k_{1}/6+k_{2}/3+k_{3}/3\right]\right]+k_{4}/6,\end{aligned} \tag{A.3}$$

where $\widehat{N}\left(\widehat{A}\right)$ is the non-linear operator applied to $\widehat{A}$, k_i terms are slope increments, and F and F^{-1} are computed numerically using the fast Fourier transform (FFT) and inverse FFT , respectively.

A.2 Fiber parameters

A.3 Theoretical Modeling of Dispersion

The ChG As_2Se_3 microwire is modeled as a step index waveguide with core index n_{core} = 2.83 and cladding index $n_{cladding}$ = 1. In order to calculate the dispersion curves, the eigenvalue equation is numerically solved for the propagation constant β of the fiber and then apply a Taylor expansion for β to derive the group velocity dispersion, and higher order dispersion β_n (n>2):

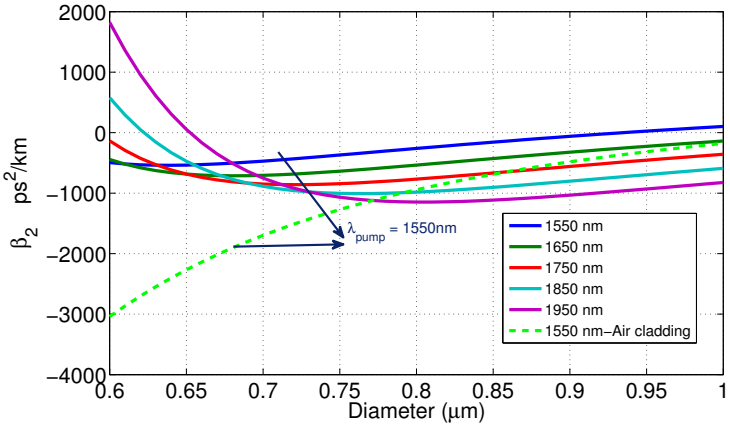

Figure A.1: *The GVD curves depicted as a function of diameters for As_2Se_3-PMMA (solid-curve) and As_2Se_3-air (dashed-curve) microwires.*

$$\left[\frac{J_m'(\kappa a)}{\kappa J_m(\kappa a)} + \frac{K_m'(\gamma a)}{\gamma K_m(\gamma a)}\right] + \left[\frac{J_m'(\kappa a)}{\kappa J_m(\kappa a)} + \frac{n_1^2 K_m'(\gamma a)}{n_2^2 \gamma K_m(\gamma a)}\right] = \left(\frac{2m\beta\left(n_1^2 - n_2^2\right)}{a\kappa^2\gamma^2}\right)^2 \tag{A.4}$$

where $\kappa^2 = n_1^2 c^2 - \beta^2$, and $\gamma^2 = \beta^2 - n_2^2 c^2$, with m being the order of the eigenvalues for the fundamental mode, and a being the radius of the core. The numerical calculation of the GVD for As_2Se_3-PMMA As_2Se_3-air microwires with different diameters and wavelengths is shown in fig. A.1. The dispersion is very sensitive to the microwire diameter.

A.4 Theoretical Modeling of Nonlinear Waveguide nonlinearity

When a fundamental soliton propagates along a fiber, it shifts toward longer wavelength. This consequently changes the transverse mode distribution of the soliton into the surrounding, and the percentage of power inside the As_2Se_3 changes (see fig. A.2). This leads to a change in the waveguide nonlinear parameter of the soliton. Also, for a broadband SC spectrum, the frequency constituents experience different waveguide nonlinearity. Thus, it is not accurate to assume that a frequency-shifted soliton or the generated SC experience a single nonlinear parameter value. In the simulation, the dependence of γ on the mean central frequency shift of the soliton and as a function of frequency for SC generation is included.

Compared to As_2Se_3 fibers, microwires can have much smaller mode areas depending on their diameters. For this, the effective area A_{eff} and the nonlinear coefficient γ are defined as a function of the diameter d for fibers (fig. A.2).

A.5 Nonlinear refractive index

To measure the magnitude of the nonlinearity several models have been developed:

• According to the bond approximation method, Lines at. al. [191] has derived $n_2(0)$ based on the two-level bond orbital approximation:

$$n_2(0) = \frac{3.4\left(n_o^2+2\right)^3\left(n_o^2-1\right)d^2}{n_o^2 E_s^2}.10^{-20}\left(\frac{m^2}{W}\right) \tag{A.5}$$

n_o is the linear refractive index of the material in the long wavelength limit (zero-frequency).

• An alternative expression to $n_2(0)$ was given by Petkov and Ewen [192] as:

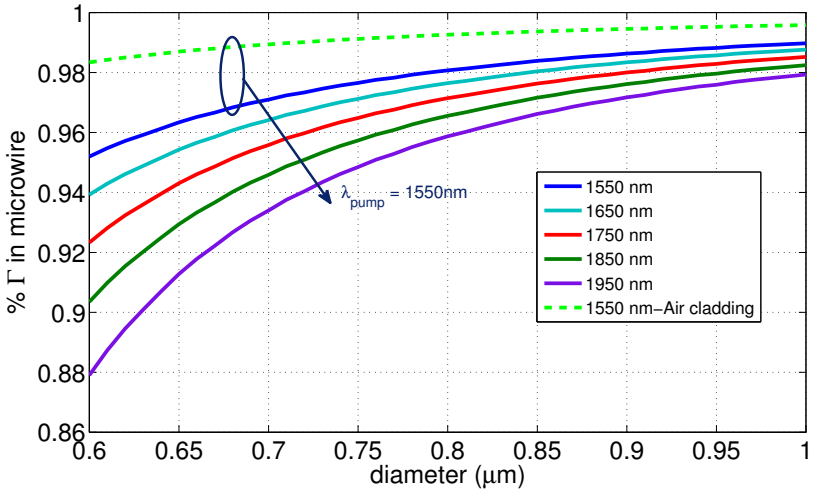

(a)

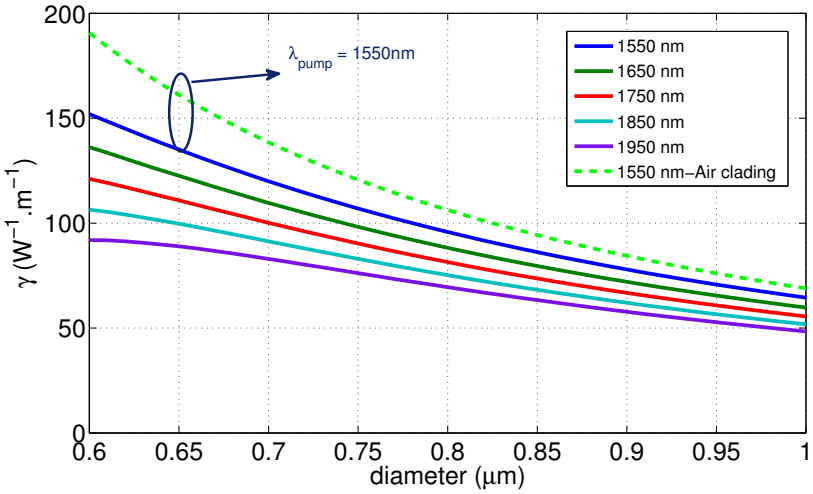

(b)

Figure A.2: *a) The waveguide nonlinearity, and b) the mode confinement inside As_2Se_3 depicted as a function of diameters for PMMA-As_2Se_3 (solid-curve) and air-As_2Se_3(dashed-curve) microwires.*

$$n_2(0) = 4.1.10^{-17} \frac{g\, S \left(n_o^2+2\right)^{1.5} \left(n_o^2-1\right)^2}{n_o^2 E_D E_s^2} \left(\frac{m^2}{W}\right) \tag{A.6}$$

where g is the anharmonicity parameter, S is an oscillator strength parameter, and E_D is the dispersion energy from the Wemple-DiDomenico model. For SCs E_D is approximately 26 eV, and $E_S$for As_2Se_3 is 4.1 eV. According to the equation derived by DiDomenico and shown below, n_o=2.709513501 at ω=0

-The dispersion of the index of refraction can be modeled as:

$$n_o^2(\omega) = 1 + \frac{E_D E_S}{\left[(E_S)^2 - (\hbar\omega)^2\right]} \tag{A.7}$$

• Shiekh-Bahae [193] has predicted the dispersion of n_2 for crsytalline solids based on the Kramers-Kronig relation and represented it by an expression G_2(x) [194, 195] . First, he calculated the two photon absorption coefficients and its dispersion using a two parabolic band model. By using the Kramers-Kronig relation, he then calculated the nonlinear index of refraction as:

$$n_2\left(\frac{m^2}{W}\right) = \frac{40\pi}{c}\frac{3.4.10^{-8}}{n_o^2 E_G^4}.G_2\left(\frac{\hbar\omega}{E_G}\right) \tag{A.8}$$

In ChG this method should be considered as an approximation, since it predicts the value of n_2 for a state-free band-gap. ChG is an amorphous material with an Urbach absorption tail. It has a continuum inter-gap states and exhibit linear absorption well below their normal band-gap. Due to this finite absorption edge, it has a large n_2 values. This is manifested as a peak in just below the half-gap before significant absorption takes place by TPA as we move claser in energy to the half-gap.

• Based on the single oscillator model, the value of n_2 can be extracted from the third-order susceptibility by using two equations [64]:

$$
\begin{aligned}
n_2 &= \frac{12\pi^2}{n_o^2 c} Re\left[\chi^{(3)}\right] \\
\chi^{(3)} &= \frac{e^4}{m^3\omega_o^6 d^4}\left[1-\left(\frac{\omega}{\omega_o}\right)^2\right]^{-4} + \frac{4ie^4}{m^3\omega_o^8 d^5}\left[1-\left(\frac{\omega}{\omega_o}\right)^2\right]^{-5} \\
&toobtain: \\
n_2\left(\frac{m^2}{W}\right) &\approx \frac{3.95.10^{-6}.e^4}{n_o^2 m^3\omega_o^6 d^5}\left[1-\left(\frac{\hbar\omega}{\hbar\omega_o}\right)^2\right]^{-4}
\end{aligned}
\tag{A.9}
$$

• Lenz [182] has combined the above two approaches of Lines and Bahae. He has used eq. (A.5) and eq. (A.8) to predict the long wavelength value of n_2 and normalize $G_2\left(\frac{\hbar\omega}{E_G}\right)$ of eq. (A.8) to unity in the long wavelength limit by multiplying it by 512/7.

$$
n_2\left(\frac{m^2}{W}\right) = \frac{3.4.10^{-20}\left(n_o^2+2\right)^3\left(n_o^2-1\right)d^2}{n_o^2 E_s^2}.G_2'\left(\frac{\hbar\omega}{E_G}\right) \tag{A.10}
$$

In this thesis, this approach is followed to calculate n_2. The parameters were adjusted to match the experimental measurements of [50]. c = 299.792458, h = 4.13566733e-3, E_d = 26, E_g = 1.78, E_s = 2.5E_g, d = 0.25.

A.6 Two photon absorption curve

Below is the matlab code to generate the whole TPA curve of As_2Se_3:

```
%-------------------------------------------------------------------------
% Two photon absorption
%-------------------------------------------------------------------------
c = 299792.458;                                %speed of ligth nm/ps
h = 4.13566733e-3; % [eV.psec],
%Plank's constant (h = 6.62606896e-34[J.sec]/1.6e-19)
```

```
%-------------------------- parameters-----------------------------
Eg = 1.78;
K = 1220;
Ep = 21;
segma = 1/16;
%-------------------------------------------------------------------------
Eph1 = 0.3:0.01:0.96;
Eph2 = 0.96:0.01:1.5;

f1 = Eph1./h;
lamda1 =(c./f1)*1e-3;

n1 = sqrt(1 + lamda1.^2.*(0.2274./(lamda1.^2-508.05159)...
 + 6.74238./(lamda1.^2-0.10545)));

f2 = Eph2./h;
lamda2 =(c./f2)*1e-3;

n2 = sqrt(1 + lamda2.^2.*(0.2274./(lamda2.^2-508.05159)...
 + 6.74238./(lamda2.^2-0.10545)));

x = Eph2./Eg;
m = 2*x;
F2 = ((m-1).^(3/2))./(m.^5);

BtpaL = 1e-20.*(K.*sqrt(Ep)./(n1.^2.*Eg.^3)).*exp(((Eg-0.12381+Eph1)./segma));
```

```
BtpaH = (K.*sqrt(Ep)./(n2.^2.*Eg.^3)).*F2;

%Experimental data
Eph3=1.78*[0.6546
0.559053
0.449424];

BBTPA=[5.35
2.795128
0.14];

figure,
plot(Eph2, BtpaH, 'k-');
hold all;
plot(Eph1, BtpaL, 'k--', Eph3, BBTPA, 'ro');
grid on;
set(gca,'FontSize',14);
xlabel('E_{photon} (ev)');
ylabel('\beta_{TPA} [cm/GW]');
```

Abstract publications

Journal publication I

Mid-infrared sources based on the soliton self-frequency shift

A. Al-kadry and M. Rochette

J. Opt. Soc. Am. B 29, 1347–1355 (2012).

Abstract: We present a method to maximize the soliton SSFS in microwires with diameter profiles varying nonuniformly along the soliton propagation path. The method is divided into two steps. The first step consists in selecting the input microwire diameter that leads to the highest rate of frequency shift per unit of propagation length. The second step consists in increasing gradually the microwire diameter along the soliton path to suppress dispersive wave emission and maintain a large rate of frequency shift per unit of propagation length. We first propose and apply a rule to select the initial diameter using the adiabatic theory. The optimal diameter profile is then achieved by maintaining the red-shifting soliton at a fixed spectral separation from the zero-dispersion wavelengths. The optimized profile supports solitons with different input energies that allow a wavelength shift up to 650 nm from the 2100 nm pump wavelength in a 20 cm microwire length. We compare our results with the SSFS generated in microwires with uniform diameter profile to illustrate the enhancement of wavelength shift in the designed nonuniform microwire.

Journal publication II

Maximized Soliton Self-Frequency Shift in Non-Uniform Microwires by the Control of Third-Order Dispersion Perturbation

A. Al-kadry and M. Rochette

J. Lightwave Technol. 31, 1462–1467 (2013).

Abstract: We present a simple method based on the soliton perturbative theory to design microwires of non-uniform diameter profiles. In contrast to previous methods, the one presented here relies on minimizing the soliton perturbation by third order dispersion (TOD) while taking into account the change of the soliton local duration along the microwire. The method leads to a design that maximizes the soliton self-frequency shift in non-uniform microwires. The microwire design comprises a unique dispersion profile such that a wavelength-shifting soliton experiences only weak perturbations from the TOD and avoids shedding its energy into the dispersive waves. The TOD perturbation is quantified with an analytic expression that is kept below a threshold value, thus keeping a soliton weakly perturbed by TOD in every position within the microwire. Numerical simulations are conducted to check the validity of the method. We consider a fundamental soliton centered at a wavelength of 2000 nm propagating in As_2Se_3 microwires of length as short as 10 cm. The results show that optimized non-uniform diameter profile allows the tuning of the self-frequency shifted soliton over a spectral range of 860 nm.

Journal publication III

Broadband supercontinuum generation in As_2Se_3 chalcogenide wires by avoiding the two-photon absorption effects

A. Al-kadry, C. Baker, M. El Amraoui, Y. Messaddeq, and M. Rochette

Opt. Lett. 38, 1185-1187 (2013).

Abstract: We report the generation of a broadband SC spanning from 1260 to 2200 nm using a 10 cm long As_2Se_3 chalcogenide (ChG) wire pumped at a wavelength of 1550 nm. Such a wide SC in As_2Se_3 is obtained by avoiding the effects of two-photon absorption normally observed at a wavelength of 1550 nm. For this purpose, the pump soliton is initially self-frequency shifted toward longer wavelength by means of the Raman effect in standard silica fiber before being launched into the ChG wire for spectral broadening.

Bibliography

[1] M. E. Zadeh and I. T. Sorokina. *Mid-Infrared Coherent Sources and Applications*. Springer, 2008.

[2] N. Nishizawa and T. Goto. "Mid-infrared photonics". *Nat. Photonics* 6.7 (2012), pp. 407–498.

[3] J. Biegert, P. Bates, and O. Chalus. "New Mid-Infrared Light Sources". *IEEE J. Sel. Topics Quantum Electron.* 18.1 (2012), pp. 531–540.

[4] D. Hudson, S. Jackson, and B. Eggleton. "Novel laser sources in the mid-Infrared". In: *Photonics (ICP), 2012 IEEE 3rd International Conference on*. 2012, pp. 381–385.

[5] R. Won. "Shining in the mid-infrared". *Nat. Photonics* 5.5 (2011), pp. 457–458.

[6] A. Schliesser, N. Picqué, and T. W. Hänsch. "Mid-infrared frequency combs". *Nat. Photonics* 6.7 (2012), pp. 440–449.

[7] I. T. Sorokina and K. L. Vodopyanov. *Solid-state mid-infrared laser sources*. Vol. 89. Springer, 2003.

[8] S. A. Diddams. "Frequency comb sources and techniques for mid-infrared spectroscopy and sensing". In: *CLEO: Science and Innovations*. Optical Society of America. 2013.

[9] S. D. Jackson. "Towards high-power mid-infrared emission from a fibre laser". *Nat. Photonics* 6.7 (2012), pp. 423–431.

[10] F. S. L. Mescia and F. Prudenzano. "New Trends in Amplifiers and Sources via Chalcogenide Photonic Crystal Fibers". *International J. Opt.* 2012.17 (2012).

[11] G. P. Agrawal. *Nonlinear fiber optics*. 4^{th}. Academic Press, 2007.

[12] F. M. Mitschke and L. F. Mollenauer. "Discovery of the soliton self-frequency shift". *Opt. Lett.* 11.10 (1986), pp. 659–661.

[13] J. P. Gordon. "Theory of the soliton self-frequency shift". *Opt. Lett.* 11.10 (1986), pp. 662–664.

[14] T. Izawa, N. Shibata, and A. Takeda. "Optical attenuation in pure and doped fused silica in the ir wavelength region". *Appl. Phys. Lett.* 31.1 (1977).

[15] J. Fatome, B. Kibler, M. El-Amraoui, J.-C. Jules, G. Gadret, F. Desevedavy, and F. Smektala. "Mid-infrared extension of supercontinuum in chalcogenide suspended core fibre through soliton gas pumping". *Electron. Lett.* 47.6 (2011), pp. 398–400.

[16] C. Xia, M. Kumar, M.-Y. Cheng, O. Kulkarni, M. Islam, A. Galvanauskas, F. L. Terry, M. Freeman, D. A. Nolan, and W. Wood. "Supercontinuum Generation in Silica Fibers by Amplified Nanosecond Laser Diode Pulses". *IEEE J. Sel. Topics Quantum Electron.* 13.3 (2007), pp. 789–797.

[17] J. Lee, J. van Howe, C. Xu, and X. Liu. "Soliton Self-Frequency Shift: Experimental Demonstrations and Applications". *IEEE J. Sel. Topics Quantum Electron.* 14.3 (2008), pp. 713–723.

[18] J. M. Dudley and J. R. Taylor. *Supercontinuum generation in optical fibers*. Cambridge University Press, 2010.

[19] J. M. Dudley, G. Genty, and S. Coen. "Supercontinuum generation in photonic crystal fiber". *Rev. Mod. Phys.* 78 (4 Oct. 2006), pp. 1135–1184.

[20] G. Genty, S. Coen, and J. M. Dudley. "Fiber supercontinuum sources (Invited)". *J. Opt. Soc. Am. B* 24.8 (Aug. 2007), pp. 1771–1785.

[21] J. M. Dudley and J. R. Taylor. "Ten years of nonlinear optics in photonic crystal fibre". *Nat. Photonics* 3.2 (2009), pp. 85–90.

[22] R. Alfano and S. Shapiro. "Observation of self-phase modulation and small-scale filaments in crystals and glasses". *Phys. Rev. Lett.* 24 (1970), pp. 592–594.

[23] R. Alfano and S. Shapiro. "Emission in the region 4000 to 7000 Å via four-photon coupling in glass". *Phys. Rev. Lett.* 24 (1970), pp. 584–587.

[24] S. Smirnov, J. Ania-Castanon, T. Ellingham, S. Kobtsev, S. Kukarin, and S. Turitsyn. "Optical spectral broadening and supercontinuum generation in telecom applications". *Opt. Fiber Technol.* 12.2 (2006), pp. 122 –147.

[25] C. Lin, V. Nguyen, and W. French. "Wideband near-ir continuum (0.7–2.1 μm) generated in low-loss optical fibres". *Electron. Lett.* 14.25 (1978), pp. 822–823.

[26] S Leon-Saval, T Birks, W Wadsworth, P St J Russell, and M Mason. "Supercontinuum generation in submicron fibre waveguides". *Opt. Express* 12.13 (2004), pp. 2864–2869.

[27] M. Foster and A. Gaeta. "Ultra-low threshold supercontinuum generation in sub-wavelength waveguides". *Opt. Express* 12.14 (July 2004), pp. 3137–3143.

[28] M. Foster, K. Moll, and A. Gaeta. "Optimal waveguide dimensions for nonlinear interactions". *Opt. Express* 12.13 (June 2004), pp. 2880–2887.

[29] J. H. V. Price et al. "Mid-IR Supercontinuum Generation From Nonsilica Microstructured Optical Fibers". *IEEE J. Sel. Topics Quantum Electron.* 13.3 (2007), pp. 738–749.

[30] G. Brambilla, F. Xu, P. Horak, Y. Jung, F. Koizumi, N. P. Sessions, E. Koukharenko, X. Feng, G. S. Murugan, J. S. Wilkinson, et al. "Optical fiber nanowires and microwires: fabrication and applications". *Advances in Optics and Photonics* 1.1 (2009), pp. 107–161.

[31] A. Zheltikov. "The physical limit for the waveguide enhancement of nonlinear-optical processes". *Opt. Spectrosc.* 95.3 (2003), pp. 410–415.

[32] T. A. Birks, W. J. Wadsworth, and P. S. J. Russell. "Supercontinuum generation in tapered fibers". *Opt. Lett.* 25.19 (2000), pp. 1415–1417.

[33] J Teipel, K Franke, D Türke, F Warken, D Meiser, M Leuschner, and H Giessen. "Characteristics of supercontinuum generationin tapered fibers using femtosecond laser pulses". *Appl. Phys. B* 77.2-3 (2003), pp. 245–251.

[34] L. Tong, R. R. Gattass, J. B. Ashcom, S. He, J. Lou, M. Shen, I. Maxwell, and E. Mazur. "Subwavelength-diameter silica wires for low-loss optical wave guiding". *Nature* 426.6968 (2003), pp. 816–819.

[35] R. R. Gattass, G. T. Svacha, L. Tong, and E. Mazur. "Supercontinuum generation in submicrometer diameter silica fibers". *Opt. Express* 14.20 (2006), pp. 9408–9414.

[36] V. Kumar, A George, J Knight, and P Russell. "Tellurite photonic crystal fiber". *Optics Express* 11.20 (2003), pp. 2641–2645.

[37] P. Domachuk, N. A. Wolchover, M. Cronin-Golomb, A. Wang, A. K. George, C. M. B. Cordeiro, J. C. Knight, and F. G. Omenetto. "Over 4000 nm bandwidth of mid-IR supercontinuum generation in sub-centimeter segments of highly nonlinear tellurite PCFs". *Opt. Express* 16.10 (May 2008), pp. 7161–7168.

[38] M. Liao, C. Chaudhari, G. Qin, X. Yan, T. Suzuki, and Y. Ohishi. "Tellurite microstructure fibers with small hexagonal core for supercontinuum generation". *Opt. Express* 17.14 (July 2009), pp. 12174–12182.

[39] I. Savelii et al. "Suspended core tellurite glass optical fibers for infrared supercontinuum generation". *Opt. Mater.* 33.11 (2011), pp. 1661 –1666.

[40] G. Qin, X. Yan, C. Kito, M. Liao, C. Chaudhari, T. Suzuki, and Y. Ohishi. "Supercontinuum generation spanning over three octaves from UV to 3.85 μm in a fluoride fiber". *Opt. Lett.* 34.13 (July 2009), pp. 2015–2017.

[41] C. Xia, M. Kumar, O. P. Kulkarni, M. N. Islam, F. L. Terry Jr, M. J. Freeman, M. Poulain, G. Mazé, et al. "Mid-infrared supercontinuum generation to 4.5 μm in ZBLAN fluoride fibers by nanosecond diode pumping". *Opt. Lett.* 31.17 (2006), pp. 2553–2555.

[42] C. Agger, C. Petersen, S. Dupont, H. Steffensen, J. K. Lyngsø, C. L. Thomsen, J. Thøgersen, S. R. Keiding, and O. Bang. "Supercontinuum generation in ZBLAN fibers—detailed comparison between measurement and simulation". *J. Opt. Soc. Am. B* 29.4 (Apr. 2012), pp. 635–645.

[43] M. Liao, C. Chaudhari, G. Qin, X. Yan, C. Kito, T. Suzuki, Y. Ohishi, M. Matsumoto, and T. Misumi. "Fabrication and characterization of a chalcogenide-tellurite composite microstructure fiber with high nonlinearity". *Opt. Express* 17.24 (Nov. 2009), pp. 21608–21614.

[44] M. El-Amraoui et al. "Microstructured chalcogenide optical fibers from As2S3 glass: towards new IR broadband sources". *Opt. Express* 18.25 (Dec. 2010), pp. 26655–26665.

[45] J. Hu, C. R. Menyuk, L. B. Shaw, J. S. Sanghera, and I. D. Aggarwal. "Generating Mid-IR Source Using As2S3-Based Chalcogenide Photonic Crystal Fibers". *Conference on Lasers and Electro-Optics/International Quantum Electron. Conference* (2009), CThN6.

[46] N. Granzow, S. P. Stark, M. A. Schmidt, A. S. Tverjanovich, L. Wondraczek, and P. S. Russell. "Supercontinuum generation in chalcogenide-silica step-index fibers". *Opt. Express* 19.21 (Oct. 2011), pp. 21003–21010.

[47] D. D. Hudson, S. A. Dekker, E. C. Mägi, A. C. Judge, S. D. Jackson, E. Li, J. S. Sanghera, L. B. Shaw, I. D. Aggarwal, and B. J. Eggleton. "Octave spanning supercontinuum in an As2S3 taper using ultralow pump pulse energy". *Opt. Lett.* 36.7 (Apr. 2011), pp. 1122–1124.

[48] M. R. Lamont, B. Luther-Davies, D.-Y. Choi, S. Madden, and B. J. Eggleton. "Supercontinuum generation in dispersion engineered highly nonlinear($\gamma = 10$ /W/m) As2S3 chalcogenide planar waveguide". *Opt. Express* 16.19 (Sept. 2008), pp. 14938–14944.

[49] J. M. Harbold, F. O. Ilday, F. W. Wise, J. S. Sanghera, V. Q. Nguyen, L. B. Shaw, and I. D. Aggarwal. "Highly nonlinear As-S-Se glasses for all-optical switching". *Opt. Lett.* 27.2 (Jan. 2002), pp. 119–121.

[50] R. E. Slusher, G. Lenz, J. Hodelin, J. Sanghera, L. B. Shaw, and I. D. Aggarwal. "Large Raman gain and nonlinear phase shifts in high-purity As2Se3 chalcogenide fibers". *J. Opt. Soc. Am. B* 21.6 (June 2004), pp. 1146–1155.

[51] K. M. Hilligsøe, T. Andersen, H. Paulsen, C. Nielsen, K. Mølmer, S. Keiding, R. Kristiansen, K. Hansen, and J. Larsen. "Supercontinuum generation in a photonic crystal fiber with two zero dispersion wavelengths". *Opt. Express* 12.6 (2004), pp. 1045–1054.

[52] M. Frosz, P. Falk, and O. Bang. "The role of the second zero-dispersion wavelength in generation of supercontinua and bright-bright soliton-pairs across the zero-dispersion wavelength". *Opt. Express* 13.16 (2005), pp. 6181–6192.

[53] G Genty, M Lehtonen, H Ludvigsen, and M Kaivola. "Enhanced bandwidth of supercontinuum generated in microstructured fibers". *Opt. Express* 12.15 (2004), pp. 3471–3480.

[54] J. Travers. "Blue extension of optical fibre supercontinuum generation". *J. Opt* 12.11 (2010), p. 113001.

[55] A Kudlinski, A. George, J. Knight, J. Travers, A. Rulkov, S. Popov, and J. Taylor. "Zero-dispersion wavelength decreasing photonic crystal fibers for ultraviolet-extended supercontinuum generation". *Opt. Express* 14.12 (2006), pp. 5715–5722.

[56] J. C. Travers, A. B. Rulkov, S. V. Popov, J. R. Taylor, A Kudlinski, A. K. George, and J. C. Knight. "Multi-Watt Supercontinuum Generation from 0.3 to 2.4 μm in PCF Tapers". In: *Conference on Lasers and Electro-Optics*. Optical Society of America. 2007.

[57] J. Stone and J. Knight. "From zero dispersion to group index matching: How tapering fibers offers the best of both worlds for visible supercontinuum generation". *Opt. Fiber Technol.* (2012).

[58] S. Stark, J. Travers, and P. S. J. Russell. "Extreme supercontinuum generation to the deep UV". *Opt. Lett.* 37.5 (2012), pp. 770–772.

[59] X. Feng, F. Poletti, A. Camerlingo, F. Parmigiani, P. Petropoulos, P. Horak, G. M. Ponzo, M. Petrovich, J. Shi, W. H. Loh, et al. "Dispersion controlled highly nonlinear fibers for all-optical processing at telecoms wavelengths". *Optical Fiber Technology* 16.6 (2010), pp. 378–391.

[60] *Amorphous Materials Inc., USA*. http://www.amorphousmaterials.com/.

[61] J. S. Sanghera, L. Shaw, and I. D. Aggarwal. "Applications of chalcogenide glass optical fibers". *C.R. Chim.* 5.12 (2002), pp. 873 –883.

[62] A Zakery and S. R. Elliott. *Optical nonlinearities in chalcogenide glasses and their applications*. Vol. 135. Springer, 2007.

[63] B. Jalali. "Nonlinear optics in the mid-infrared". *Nat. Photonics* 4 (2010), pp. 506–508.

[64] R. Boyd. *Nonlinear Optics*. 3^{rd}. Springer Series in Optical Sciences, 2008.

[65] R. H. Stolen, J. P. Gordon, W. J. Tomlinson, and H. A. Haus. "Raman response function of silica-core fibers". *J. Opt. Soc. Am. B* 6.6 (1989), pp. 1159–1166.

[66] A. Seddon. "Chalcogenide glasses: a review of their preparation, properties and applications". *J. Non-Cryst. Solids* 184.0 (1995), pp. 44 –50.

[67] N. Akhmediev and M. Karlsson. "Cherenkov radiation emitted by solitons in optical fibers". *Phys. Rev. A* 51 (3 1995), pp. 2602–2607.

[68] A. M. Al-kadry and M. Rochette. "Mid-infrared sources based on the soliton self-frequency shift". *J. Opt. Soc. Am. B* 29 (6 2012), pp. 1347–1355.

[69] A. Al-Kadry and M. Rochette. "Maximized Soliton Self-Frequency Shift in Non-Uniform Microwires by the Control of Third-Order Dispersion Perturbation". *J. Lightwave Technol.* 31.9 (2013), pp. 1462–1467.

[70] A. Al-kadry, C. Baker, M. El Amraoui, Y. Messaddeq, and M. Rochette. "Broadband supercontinuum generation in As2Se3 chalcogenide wires by avoiding the two-photon absorption effects". *Opt. Lett.* 38.7 (2013), pp. 1185–1187.

[71] A. Al-kadry and M Rochette. "Mid-infrared sources based on the soliton self-frequency shift". In: *Proceedings of SPIE*. Vol. 8007. 2011, p. 80070D.

[72] A. Al-Kadry and M. Rochette. "Optimization of optical soliton self-frequency shifting towards the mid-infrared". In: *Fibre and Optical Passive Components (WFOPC), 2011 7th Workshop on*. IEEE. 2011, pp. 1–4.

[73] A. Al-Kadry and M. Rochette. "Widely tunable soliton frequency shifting for mid-infrared applications". In: *Photonics Conference (PHO), 2011 IEEE*. IEEE. 2011, pp. 59–60.

[74] A. Al-kadry, C. Baker, M. El-Amraoui, Y. Messaddeq, and M. Rochette. "Broadband Supercontinuum in As2Se3 Wires by Suppression of Two-photon Absorption". In: *CLEO: Science and Innovations*. Optical Society of America. 2013.

[75] M. M. Hasegawa Akira. *Optical Solitons in Fibers*. 3^{rd}. Springer Series in Photonics, 2003.

[76] A. Konyukhov, E. Romanova, and V. Shiryaev. "Chalcogenide glasses as a medium for controlling ultrashort IR pulses: Part I". *Opt. Spectrosc.* 110.3 (2011), pp. 442–448.

[77] J. A. Savage. "Optical properties of chalcogenide glasses". *J. Non-Cryst. Solids* 47.1 (1982), pp. 101–115.

[78] *Coractive Inc, Canada*. www.coractive.com.

[79] T. Birks, K. Oakley, et al. "Control of optical fibre taper shape". *Electron. Lett.* 27.18 (1991), pp. 1654–1656.

[80] E. C. Mägi, L. B. Fu, H. C. Nguyen, M. R. Lamont, D. I. Yeom, and B. J. Eggleton. "Enhanced Kerr nonlinearity in sub-wavelength diameter As2Se3 chalcogenide fiber tapers". *Opt. Express* 15.16 (Aug. 2007), pp. 10324–10329.

[81] F. Warken and H. Giessen. "Fast profile measurement of micrometer-sized tapered fibers with better than 50-nm accuracy". *Opt. Lett.* 29.15 (2004), pp. 1727–1729.

[82] J. S. Sanghera et al. "Development and Infrared Applications of Chalcogenide Glass Optical Fibers". *Fiber Integr. Opt.* 19.3 (2000), pp. 251–274.

[83] C. Moynihan, P. Macedo, M. Maklad, R. Mohr, and R. Howard. "Intrinsic and impurity infrared absorption in As_2 Se_3 glass". *J. Non-Cryst. Solids* 17.3 (1975), pp. 369–385.

[84] V. Shiryaev, S. Smetanin, D. Ovchinnikov, M. Churbanov, E. Kryukova, and V. Plotnichenko. "Effects of oxygen and carbon impurities on the optical transmission of As2Se3 glass". *Inorg. Mater.* 41.3 (2005), pp. 308–314.

[85] J. Travers, R. Kennedy, S. Popov, J. Taylor, H Sabert, and B Mangan. "Extended continuous-wave supercontinuum generation in a low-water-loss holey fiber". *Opt. Lett.* 30.15 (2005), pp. 1938–1940.

[86] S. A. Dekker, A. C. Judge, R. Pant, I. Gris-Sánchez, J. C. Knight, C. M. de Sterke, and B. J. Eggleton. "Highly-efficient, octave spanning soliton self-frequency shift using a specialized photonic crystal fiber with low OH loss". *Opt. Express* 19.18 (2011), pp. 17766–17773.

[87] Q. Coulombier, L. Brilland, P. Houizot, T. Chartier, T. N. N'Guyen, F. Smektala, G. Renversez, A. Monteville, D. Méchin, T. Pain, et al. "Casting method for producing low-loss chalcogenide microstructured optical fibers". *Optics Express* 18.9 (2010), pp. 9107–9112.

[88] I Gris-Sánchez, B. J. Mangan, and J. C. Knight. "Reducing spectral attenuation in small-core photonic crystal fibers". *Opt. Mater. Express* 1.2 (2011), pp. 179–184.

[89] G. M. Hale and M. R. Querry. "Optical constants of water in the 200-nm to 200-μm wavelength region". *Appl. Opt.* 12.3 (1973), pp. 555–563.

[90] M. Churbanov, I. Scripachev, G. Snopatin, V. Shiryaev, and V. Plotnichenko. *High-purity glasses based on arsenic chalcogenides*. Tech. rep. DTIC Document, 2001.

[91] D. Marcuse. "Mode conversion caused by surface imperfections of a dielectric slab waveguide". *Bell Syst. Tech. J* 48.10 (1969), pp. 3187–3215.

[92] F. Ladouceur. "Roughness, inhomogeneity, and integrated optics". *IEEE/OSA J. Lightw. Technol.* 15.6 (1997), pp. 1020–1025.

[93] G. Zhai and L. Tong. "Roughness-induced radiation losses in optical micro or nanofibers". *Opt. Express* 15.21 (2007), pp. 13805–13816.

[94] G. Brambilla, V. Finazzi, and D. Richardson. "Ultra-low-loss optical fiber nanotapers". *Opt. Express* 12.10 (2004), pp. 2258–2263.

[95] K. Blow and D. Wood. "Theoretical description of transient stimulated Raman scattering in optical fibers". *IEEE J. Quantum Electron.* 25.12 (1989), pp. 2665–2673.

[96] E. W. Van Stryland, H Vanherzeele, M. A. Woodall, M. Soileau, A. L. Smirl, S. Guha, and T. F. Boggess. "Two photon absorption, nonlinear refraction, and optical limiting in semiconductors". *Opt. Eng.* 24.4 (1984), pp. 244613–244613.

[97] J. Hult. "A Fourth-Order Runge–Kutta in the Interaction Picture Method for Simulating Supercontinuum Generation in Optical Fibers". *J. Lightwave Technol.* 25.12 (2007), pp. 3770–3775.

[98] J. S. Sanghera, L. B. Shaw, P. Pureza, V. Q. Nguyen, D. Gibson, L. Busse, I. D. Aggarwal, C. M. Florea, and F. H. Kung. "Nonlinear Properties of Chalcogenide Glass Fibers". *Int. J. Appl. Glass Sci.* 1.3 (2010), pp. 296–308.

[99] J. S. Russell. "Report on waves". In: *14th meeting of the British Association for the Advancement of Science*. Vol. 311. 1844, p. 390.

[100] A. Hasegawa and F. Tappert. "Transmission of stationary nonlinear optical pulses in dispersive dielectric fibers. I. Anomalous dispersion". *Appl. Phys. Lett.* 23.3 (1973), pp. 142–144.

[101] L. F. Mollenauer, R. H. Stolen, and J. P. Gordon. "Experimental Observation of Picosecond Pulse Narrowing and Solitons in Optical Fibers". *Phys. Rev. Lett.* 45 (13 1980), pp. 1095–1098.

[102] A. Hasegawa and Y. Kodama. "Amplification and reshaping of optical solitons in a glass fiber—I". *Opt. Lett.* 7.6 (1982), pp. 285–287.

[103] A. Hasegawa. "Amplification and reshaping of optical solitons in a glass fiber-IV: Use of the stimulated Raman process". *Opt. Lett.* 8.12 (1983), pp. 650–652.

[104] K. Blow, N. Doran, and D. Wood. "Generation and stabilization of short soliton pulses in the amplified nonlinear Schrödinger equation". *J. Opt. Soc. Am. B* 5.2 (1988), pp. 381–391.

[105] H. Kuehl. "Solitons on an axially nonuniform optical fiber". *J. Opt. Soc. Am. B* 5.3 (1988), pp. 709–713.

[106] E. Dianov, P. Mamyshev, A. Prokhorov, and S. Chernikov. "Generation of a train of fundamental solitons at a high repetition rate in optical fibers". *Opt. Lett.* 14.18 (1989), pp. 1008–1010.

[107] P. Beaud, W. Hodel, B. Zysset, and H. Weber. "Ultrashort pulse propagation, pulse breakup, and fundamental soliton formation in a single-mode optical fiber". *IEEE J. Quantum Electron.* 23.11 (1987), pp. 1938 –1946.

[108] E. Golovchenko, E. Dianov, A. Prokhorov, and V. Serkin. "Decay of optical solitons". *JETP Lett* 42.2 (1985), pp. 87–91.

[109] E. Dianov and V Mamyshev. "Stimulated-Raman conversion of multisoliton pulses in". *JETP Lett* 41.6 (1985).

[110] P. Wai, C. R. Menyuk, Y. Lee, and H. Chen. "Nonlinear pulse propagation in the neighborhood of the zero-dispersion wavelength of monomode optical fibers". *Opt. Lett.* 11.7 (1986), pp. 464–466.

[111] I. Cristiani, R. Tediosi, L. Tartara, and V. Degiorgio. "Dispersive wave generation by solitons in microstructured optical fibers". *Opt. Express* 12.1 (2004), pp. 124–135.

[112] J. C. K. D. V. Skryabin F. Luan and P. S. J. Russell. "Soliton self-frequency shift cancellation in photonic crystal fibers". *Science* 301 (5640 2003), pp. 1705–1708.

[113] G. P. Agrawal. "Nonlinear fiber optics: its history and recent progress [Invited]". *Journal of the Optical Society of America-B-Optical Physics* 28.12 (2011), A1.

[114] A. C. Judge, O. Bang, B. J. Eggleton, B. T. Kuhlmey, E. C. Mägi, R. Pant, and C. M. de Sterke. "Optimization of the soliton self-frequency shift in a tapered photonic crystal fiber". *J. Opt. Soc. Am. B* 26.11 (2009), pp. 2064–2071.

[115] D. A. Chestnut and J. R. Taylor. "Soliton self-frequency shift in highly nonlinear fiber with extension by external Raman pumping". *Opt. Lett.* 28.24 (2003), pp. 2512–2514.

[116] X. Liu, C. Xu, W. H. Knox, J. K. Chandalia, B. J. Eggleton, S. G. Kosinski, and R. S. Windeler. "Soliton self-frequency shift in a short tapered air–silica microstructure fiber". *Opt. Lett.* 26.6 (2001), pp. 358–360.

[117] B. Washburn, S. Ralph, P. Lacourt, J. Dudley, W. Rhodes, R. Windeler, and S. Coen. "Tunable near-infrared femtosecond soliton generation in photonic crystal fibres". *Electron. Lett.* 37.25 (2001), pp. 1510 –1512.

[118] I. Cormack, D. Reid, W. Wadsworth, J. Knight, and P. Russell. "Observation of soliton self-frequency shift in photonic crystal fibre". *Electron. Lett.* 38.4 (2002), pp. 167 –169.

[119] D. G. Ouzounov, F. R. Ahmad, D. Muller, N. Venkataraman, M. T. Gallagher, M. G. Thomas, J. Silcox, K. W. Koch, and A. L. Gaeta. "Generation of Megawatt Optical Solitons in Hollow-Core Photonic Band-Gap Fibers". *Science* 301.5640 (2003), pp. 1702–1704.

[120] S. V. Kobtsev, N. V. Fateevand, and S. V. Smirnov. "Generation of self-frequency-shifted solitons in tapered fibers in the presence of femtosecond pumping". *Laser Phys.* 14.5 (2004), pp. 748–751.

[121] J. Lægsgaard. "Soliton formation in hollow-core photonic bandgap fibers". *Appl. Phys. B* 95.2 (2009), pp. 293–300.

[122] A. Ivanov, A. Podshivalov, and A. Zheltikov. "Frequency-shifted megawatt soliton output of a hollow photonic-crystal fiber for time-resolved coherent anti-Stokes Raman scattering microspectroscopy". *Opt. Lett.* 31.22 (2006), pp. 3318–3320.

[123] F. Gèrôme, P Dupriez, J Clowes, J. Knight, and W. Wadsworth. "High power tunable femtosecond soliton source using hollow-core photonic bandgap fiber, and its use for frequency doubling". *Opt. Express* 16.4 (2008), pp. 2381–2386.

[124] A. V. Gorbach and D. V. Skryabin. "Soliton self-frequency shift, non-solitonic radiation and self-induced transparency in air-core fibers". *Opt. Express* 16.7 (2008), pp. 4858–4865.

[125] N González-Baquedano, I Torres-Gómez, N Arzate, A Ferrando, and D. Ceballos-Herrera. "Pulse quality analysis on soliton pulse compression and soliton self-frequency shift in a hollow-core photonic bandgap fiber". *Opt. Express* 21.7 (2013), pp. 9132–9143.

[126] J. C. Knight, T. A. Birks, P. S. J. Russell, and D. M. Atkin. "All-silica single-mode optical fiber with photonic crystal cladding". *Opt. Lett.* 21.19 (1996), pp. 1547–1549.

[127] J. Knight, J. Arriaga, T. Birks, A. Ortigosa-Blanch, W. Wadsworth, and P. Russell. "Anomalous dispersion in photonic crystal fiber". *IEEE Photon. Technol. Lett.* 12.7 (2000), pp. 807 –809.

[128] N. Nishizawa and T. Goto. "Compact system of wavelength-tunable femtosecond soliton pulse generation using optical fibers". *IEEE Photon. Technol. Lett.* 11.3 (1999), pp. 325 –327.

[129] M.-C. Chan, S.-H. Chia, T.-M. Liu, T.-H. Tsai, M.-C. Ho, A. A. Ivanov, A. M. Zheltikov, J.-Y. Liu, H.-L. Liu, and C.-K. Sun. "1.2-2.2-μm Tunable Raman Soliton Source Based on a Cr:Forsterite-Laser and a Photonic-Crystal Fiber". *IEEE Photon.Technol. Lett.* 11.20 (2008), p. 900.

[130] H. Lim, J. Buckley, A. Chong, and F. Wise. "Fibre-based source of femtosecond pulses tunable from 1.0 to 1.3 mum". *Electron. Lett.* 40.24 (2004), pp. 1523 –1525.

[131] I. Gris-Sánchez, B. Mangan, and J. Knight. "Reducing spectral attenuation in small-core photonic crystal fibers". *Opt. Mater. Express* 1.2 (2011), pp. 179–184.

[132] C. Baker and M. Rochette. "A generalized heat-brush approach for precise control of the waist profile in fiber tapers". *Opt. Mater. Express* 1.6 (2011), pp. 1065–1076.

[133] X. Yan, C. Kito, S. Miyoshi, M. Liao, T. Suzuki, and Y. Ohishi. "Raman transient response and enhanced soliton self-frequency shift in ZBLAN fiber". *J. Opt. Soc. Am. B* 29.2 (2012), pp. 238–243.

[134] A. C. Judge, S. A. Dekker, R. Pant, C. M. de Sterke, and B. J. Eggleton. "Soliton self-frequency shift performance in As_2 S_3 waveguides". *Opt. Express* 18.14 (2010), pp. 14960–14968.

[135] O Vanvincq, A Kudlinski, A Bétourné, Y Quiquempois, and G Bouwmans. "Extreme deceleration of the soliton self-frequency shift by the third-order dispersion in solid-core photonic bandgap fibers". *J. Opt. Soc. Am. B* 27.11 (2010), pp. 2328–2335.

[136] J. G. Kuzyk. *Polymer Fiber Optics: Materials, Physics, and Application*. CRC press, 2009.

[137] H. Lin, W. Dechent, D. Day, and J. Stoffer. "Preparation and properties of mid-infrared glass fibres and poly (chlorotrifluoroethylene) composites". *Journal of Mater. Sci.* 32 (24 1997), pp. 6573–6578.

[138] G. Snopatin, V. Shiryaev, V. Plotnichenko, E. Dianov, and M. Churbanov. "High-purity chalcogenide glasses for fiber optics". *Inorg. Mater.* 45 (13 2009), pp. 1439–1460.

[139] J. Love. "Spot size, adiabaticity and diffraction in tapered fibres". *Electron. Lett.* 23.19 (1987), pp. 993–994.

[140] J. Herrmann and A. Nazarkin. "Soliton self-frequency shift for pulses with a duration less than the period of molecular oscillations". *Opt. Lett.* 19.24 (1994), pp. 2065–2067.

[141] R. Pant, A. C. Judge, E. C. Magi, B. T. Kuhlmey, M. de Sterke, and B. J. Eggleton. "Characterization and optimization of photonic crystal fibers for enhanced soliton self-frequency shift". *J. Opt. Soc. Am. B* 27.9 (2010), pp. 1894–1901.

[142] J. N. Elgin. "Soliton propagation in an optical fiber with third-order dispersion". *Opt. Lett.* 17.20 (Oct. 1992), pp. 1409–1410.

[143] P. K. A. Wai, H. H. Chen, and Y. C. Lee. "Radiations by "solitons" at the zero group-dispersion wavelength of single-mode optical fibers". *Phys. Rev. A* 41 (1 Jan. 1990), pp. 426–439.

[144] J. N. Elgin. "Perturbations of optical solitons". *Phys. Rev. A* 47 (5 May 1993), pp. 4331–4341.

[145] F. Biancalana, D. V. Skryabin, and A. V. Yulin. "Theory of the soliton self-frequency shift compensation by the resonant radiationin photonic crystal fibers". *Phys. Rev. E* 70 (1 July 2004), p. 016615.

[146] S. Roy, S. K. Bhadra, and G. P. Agrawal. "Dispersive waves emitted by solitons perturbed by third-order dispersion inside optical fibers". *Phys. Rev. A* 79 (2 Feb. 2009), p. 023824.

[147] H. Steffensen, C. Agger, and O. Bang. "Influence of two-photon absorption on soliton self-frequency shift". *J. Opt. Soc. Am. B* 29.3 (Mar. 2012), pp. 484–492.

[148] W. J. Wadsworth, A. Ortigosa-Blanch, J. C. Knight, T. A. Birks, T.-P. M. Man, and P. S. J. Russell. "Supercontinuum generation in photonic crystal fibers and optical fiber tapers: a novel light source". *J. Opt. Soc. Am. B* 19.9 (2002), pp. 2148–2155.

[149] T. Morioka, K. Mori, and M. Saruwatari. "More than 100-wavelength-channel picosecond optical pulse generation from single laser source using supercontinuum in optical fibres". *Electron. Lett.* 29.10 (1993), pp. 862–864.

[150] H. R. H. T. W. Udem Th. "Optical frequency metrology". *Nature* 416 (2002), pp. 233–237.

[151] I. Hartl, X. D. Li, C. Chudoba, R. K. Ghanta, T. H. Ko, J. G. Fujimoto, J. K. Ranka, and R. S. Windeler. "Ultrahigh-resolution optical coherence tomography using continuum generation in an air–silica microstructure optical fiber". *Opt. Lett.* 26.9 (May 2001), pp. 608–610.

[152] A. Labruyère, A. Tonello, V. Couderc, G. Huss, and P. Leproux. "Compact supercontinuum sources and their biomedical applications". *Opt. Fiber Technol.* 18.5 (2012), pp. 375 –378.

[153] L. Froehly and J. Meteau. "Supercontinuum sources in optical coherence tomography: A state of the art and the application to scan-free time domain correlation techniques and depth dependant dispersion compensation". *Opt. Fiber Technol.* 18.5 (2012), pp. 411 –419.

[154] K. Namjou, C. B. Roller, and P. J. McCann. "The Breathmeter-A new laser device to analyze your health". *Circuits and Devices Magazine, IEEE* 22.5 (2006), pp. 22–28.

[155] S. Sanders. "Wavelength-agile fiber laser using group-velocity dispersion of pulsed super-continua and application to broadband absorption spectroscopy". English. *Appl. Phys. B* 75.6-7 (2002), pp. 799–802.

[156] K. Lindfors, T. Kalkbrenner, P. Stoller, and V. Sandoghdar. "Detection and Spectroscopy of Gold Nanoparticles Using Supercontinuum White Light Confocal Microscopy". *Phys. Rev. Lett.* 93 (3 July 2004), p. 037401.

[157] F. K. Tittel, D. Richter, and A. Fried. "Mid-infrared laser applications in spectroscopy". In: *Solid-State Mid-Infrared Laser Sources*. Springer, 2003, pp. 458–529.

[158] B. L.-D. B. J. Eggleton and K. Richardson. "Chalcogenide photonics". *Nat. Photon.* 5 (2011), pp. 1749–4885.

[159] C. Baker and M. Rochette. "High Nonlinearity and Single-Mode Transmission in Tapered Multimode As2Se3-PMMA Fibers". *Photonics Journal, IEEE* 4.3 (2012), pp. 960–969.

[160] D.-I. Yeom, E. C. Mägi, M. R. E. Lamont, M. A. F. Roelens, L. Fu, and B. J. Eggleton. "Low-threshold supercontinuum generation in highly nonlinear chalcogenide nanowires". *Opt. Lett.* 33.7 (2008), pp. 660–662.

[161] M. Sheik-Bahae, D. Hutchings, D. Hagan, and E. Van Stryland. "Dispersion of bound electron nonlinear refraction in solids". *IEEE J. Quantum Electron.* 27.6 (1991), pp. 1296–1309.

[162] J Troles, F Smektala, G Boudebs, and A Monteil. "Third order nonlinear optical characterization of new chalcohalogenide glasses containing lead iodine". *Opt. Mater.* 22.4 (2003), pp. 335 –343.

[163] V. Mizrahi, M. A. Saifi, M. J. Andrejco, K. W. DeLong, and G. I. Stegeman. "Two-photon absorption as a limitation to all-optical switching". *Opt. Lett.* 14.20 (Oct. 1989), pp. 1140–1142.

[164] A. Tuniz, G. Brawley, D. J. Moss, and B. J. Eggleton. "Two-photon absorption effects on Raman gain in single mode As2Se3 chalcogenide glass fiber". *Opt. Express* 16.22 (Oct. 2008), pp. 18524–18534.

[165] R. Ahmad and M. Rochette. "Chalcogenide optical parametric oscillator". *Opt. Express* 20.9 (Apr. 2012), pp. 10095–10099.

[166] N. F. Nott and E. A. Davis. *Electronic Processes in Non-Crystalline Materials*. 2^{nd}. Oxford U. Press, 1979.

[167] T. A. Birks and Y. W. Li. "The shape of fiber tapers". *J. Lightw. Technol.* 10.4 (1992), pp. 432–438.

[168] J. Hu, C. R. Menyuk, L. B. Shaw, J. S. Sanghera, and I. D. Aggarwal. "Computational study of 3–5 μm source created by using supercontinuum generation in As2S3 chalcogenide fibers with a pump at 2 μm". *Opt. Lett.* 35.17 (Sept. 2010), pp. 2907–2909.

[169] B. Kuyken, X. Liu, R. M. O. Jr., R. Baets, G. Roelkens, and W. M. J. Green. "Mid-infrared to telecom-band supercontinuum generation in highly nonlinear silicon-on-insulator wire waveguides". *Opt. Express* 19.21 (Oct. 2011), pp. 20172–20181.

[170] X. Gai, D.-Y. Choi, S. Madden, Z. Yang, R. Wang, and B. Luther-Davies. "Supercontinuum generation in the mid-infrared from a dispersion-engineered As2S3 glass rib waveguide". *Opt. Lett.* 37.18 (Sept. 2012), pp. 3870–3872.

[171] F Silva, D. Austin, A Thai, M Baudisch, M Hemmer, D Faccio, A Couairon, and J Biegert. "Multi-octave supercontinuum generation from mid-infrared filamentation in a bulk crystal". *Nat. Commun.* 3 (2012), p. 807.

[172] J. Geng, Q. Wang, and S. Jiang. "High-spectral-flatness mid-infrared supercontinuum generated from a Tm-doped fiber amplifier". *Appl. Opt.* 51.7 (Mar. 2012), pp. 834–840.

[173] W. Gao, M. E. Amraoui, M. Liao, H. Kawashima, Z. Duan, D. Deng, T. Cheng, T. Suzuki, Y. Messaddeq, and Y. Ohishi. "Mid-infrared supercontinuum generation in a suspended-core As2S3 chalcogenide microstructured optical fiber". *Opt. Express* 21.8 (Apr. 2013), pp. 9573–9583.

[174] N. Ducros, A. Labruyère, S. Février, F. Morin, F. Druon, M. Hanna, P. Georges, R. Buczynski, D. Pysz, and R. Stepien. "Mid-Infrared Supercontinuum Generation in Lead-Bismuth-Gallium Oxide Glass Photonic Crystal Fiber". In: *Conference on Lasers and Electro-Optics*. Optical Society of America. 2010.

[175] V. Kamynin, A. Kurkov, and V. Mashinsky. "Supercontinuum generation up to 2.7 μm in the germanate-glass-core and silica-glass-cladding fiber". *Laser Phys. Lett.* 9.3 (2012), pp. 219–222.

[176] O. P. Kulkarni, V. V. Alexander, M. Kumar, M. J. Freeman, M. N. Islam, F. L. Terry Jr, M. Neelakandan, A. Chan, et al. "Supercontinuum generation from 1.9 to 4.5 μm in ZBLAN fiber with high average power generation beyond 3.8 μm using a thulium-doped fiber amplifier". *J. Opt. Soc. Am. B* 28.10 (2011), pp. 2486–2498.

[177] D. Deng, W. Gao, M. Liao, Z. Duan, T. Cheng, T. Suzuki, and Y. Ohishi. "Supercontinuum generation from a multiple-ring-holes tellurite microstructured optical fiber pumped by a 2 μm mode-locked picosecond fiber laser". *Appl. Opt.* 52.16 (2013), pp. 3818–3823.

[178] I Savelli, O Mouawad, J. Fatome, B. Kibler, F Désévédavy, G. Gadret, J.-C. Jules, P. Bony, H Kawashima, W Gao, et al. "Mid-infrared 2000-nm bandwidth supercontinuum generation in suspended-core microstructured Sulfide and Tellurite optical fibers". *Opt. Express* 20.24 (2012), pp. 27083–27093.

[179] L. Shaw, P. Thielen, F. Kung, V. Nguyen, J. Sanghera, and I. Aggarwal. "IR supercontinuum generation in As-Se photonic crystal fiber". In: *Conf. Adv. Solid State Lasers (ASSL), Seattle, WA*. 2005.

[180] M. J. Thorpe, D. Balslev-Clausen, M. S. Kirchner, and J. Ye. "Cavity-enhanced optical frequency comb spectroscopy: application to human breath analysis". *Opt. Express* 16.4 (2008), pp. 2387–2397.

[181] H. Thiel. "Low power laser therapy—an introduction and a review of some biological effects". *The Journal of the Canadian Chiropractic Association* 30.3 (1986), p. 133.

[182] G Lenz, J Zimmermann, T Katsufuji, M. Lines, H. Hwang, S Spälter, R. Slusher, S.-W. Cheong, J. Sanghera, and I. Aggarwal. "Large Kerr effect in bulk Se-based chalcogenide glasses". *Opt. Lett.* 25.4 (2000), pp. 254–256.

[183] T. A. Cerni. "An infrared hygrometer for atmospheric research and routine monitoring". *J. Atmos. Oceanic Technol.* 11 (1994), pp. 445–462.

[184] D. D. Weis and G. E. Ewing. "Absorption anomalies in ratio and subtraction FT-IR spectroscopy". *Anal. Chem.* 70.15 (1998), pp. 3175–3183.

[185] S. Danto, D. Thompson, P. Wachtel, J. D. Musgraves, K. Richardson, and B. Giroire. "A Comparative Study of Purification Routes for As2Se3 Chalcogenide Glass". *Int. J. Appl. Glass Sci.* (2012).

[186] B Wetzel, A Stefani, L Larger, P. Lacourt, J. Merolla, T Sylvestre, A Kudlinski, A Mussot, G Genty, F Dias, et al. "Real-time full bandwidth measurement of spectral noise in supercontinuum generation". *Scientific reports* 2 (2012).

[187] J. M. Dudley, L. Provino, N. Grossard, H. Maillotte, R. S. Windeler, B. J. Eggleton, and S. Coen. "Supercontinuum generation in air–silica microstructured fibers with nanosecond and femtosecond pulse pumping". *J. Opt. Soc. Am. B* 19.4 (2002), pp. 765–771.

[188] S. Coen, A. H. L. Chau, R. Leonhardt, J. D. Harvey, J. C. Knight, W. J. Wadsworth, and P. S. J. Russell. "Supercontinuum generation by stimulated Raman scattering and parametric four-wave mixing in photonic crystal fibers". *J. Opt. Soc. Am. B* 19.4 (2002), pp. 753–764.

[189] M. H. Frosz, O. Bang, and A. O. Bjarklev. "Soliton collision and Raman gain regimes in continuous-wave pumped supercontinuum generation". *Opt. Express* 14.20 (2006), pp. 9391–9407.

[190] A. Rieznik, A. Heidt, P. Konig, V. Bettachini, and D. Grosz. "Optimum integration procedures for supercontinuum simulation". *Photonics Journal, IEEE* 4.2 (2012), pp. 552–560.

[191] M. Lines. "Oxide glasses for fast photonic switching: A comparative study". *J. Appl. Phys.* 69.10 (1991), pp. 6876–6884.

[192] K Petkov and P. Ewen. "Photoinduced changes in the linear and non-linear optical properties of chalcogenide glasses". *J. Non-Cryst. Solids* 249.2 (1999), pp. 150–159.

[193] M Sheik-Bahae, D. Hagan, and E. Van Stryland. "Dispersion and band-gap scaling of the electronic Kerr effect in solids associated with two-photon absorption". *Phys. Rev. Lett.* 65.1 (1990), p. 96.

[194] N. Boling, A. Glass, and A Owyoung. "Empirical relationships for predicting nonlinear refractive index changes in optical solids". *IEEE J. Quantum Electron.* 14.8 (1978), pp. 601–608.

[195] R. DeSalvo, A. A. Said, D. J. Hagan, E. W. Van Stryland, and M. Sheik-Bahae. "Infrared to ultraviolet measurements of two-photon absorption and n_2 in wide bandgap solids". *IEEE J. Quantum Electron.* 32.8 (1996), pp. 1324–1333.